NTNU – Trondheim
Norwegian University of
Science and Technology

Aerodynamic stability of slender suspension bridges

Simen L Walbækken

Civil and Environmental Engineering
Submission date: June 2013
Supervisor: Einar Norleif Strømmen, KT
Co-supervisor: Kristian Berntsen, Vegdirektoratet
Bjørn Isaksen, Vegdirektoratet

Norwegian University of Science and Technology
Department of Structural Engineering

Department of Structural Engineering
Faculty of Engineering Science and Technology
NTNU- Norwegian University of Science and Technology

ACCESSIBILITY

Open

MASTER THESIS 2013

SUBJECT AREA:	DATE:	NO. OF PAGES:
Bridge aerodynamics.	09.06.2013	128

TITLE:

Aerodynamic stability of slender suspension bridges

Aerodynamisk stabilitet av lange slanke hengebruer

BY:

Simen L. Walbækken

SUMMARY:
This thesis studies the aerodynamic stability of a proposed suspension bridge crossing the Sognefjord. Such a bridge will require a main span of approximately 3700 m, almost double the span length of the current record holder. For such a long span and slender suspension bridge its aerodynamic properties are highly important.

A comparison of the aerodynamic stability limits using three different configurations of a so-called vented or dual box girder has been done. The only difference in each configuration is the center-to-center distance between the individual box girders. The design of the individual girders and the cable system is kept constant.

A modal approach to solving the equation of motion has been employed where the eigenfrequencies and eigenmodes have been computed using a computer program called ALVSAT. The numerical calculations of stability limits as well as dynamic response have been done using self-written MATLAB scripts based on well-established theory of bridge aerodynamics. Aerodynamic derivatives have been obtained from wind tunnel tests on the similar cross section of the proposed Brusymfonien bridge.

The results obtained show an increasing critical mean wind velocity with increasing the center-to-center widths between the box sections. For the widest dual box girder, no stability limits were found. The response results confirm the stability limits and indicate a stabilization effect of the dual box girders at wind velocities below the point of modal coupling.

RESPONSIBLE TEACHER: Professor Dr. Ing. Einar Strømmen

SUPERVISOR(S): Bjørn Isaksen (SVV), Kristian Berntsen (SVV)

CARRIED OUT AT: Department of Structural Engineering

MASTEROPPGAVE 2013

Konstruksjonsteknikk

for

Simen Walbækken

AERODYNAMISK STABILITET AV LANGE SLANKE HENGEBRUER

Aerodynamic stability of slender suspension bridges

I Norge er det for tiden under planlegging og bygging en rekke meget slanke brukonstruksjoner, for eksempel Hardangerbroen som er en klassisk hengebro og Hålogalandsbroen som er under utredning i to alternative utgaver, ett alternativ som en vanlig hengebro og et annet i form av den såkalte "Brusymfonien". Begge har hovedspenn på betydelig mer enn 1000 m. De er svært utsatt for den dynamiske lastvirkningen fra vind, men begge er håndterbare innenfor dagens teknologi. Det er imidlertid også under utredning en kryssing av Sognefjorden som innebærer en bro med spenn på opp til tre kilometer, og i dette tilfellet er det usikkert i hvilken grad man vil være i stand til å oppnå en konstruktiv utførelse med tilfredsstillende aerodynamisk egenskaper. Det har i den forbindelse blitt foreslått å undersøke muligheten for addere dempning til systemet ved hjelp av en eller flere massedempere. Hensikten med denne oppgaven er nettopp å se på mulige utførelser av fjordkryssinger i denne spennvidden, hvor det legges spesiell vekt på å undersøke i hvilken grad massedempere (TMD) kan bidra. Arbeidet foreslås lagt opp etter følgende plan:

1. Studenten setter seg inn i teorien for hengebroens virkemåte (men det er ikke hensikten at dette skal munne ut i en omfattende utredning).
2. Studenten setter seg inn i teorien for aerodynamisk stabilitet av slanke broer, spesielt med hensyn til koblede vertikal- og torsjonssvingninger, dvs. "flutter" (se *Strømmen: Theory of bridge aerodynamics, Springer 2006*).
3. For en eller flere aktuelle utførelser utførelser (avtales med veileder og Sivilingeniør K. Berntsen i Vegdirektoratet) skal det foretas en utredning med sikte på å kvantifisere de viktigste mekaniske egenskapene (dvs. aktuelle masse- og stivhetsegenskaper). Basert på regnemaskinprogrammet Alvsat skal det deretter foretas beregninger av de aktuelle egenfrekvensene og tilhørende egensvingeformene som er avgjørende for stabilitetsgrensen. (I den grad tiden tillater det skal disse beregningene utføres i form av et parameterstudium.)
4. For tilfellene som er behandlet under punkt 3 skal det foretas beregninger av stabilitetsgrensen. Beregningen skal baseres på en mest mulig generell teori (se punkt 2 ovenfor) og en løsning i Matlab.
5. For det samme tilfellet skal det foretas en undersøkelse i hvilken grad en eller flere massedempere vil kunne forbedre de dynamiske egenskapene til systemet.

Studenten kan selv velge hvilke problemstillinger han ønsker å legge vekt på. Oppgaven skal gjennomføres i samarbeid med Siv.ing. Kristian Berntsen og Dr.ing. Bjørn Isaksen i Vegdirektoratet.

NTNU, 2013-01-03

Einar Strømmen

Preface

This thesis is the final part of my Master's degree at the Norwegian university of science and technology.

I would like to thank Professor Dr. Ing. Einar Strømmen at the university for his help and guidance with this thesis. I would also like to thank Kristian Berntsen at the Norwegian public roads administration for answering all my questions and providing information on the bridge design.

Trondheim, June 9th 2013

Simen L. Walbækken

Abstract

This thesis studies the aerodynamic stability of a proposed suspension bridge crossing the Sognefjord. Such a bridge will require a main span of approximately 3700 m, almost double the span length of the current record holder. For such a long span and slender suspension bridge its aerodynamic properties becomes highly important.

A comparison of the aerodynamic stability limits using three different configurations of a so-called vented or dual box girder has been done. The only difference in each configuration is the center-to-center distance between the individual box girders. The design of the individual girders and the cable system is kept constant.

A modal approach to solving the equation of motion has been employed where the eigenfrequencies and eigenmodes have been computed using a computer program called ALVSAT [1]. The numerical calculations of stability limits as well as dynamic response have been done using self-written MATLAB [2] scripts based on well-established theory of bridge aerodynamics. Aerodynamic derivatives used are from wind tunnel tests on the similar cross section of the proposed Brusymfonien bridge [3].

The results obtained show an increasing critical mean wind velocity with increasing the center-to-center widths between the box girders. For the widest dual box girder, no stability limits were found. The response results confirm the stability limits and indicate a stabilization effect of the dual box girders at wind velocities below the point of modal coupling.

Sammendrag

Denne oppgaven undersøker aerodynamisk stabilitet av en foreslått ett-spenns hengebro over Sognefjorden. Dette vil kreve en spennlengde på omtrent 3700 m, som er det dobbelte av dagens rekordholder. En hengebro med ett spenn i denne lengden vil være veldig slank og viktigheten av dens aerodynamiske egenskaper er derfor stor.

En sammenligning av aerodynamisk stabilitet av tre utførelser av et såkalt dobbelt kassetverrsnitt har blitt gjort. Forskjellen på utførelsene er senteravstanden mellom de to stivhetsbærerne, mens stivhetsbærerne i seg selv og kabelsystemet er uendret.

Løsningen av svingelingene baserer seg på en modal framgangsmåte, hvor egenfrekvensene og egensvingemodene er beregnet ved hjelp av datamaskinprogrammet ALVSAT [1]. De numeriske beregningene av stabilitetsgrenser og dynamisk respons er gjort ved hjelp av selv skrevne MATLAB [2] rutiner og er basert på godt etablert teori innen bro-aerodynamikk. Aerodynamisk deriverte fra vindtunneltester er tatt fra en rapport på det lignende tverrsnittet til den foreslåtte broen Brusymfonien [3].

Resultatene viser en økende kritisk middelvindhastighet når senteravstanden mellom kassetverrsnittene økes. For det dobble tverrsnittet med bredest senteravstand ble det ikke funnet noen stabilitetsgrense. Responsberegningene bekrefter stabilitetsgrensene i tillegg til å indikere en stabiliserende effekt ved lavere middelvindhastigheter for slike tverrsnitt.

Contents

Notation

Matrices and vectors

Matrices are in general bold upper case Latin or Greek letters, e.g. $\mathbf{Q}$ and $\mathbf{\Phi}$.
Vectors are in general bold lower case Latin or Greek letters, e.g. $\mathbf{q}$ and $\boldsymbol{\varphi}$
$diag[\cdot]$ is a diagonal matrix whose content is written within the brackets.
$\det(\cdot)$ is the determinant of the matrix within the brackets.

Superscript and bars above symbols

Superscript T indicates the transposed of a vector or matrix.
Superscript * indicates the complex conjugate of a quantity.
Dots above symbols indicates its derivative with respect to time.
A prime on a variable indicates its derivative with respect to a relevant variable except t.
A bar (–) above a symbol indicates its average value, e.g. $\bar{r}$.
A tilde (˜) above a symbol indicates that it is a modal quantity, e.g. $\tilde{m}$.
A hat (ˆ) above a symbol indicates a normalized quantity, e.g. $\hat{H}$.

The use of indices and superscript

Index x, y, or z refers to corresponding structural axis.
Index x_f,y_f or z_f refers to corresponding flow axis.
u, v or w refer to flow components.
i and j are mode shape numbers.
n refers to the u, v or w flow component.
D, L, or M refer drag, lift and moment.
tot is short for total.
ae is short for aerodynamic, indicates a flow induced quantity.
cr is short for critical.
max is short for maximum.

r is short for response.
sb is short for single box.
tg is short for transverse girder.
hc is short for hanger cable.
c is short for cables indicating main cables.
T is short of traffic.
G is short for self-weight.

Abbreviations

cg is short for center of gravity.
sc is short for shear center.
cc is short for centroid.
c/c is short for center-to-center distance.
exp is short for exposed, meaning flow exposed part, e.g. L_{exp}.

Latin letters

A Area, cross-sectional area.
A_n Wind spectrum coefficient ($n = u, v, w$).
$A_1^* - A_6^*$ Aerodynamic derivatives associated with torsional motion.
a Fourier constant.
$\mathbf{a}_r$, $\mathbf{a}_q$ Fourier coefficient associated with response or load.
$\mathbf{a}_\eta$, $\mathbf{a}_{\tilde{Q}}$ Fourier coefficient associated with modal response or load.
$\mathbf{B}$ Cross-sectional width.
$\mathbf{B}_q$, $\hat{\mathbf{B}}_q$ Buffeting dynamic load coefficient matrix at cross-sectional level.
$\mathbf{b}_q$, $\hat{\mathbf{b}}_q$ Mean wind load coefficient vector.
$\mathbf{C}$ Matrix containing damping coefficients.
$\mathbf{C}_{ae}$ Aerodynamic damping coefficient matrix.
$\bar{C}$ Force coefficients at mean angle of incidence.
C' Slope of load coefficient curves at mean angle of incidence.
C_w Cross sectional warping constant.
Co Co-spectral density.
$\mathbf{Cov}_{rr}$ Matrix containing covariance of response quantities.
D Cross-sectional depth.
$\mathbf{E}$ Modulus of elasticity.
$\hat{E}$, $\hat{\mathbf{E}}$ Impedance, impedance matrix.
e Eccentricity between shear center and center of gravity or centroid.
e_c Cable sag.
F Force.
f Frequency in Hertz [Hz].

f_{cbu} Cable ultimate tensile strength.
g Gravitational constant.
$\mathbf{G}$ Shear modulus of elasticity.
$\bar{H}$ Static horizontal cable force.
$H_1^* - H_6^*$ Aerodynamic derivatives associated with the across-wind motion.
$\hat{H}_\eta$, $\hat{\mathbf{H}}_\eta$ Normalized modal frequency response function, normalized modal frequency response matrix.
I_T St Venants torsion constant.
I_u, I_w Turbulence intensity of flow components u, w.
I_y, I_z Second moment of area with respect to axis y, z.
$\mathbf{I}$ Identity matrix.
i The imaginary unit or index variable.
j Index variable.
$\mathbf{K}$ Stiffness matrix.
$\mathbf{K}_{ae}$ Aerodynamic stiffness matrix.
k_p Peak factor.
k_T Terrain roughness factor.
L, L_{exp} Length, wind exposed length.
${}^mL_n$ Integral length scales ($m = x_f, y_f, z_f$, $n = u, v, w$).
m, $\mathbf{M}$ Distributed mass or mass matrix.
$\tilde{m}_i$ Modally equivalent distributed mass for mode i.
N Number.
$\bar{N}$ Static cable axial force.
n Index variable.
$P_1^* - P_6^*$ Aerodynamic derivatives associated with along-wind motion.
q Distributed load.
$\mathbf{q}$, $\tilde{\mathbf{Q}}$ Wind load vector, modal wind load vector.
r, $\mathbf{r}$ Cross-sectional displacement or radial distance, displacement vector.
S, $\mathbf{S}$ Auto or cross-spectral density, cross-spectral density matrix.
S_{rr}, $\mathbf{S}_{rr}$ Auto spectral or cross-spectral density associated with response, cross spectral density matrix associated with response.
t Time.
u Fluctuating along-wind horizontal velocity component.
V Mean wind velocity.
v Fluctuating across wind horizontal velocity component.
w Fluctuating across wind vertical component.
x, y, z Cartesian structural coordinates, with origo in shear center, x in the span-wise direction and z vertical.
x_f, y_f, z_f Cartesian flow axis (x_f in the main flow direction and z_f vertical).
x_r Chosen span-wise position for response calculation.

z_0 Terrain roughness length.

Greek letters

α Angle of incidence.
β Coefficient.
γ Coefficient, safety coefficient.
ζ**,**$\boldsymbol{\zeta}$ Damping ratio, damping ratio matrix.
η**,** $\boldsymbol{\eta}$ Generalized coordinate, vector containing N_{mod} η components.
θ Index indicating cross-sectional rotation (about shear center).
$\boldsymbol{\kappa}_{ae}$ Reduced modal aerodynamic stiffness matrix.
ρ Density coefficient, e.g. of air.
ρ_{rr} Covariance coefficients.
σ**,** σ^2 Standard deviation, variance.
$\boldsymbol{\Phi}$ $3 \cdot N_{mod}$ matrix containing all mode shapes φ_i.
$\boldsymbol{\Phi}_r$ Mode shape amplitude matrix at span-wise location at $x = x_r$.
$\boldsymbol{\varphi}$ 3 by 1 mode shape vector containing components ϕ_y, ϕ_z, ϕ_θ.
ψ Normalized mode shape integral.
ω Circular frequency.
ω_i Still air eigenfrequency associated with mode i.
$\omega_i(V)$ Resonance frequency associated with mode i at mean wind velocity V.

Chapter 1

Introduction

As a part of the proposed coastal highway route E39 of the Norwegian public roads administration (NPRA), several fjords must be crossed. One of the main objectives of this public transportation project is to replace the numerous ferry connections along the existing highway with bridges. The widest of the fjords is the Sognefjord, where a bridge will require to span a distance of about $3700\,m$. One of the bridge designs in consideration is a single-span suspension bridge. The design traffic capacity will only require a two lane roadway and two walking/bicycle paths, rendering the required width of the bridge deck quite small. With a main span of $3700\,m$ this proposed bridge will be very slender, making its aerodynamic properties very important.

For high wind loads motion induced effects between a bridge girder and the surrounding flow may cause the structure to become unstable and ultimately lead to structural collapse, see fig. 1.1. Such motion induced effects are more prone to occur the more slender the bridge. The identification of such stability limits is therefore crucial when considering bridge designs of slender suspension bridges.

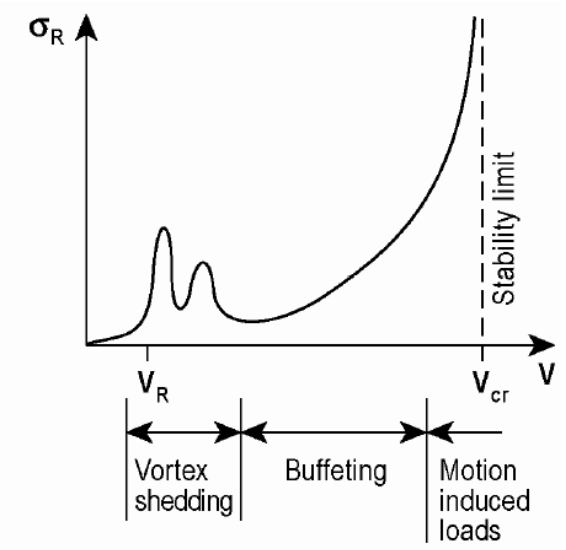

Figure 1.1: Dynamic response with increasing mean wind velocity [4].

The goal of this thesis is to identify the stability limits of a single-span suspension bridge crossing the Sognefjord, i.e. a main span of 3700 m. The computations will be based on well established theory of bridge aerodynamics.

The theory of aerodynamics of line-like bridge type structures is the topic of chapter 2. A short summary on the function of the suspension bridge as a structure is presented in chapter 3. Chapter 4 contains computations of cross sectional properties for the chosen cross sections, and chapter 5 presents the numerical results obtained based on the previous chapters. Finally chapter 6 concludes the thesis.

Chapter 2

Aerodynamics

2.1 Dynamics of line-like structures

Problems in structural dynamics begin with the well known equation of motion, which in matrix notation may be written

$$\mathbf{M} \cdot \ddot{\mathbf{r}} + \mathbf{C} \cdot \dot{\mathbf{r}} + \mathbf{K} \cdot \mathbf{r} = \mathbf{q} \tag{2.1}$$

where $\mathbf{M}$, $\mathbf{C}$, $\mathbf{K}$ are the structural mass, damping and stiffness matrices respectively, and $\mathbf{q}$ is the externally applied load. $\mathbf{r}$ is the structural displacement, and $\dot{\mathbf{r}}$ and $\ddot{\mathbf{r}}$ are the first and second order derivatives of displacement with respect to time, namely structural velocity and acceleration.

In this thesis a continuous approach to the structural properties and displacements are employed, i.e. for a line-like bridge type structure the relevant degrees of freedom are

$$\mathbf{r} = \mathbf{r}(x,t) = \begin{bmatrix} r_y(x,t) & r_z(x,t) & r_\theta(x,t) \end{bmatrix}^T \tag{2.2}$$

where y, z and θ are lateral, vertical and torsional movement as shown in fig. 2.1.

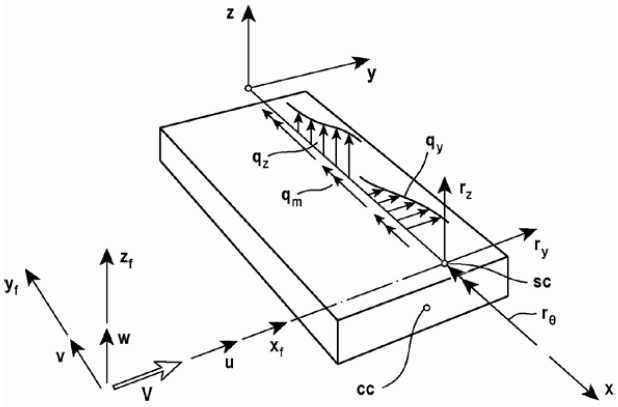

Figure 2.1: Displacement, load and flow axis definition [5].

With this continuous approach to the displacements, and assuming shear center, centroid and center of gravity coincide, the content of **M**, **C** and **K** are the distributed mass, damping and stiffness:

$$\mathbf{M} = \begin{bmatrix} m_y(x) & 0 & 0 \\ 0 & m_z(x) & 0 \\ 0 & 0 & m_\theta(x) \end{bmatrix} \tag{2.3}$$

$$\mathbf{C} = \begin{bmatrix} c_y(x) & 0 & 0 \\ 0 & c_z(x) & 0 \\ 0 & 0 & c_\theta(x) \end{bmatrix} \tag{2.4}$$

$$\mathbf{K} = \begin{bmatrix} k_y(x) & 0 & 0 \\ 0 & k_z(x) & 0 \\ 0 & 0 & k_\theta(x) \end{bmatrix} \tag{2.5}$$

and **q** is the externally applied distributed load.

$$\mathbf{q}(x,t) = \begin{bmatrix} q_y(x,t) \\ q_z(x,t) \\ q_\theta(x,t) \end{bmatrix} \tag{2.6}$$

Solving the equation of motion is in the following done by the modal approach. The assumption of the modal approach is that the displacement solution is a combination some characteristic eigenmodes and time-dependent generalized coordinates, this is a linear approach requiring the assumption of small displacements.

The solution to equation of motion is then

$$\mathbf{r}(x,t) = \sum_{n=1}^{N_{mod}} \boldsymbol{\varphi}_i(x)\eta_i(t) = \boldsymbol{\Phi}(x) \cdot \boldsymbol{\eta}(t) \tag{2.7}$$

where $\boldsymbol{\Phi}(x) = [\boldsymbol{\varphi}_1(x) \cdots \boldsymbol{\varphi}_i(x) \cdots \boldsymbol{\varphi}_{N_{mod}}(x)]$ is the eigenmode matrix containing the eigenmodes $\boldsymbol{\varphi_i} = [\phi_{y_i}\ \phi_{z_i}\ \phi_{\theta_i}]^T$ and $\boldsymbol{\eta} = [\eta_1(t) \cdots \eta_i(t) \cdots \eta_{Nmod}(t)]^T$ are the time-dependent generalized coordinates. N_{mod} is the number of eigenmodes chosen to represent the total response.

The eigenmodes, along with the undamped eigenfrequencies – ω_i, are obtained by solving the general eigenvalue problem of structural dynamics

$$(\mathbf{K} - \omega_i^2 \mathbf{M}) \cdot \boldsymbol{\varphi_i} = \mathbf{0} \tag{2.8}$$

By applying the principal of virtual work and introducing the modal representation of the displacement and its derivatives, one can deduce the modal equation of motion given below [5, 6].

$$\tilde{\mathbf{M}} \cdot \ddot{\boldsymbol{\eta}} + \tilde{\mathbf{C}} \cdot \dot{\boldsymbol{\eta}} + \tilde{\mathbf{K}} \cdot \boldsymbol{\eta} = \tilde{\mathbf{Q}} \tag{2.9}$$

where the matrices are given as

$$\tilde{\mathbf{M}} = diag[\tilde{M}_i] \quad , \quad \tilde{M}_i = \int_L \boldsymbol{\varphi}_i^T \cdot \mathbf{M} \cdot \boldsymbol{\varphi}_i \, dx \tag{2.10}$$

$$\tilde{\mathbf{C}} = diag[\tilde{C}_i] \quad , \quad \tilde{C}_i = 2\tilde{M}_i \omega_i \zeta_i \tag{2.11}$$

$$\tilde{\mathbf{K}} = diag[\tilde{K}_i] \quad , \quad \tilde{K}_i = \omega_i^2 \tilde{M}_i \tag{2.12}$$

where ζ_i is the modal damping ratio, which is usually chosen based on experience or given by relevant building regulations.

The modal load-vector is given by

$$\tilde{\mathbf{Q}} = [\tilde{Q}_1\ \cdots\ \tilde{Q}_i\ \cdots\ \tilde{Q}_{N_{mod}}]^T \quad , \quad \tilde{Q}_i = \int_{L_{exp}} \boldsymbol{\varphi}_i \cdot \mathbf{q} \, dx \tag{2.13}$$

Establishing the eigenfrequencies and eigenmodes for a single-span suspension bridge is discussed in ch. 3. The next section will deal with establishing a load vector for the aerodynamic case of wind-loading.

2.2 Wind-load on a line-like structure

2.2.1 Load vector establishment

Wind flow is assumed to consist of a mean time-invariant component in the main flow direction and a fluctuating (turbulence) component in each of the flow directions. The wind flow is defined in its own coordinate system (x_f, y_f, z_f), the components of the flow are defined as $U(x_f, y_f, z_f, t) = V(x_f, y_f, z_f) + u(x_f, y_f, z_f, t)$, $v(x_f, y_f, z_f, t)$ and $w(x_f, y_f, z_f, t)$, where $V(x_f, y_f, z_f)$ is the mean time invariant wind velocity, see fig. 2.1.

Aerodynamic forces acting on a structure are in general split into three parts: drag, lift and aerodynamic moment. The basic assumption is that these forces may be calculated from the instantaneous velocity pressure of the flow-structure system and some load coefficients characteristic for the structure at hand. These load coefficients are usually determined by experimental testing of model sections. Another assumption is that sufficient accuracy is retained if we linearize the turbulence components, this requires the turbulence components to be small compared to V. Structural displacements and rotations are again also assumed small. An instantaneous "snap-shot" of the flow-structure system of a bridge-type structure is shown in the figure below.

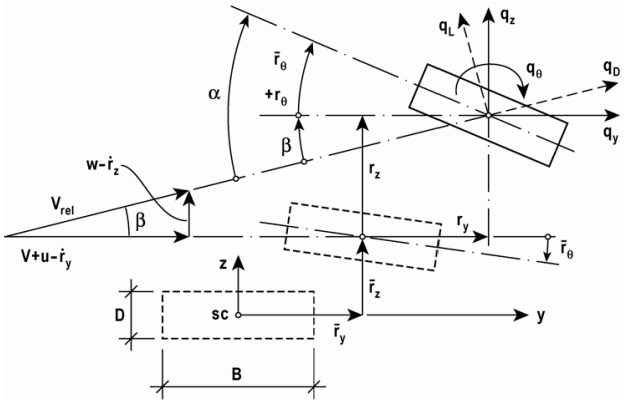

Figure 2.2: Instantaneous velocity pressure on a plate [5].

As the wind flow is split into a mean time-invariant and a fluctuating part, so is the aerodynamic loading of the structure. The mean loading cause the mean displacements $\bar{r}_y(x)$, $\bar{r}_z(x)$ and $\bar{r}_\theta(x)$ and the fluctuating forces causes the structure to oscillate about this position with the displacements $r_y(x,t)$, $r_z(x,t)$ and $r_\theta(x,t)$. In this configuration the instantaneous flow-incidence dependent cross-

sectional drag, lift and moment in the flow axes are defined by

$$\begin{bmatrix} q_D(x,t) \\ q_L(x,t) \\ q_M(x,t) \end{bmatrix} = \frac{1}{2}\rho V_{rel}^2 \cdot \begin{bmatrix} D \cdot C_D(\alpha) \\ B \cdot C_L(\alpha) \\ B^2 \cdot C_M(\alpha) \end{bmatrix} \tag{2.14}$$

where V_{rel} is the relative wind velocity and α is the angle of flow incidence.

In the structural axis system the load is given by

$$\mathbf{q}_{tot}(x,t) = \begin{bmatrix} q_y \\ q_z \\ q_\theta \end{bmatrix}_{tot} = \begin{bmatrix} \cos\beta & -\sin\beta & 0 \\ \sin\beta & \cos\beta & 0 \\ 0 & 0 & 1 \end{bmatrix} \cdot \begin{bmatrix} q_D \\ q_L \\ q_M \end{bmatrix} \tag{2.15}$$

where

$$\beta = \arctan\left(\frac{w - \dot{r}_z}{V + u - \dot{r}_y}\right) \tag{2.16}$$

By assuming that the fluctuating wind flow components $u(x,t)$ and $w(x,t)$ are small compared to V, and that the cross sectional rotations are small, one may linearize to get the following

$$\sin\beta \approx \tan\beta \approx \beta \approx \frac{w - \dot{r}_z}{V + u - \dot{r}_y} \approx \frac{w - \dot{r}_z}{V} \tag{2.17}$$

thus

$$\begin{aligned} V_{rel}^2 &= (V + u - \dot{r}_y)^2 + (w - \dot{r}_z)^2 \approx V^2 + 2Vu - 2V\dot{r}_y \\ \alpha &= \bar{r}_\theta + r_\theta + \beta \approx \bar{r}_\theta + r_\theta + \frac{w}{V} - \frac{\dot{r}_z}{V} \end{aligned} \tag{2.18}$$

The non-linear drag, lift and aerodynamic moment coefficients are also linearized and replaced by

$$\begin{bmatrix} C_D(\alpha) \\ C_L(\alpha) \\ C_M(\alpha) \end{bmatrix} = \begin{bmatrix} \bar{C}_D(\bar{\alpha}) \\ \bar{C}_L(\bar{\alpha}) \\ \bar{C}_M(\bar{\alpha}) \end{bmatrix} + \alpha_f \cdot \begin{bmatrix} C'_D(\bar{\alpha}) \\ C'_L(\bar{\alpha}) \\ C'_M(\bar{\alpha}) \end{bmatrix} \tag{2.19}$$

where $\bar{\alpha}$ and α_f are the mean and fluctuating angle of incidence, and C'_D, C'_L and C'_M are the slopes of the coefficient curves at $\bar{\alpha}$.

From eq. 2.18 it is seen that $\bar{\alpha} = \bar{r}_\theta$ and $\alpha_f = r_\theta + w/V - \dot{r}_z/V$.

Combining the above equations 2.15, 2.18 and 2.19, dropping the use of $(\bar{\alpha})$ for simplicity and discarding higher order terms the following is obtained

$$\begin{bmatrix} q_y \\ q_z \\ q_\theta \end{bmatrix}_{tot} = \rho V \left(\tfrac{V}{2} + u - \dot{r}_y\right) \left\{ \begin{bmatrix} D\bar{C}_D \\ B\bar{C}_L \\ B^2\bar{C}_M \end{bmatrix} + \left(r_\theta + \frac{w}{V} - \frac{\dot{r}_z}{V}\right) \begin{bmatrix} DC'_D \\ BC'_L \\ B^2C'_M \end{bmatrix} + \frac{w - \dot{r}_z}{V} \begin{bmatrix} -B\bar{C}_L \\ D\bar{C}_D \\ 0 \end{bmatrix} \right\} \tag{2.20}$$

which in terms of displacements and wind velocity is

$$\mathbf{q}_{tot}(x,t) = \bar{\mathbf{q}} + \mathbf{B}_q \cdot \mathbf{v} + \mathbf{C}_{ae} \cdot \dot{\mathbf{r}} + \mathbf{K}_{ae} \cdot \mathbf{r} \tag{2.21}$$

where $\mathbf{v}(x,t) = \begin{bmatrix} u & w \end{bmatrix}^T$ and $\mathbf{r}(x,t) = \begin{bmatrix} r_y & r_z & r_\theta \end{bmatrix}^T$ and:

$$\bar{\mathbf{q}} = \frac{\rho V^2 B}{2} \begin{bmatrix} (D/B)\bar{C}_D \\ \bar{C}_L \\ B\bar{C}_M \end{bmatrix} = \frac{\rho V^2 B}{2} \cdot \hat{\mathbf{b}}_q \tag{2.22}$$

$$\mathbf{B}_q(x) = \frac{\rho V^2 B}{2} \begin{bmatrix} 2(D/B)\bar{C}_D & ((D/B)C'_D - \bar{C}_L) \\ 2\bar{C}_L & (C'_L + (D/B)\bar{C}_D) \\ 2\bar{C}_M & BC'_M \end{bmatrix} = \frac{\rho V^2 B}{2} \hat{\mathbf{B}}_q \tag{2.23}$$

$$\mathbf{C}_{ae}(x) = -\frac{\rho V^2 B}{2} \begin{bmatrix} 2(D/B)\bar{C}_D & ((D/B)C'_D - \bar{C}_L) & 0 \\ 2\bar{C}_L & (C'_L + (D/B)\bar{C}_D) & 0 \\ 2\bar{C}_M & BC'_M & 0 \end{bmatrix} \tag{2.24}$$

$$\mathbf{K}_{ae}(x) = \frac{\rho V^2 B}{2} \begin{bmatrix} 0 & 0 & (D/B)C'_D \\ 0 & 0 & C'_L \\ 0 & 0 & BC'_M \end{bmatrix} \tag{2.25}$$

It is apparent that the total loading consists of a mean static part $\bar{\mathbf{q}}(x)$ and a fluctuating part

$$\mathbf{q}(x,t) = \mathbf{B}_q \cdot \mathbf{v} + \mathbf{C}_{ae} \cdot \dot{\mathbf{r}} + \mathbf{K}_{ae} \cdot \mathbf{r} \tag{2.26}$$

where $\mathbf{B}_q \cdot \mathbf{v}$ is the dynamic loading associated with turbulence in the oncoming flow, and $\mathbf{C}_{ae} \cdot \dot{\mathbf{r}}$ and $\mathbf{K}_{ae} \cdot \mathbf{r}$ are the motion induced loading. $\mathbf{C}_{ae}$ and $\mathbf{K}_{ae}$ are called the aerodynamic damping and stiffness. Note that the aerodynamic mass $\mathbf{M}_{ae}$ is most often considered negligible in wind engineering [4] and is therefore not included. Since this expression is linear, the theory is applicable in both time and frequency domain.

2.2.2 Aerodynamic derivatives

Frequency domain versions of $\mathbf{C}_{ae}$ and $\mathbf{K}_{ae}$ are given by

$$\mathbf{C}_{ae} = \begin{bmatrix} P_1 & P_5 & P_2 \\ H_5 & H_1 & H_2 \\ A_5 & A_1 & A_2 \end{bmatrix} \quad \text{and} \quad \mathbf{K}_{ae} = \begin{bmatrix} P_4 & P_6 & P_3 \\ H_6 & H_4 & H_3 \\ A_6 & A_4 & A_3 \end{bmatrix} \tag{2.27}$$

where the coefficients are functions of the frequency of motion, the mean wind velocity and the shape of the cross section. These coefficients may be determined from wind tunnel testing, generally in three different approaches, see [4]. It has been considered convenient to normalize the coefficients further, so as

$$\mathbf{C}_{ae} = \frac{\rho B^2}{2} \cdot \omega_i(V) \cdot \hat{\mathbf{C}}_{ae} \quad \text{and} \quad \mathbf{K}_{ae} = \frac{\rho B^2}{2} \cdot [\omega_i(V)]^2 \cdot \hat{\mathbf{K}}_{ae} \tag{2.28}$$

where $\omega_i(V)$ is the mean wind velocity dependent resonance frequency of eigenmode i and the reduced matrices are given as

$$\hat{\mathbf{C}}_{ae} = \begin{bmatrix} P_1^* & P_5^* & BP_2^* \\ H_5^* & H_1^* & BH_2^* \\ BA_5^* & BA_1^* & B^2A_2^* \end{bmatrix} \quad \text{and} \quad \hat{\mathbf{K}}_{ae} = \begin{bmatrix} P_4^* & P_6^* & BP_3^* \\ H_6^* & H_4^* & BH_3^* \\ BA_6^* & BA_4^* & B^2A_3^* \end{bmatrix} \tag{2.29}$$

These non-dimensional coefficients P_k^*, H_k^*, A_k^* $k = 1 - 6$ are what are called the aerodynamic derivatives, and are given in eq. 2.30.

$$\begin{bmatrix} P_1^* & H_1^* & A_1^* \\ P_2^* & H_2^* & A_2^* \\ P_3^* & H_3^* & A_3^* \\ P_4^* & H_4^* & A_4^* \\ P_5^* & H_5^* & A_5^* \\ P_6^* & H_6^* & A_6^* \end{bmatrix} = \begin{bmatrix} -2\bar{C}_D \frac{D}{B} \hat{V}_i & -\left(C'_L + \bar{C}_D \frac{D}{B}\right) \hat{V}_i & -C'_M \hat{V}_i \\ 0 & 0 & 0 \\ C'_D \frac{D}{B} \hat{V}_i^2 & C'_L \hat{V}_i^2 & C'_M \hat{V}_i^2 \\ 0 & 0 & 0 \\ \left(\bar{C}_L - C'_D \frac{D}{B}\right) \hat{V}_i & -2\bar{C}_L \hat{V}_i & -2\bar{C}_M \hat{V}_i \\ 0 & 0 & 0 \end{bmatrix} \tag{2.30}$$

where $\hat{V}_i = \frac{V}{B\omega_i(V)}$ is the reduced velocity, which is dependent on the in-wind resonance frequency $\omega_i(V)$. This dependency causes the need for some kind of iteration scheme when solving dynamics problems including these coefficients.

2.3 Aerodynamic stability

2.3.1 Impedance matrix

To find any aerodynamic stability limits one must first look at solving the equation of motion as discussed in sec. 2.1 with the load-vector being that of wind-load, as discussed in the previous section.

$$\mathbf{M}_0 \cdot \ddot{\mathbf{r}}_{tot}(x,t) + \mathbf{C}_0 \cdot \dot{\mathbf{r}}_{tot}(x,t) + \mathbf{K}_0 \cdot \mathbf{r}_{tot}(x,t) = \mathbf{q}_{tot}(x,t) \tag{2.31}$$

where the subscript "0" indicates that this is the property of the structure in still air ($V = 0$) and

$$\mathbf{r}_{tot}(x,t) = \bar{\mathbf{r}}(x) + \mathbf{r}(x,t) \quad \text{and} \quad \mathbf{q}_{tot}(x,t) = \bar{\mathbf{q}}(x) + \mathbf{q}(x,t) \tag{2.32}$$

As is seen the total displacement and wind load both comprise a mean time-invariant static part and a dynamic part. Computing the static part is considered trivial, so moving forward only the dynamic part will be the focus, thus

$$\mathbf{M}_0 \cdot \ddot{\mathbf{r}}(x,t) + \mathbf{C}_0 \cdot \dot{\mathbf{r}}(x,t) + \mathbf{K}_0 \cdot \mathbf{r}(x,t) = \mathbf{q}(x,t) \tag{2.33}$$

By substituting eq. 2.26 into the equation above yields

$$\mathbf{M}_0 \cdot \ddot{\mathbf{r}}(x,t) + \mathbf{C}_0 \cdot \dot{\mathbf{r}}(x,t) + \mathbf{K}_0 \cdot \mathbf{r}(x,t) = \mathbf{B}_q \cdot \mathbf{v} + \mathbf{C}_{ae} \cdot \dot{\mathbf{r}} + \mathbf{K}_{ae} \cdot \mathbf{r} \tag{2.34}$$

which by introducing the modal displacement $\mathbf{r}(x,t) = \boldsymbol{\Phi} \cdot \boldsymbol{\eta}$ and employing the principal of virtual work as discussed earlier, the modal equilibrium is obtained

$$\tilde{\mathbf{M}}_0 \cdot \ddot{\boldsymbol{\eta}}(t) + \tilde{\mathbf{C}}_0 \cdot \dot{\boldsymbol{\eta}}(t) + \tilde{\mathbf{K}}_0 \cdot \boldsymbol{\eta}(t) = \tilde{\mathbf{Q}}(x,t) + \tilde{\mathbf{C}}_{ae} \cdot \dot{\boldsymbol{\eta}}(t) + \tilde{\mathbf{K}}_{ae} \cdot \boldsymbol{\eta}(t) \tag{2.35}$$

where $\tilde{\mathbf{M}}_0$, $\tilde{\mathbf{C}}_0$ and $\tilde{\mathbf{K}}_0$ are given in eq. 2.9-2.11, and $\tilde{\mathbf{C}}_{ae}$ and $\tilde{\mathbf{K}}_{ae}$ are N_{mod} by N_{mod} matrices whose elements are given by

$$\tilde{C}_{ae_{ij}} = \int_{L_{exp}} \boldsymbol{\varphi}_i^T \cdot \mathbf{C}_{ae} \cdot \boldsymbol{\varphi}_j \, dx \tag{2.36}$$

and

$$\tilde{K}_{ae_{ij}} = \int_{L_{exp}} \boldsymbol{\varphi}_i^T \cdot \mathbf{K}_{ae} \cdot \boldsymbol{\varphi}_j \, dx \tag{2.37}$$

where the elements of $\mathbf{C}_{ae}$ and $\mathbf{K}_{ae}$ are given in sec. 2.2.2. And finally:

$$\tilde{Q}_i = \int_{L_{exp}} \boldsymbol{\varphi}_i^T \cdot \mathbf{B}_q \cdot \mathbf{v} \, dx \tag{2.38}$$

By moving $\tilde{\mathbf{C}}_{ae}$ and $\tilde{\mathbf{K}}_{ae}$ to the left hand side of eq. 2.35 and transitioning to the frequency domain by taking the Fourier transform of either side, we obtain

$$[-\tilde{\mathbf{M}}_0\omega^2 + (\tilde{\mathbf{C}}_0 - \tilde{\mathbf{C}}_{ae})i\omega + (\tilde{\mathbf{K}}_0 - \tilde{\mathbf{K}}_{ae})] \cdot \mathbf{a}_\eta(\omega) = \mathbf{a}_{\tilde{Q}}(\omega) \tag{2.39}$$

where

$$\begin{aligned} \mathbf{a}_\eta &= [a_{\eta_1} \cdots a_{\eta_i} \cdots a_{\eta_N}]^T \\ \mathbf{a}_{\tilde{Q}} &= [a_{\tilde{Q}_1} \cdots a_{\tilde{Q}_i} \cdots a_{\tilde{Q}_N}]^T \end{aligned} \tag{2.40}$$

are the Fourier amplitudes of the N number of frequencies included.

By premultiplying eq. 2.39 by $\tilde{\mathbf{K}}_0^{-1}$ the following is obtained

$$\hat{\mathbf{H}}_\eta^{-1} \cdot \mathbf{a}_\eta(\omega) = \mathbf{a}_{\hat{Q}}(\omega) \tag{2.41}$$

where $\hat{\mathbf{H}}_\eta$ is the non-dimensional frequency-response-matrix and $\mathbf{a}_{\hat{Q}}(\omega)$ is the reduced modal load vector.

$$\mathbf{a}_{\hat{Q}}(\omega) = \tilde{\mathbf{K}}_0^{-1} \cdot \mathbf{a}_{\tilde{Q}}(\omega) \tag{2.42}$$

$$\hat{\mathbf{H}}_\eta(\omega, V) = \left\{ \mathbf{I} - \boldsymbol{\kappa}_{ae} - \left(\omega \cdot diag\left[\frac{1}{\omega_i}\right] \right)^2 + 2i\omega \cdot diag\left[\frac{1}{\omega_i}\right] \cdot (\boldsymbol{\zeta} - \boldsymbol{\zeta}_{ae}) \right\}^{-1} \tag{2.43}$$

where $\mathbf{I}$ is the N_{mod} by N_{mod} identity matrix and

$$\left.\begin{aligned} \boldsymbol{\kappa}_{ae} &= \tilde{\mathbf{K}}_0^{-1} \cdot \tilde{\mathbf{K}}_{ae} \\ \boldsymbol{\zeta} &= diag[\zeta_i] \\ \boldsymbol{\zeta}_{ae} &= \frac{1}{2} \cdot diag[\omega_i] \cdot \left(\tilde{\mathbf{K}}_0^{-1} \cdot \tilde{\mathbf{C}}_{ae} \right) \end{aligned}\right\} \tag{2.44}$$

The inverse of the frequency-response matrix is called the impedance matrix and denoted $\hat{\mathbf{E}}_\eta(\omega, V)$. When this matrix approaches singularity, i.e. absolute value of the determinant goes to zero, the frequency-response matrix and thus the displacement response approaches infinity thereby marking a stability limit. Note that as the turbulence components are contained in $\mathbf{a}_{\hat{Q}}$, it is the mean wind velocity V which is critical to loss of stability.

The structure approaches these stability limits as the properties of the combined flow-structure system are greatly altered by motion-induced effects at high flow velocities, specifically $\boldsymbol{\zeta}_{ae}$ affects the system's damping and $\boldsymbol{\kappa}_{ae}$ affects the system's stiffness.

These stability limits may be found by finding the critical mean wind velocities $V = V_{cr}$ at which there is a mean wind velocity dependent resonance frequency $\omega_i(V) = \omega_r$, associated with mode i, such that

$$|\det(\hat{\mathbf{E}}_\eta(\omega_r, V_{cr}))| = 0 \tag{2.45}$$

Since $\hat{\mathbf{E}}_\eta(\omega, V)$ contains complex quantities, we may split the determinant into a real and an imaginary part which must both be zero simultaneously at a stability limit:

$$\mathrm{Re}(\det(\hat{\mathbf{E}}_\eta)) = 0 \quad \text{and} \quad \mathrm{Im}(\det(\hat{\mathbf{E}}_\eta)) = 0 \tag{2.46}$$

The roots will contain both a V_{cr} and an ω_r and by inspecting these values the type of stability problem may be identified. In bridge engineering there are four types of motion-induced stability problems: a static stability limit in torsion called static divergence, a dynamic stability limit of vertical movement called galloping, a dynamic stability limit in torsion, and flutter - which is a stability limit of combined vertical and torsional movement [4].

These stability limits are thus associated with the displacements $r_z(x,t)$ and $r_\theta(x,t)$. Finding these limits may then be done by identifying two low frequency mode-shapes, $\boldsymbol{\varphi}_1$ and $\boldsymbol{\varphi}_2$, which are highly influential to the total response. One of them with a predominant ϕ_z component and the other with a predominant ϕ_θ component. For the case of two modes as described above

$$\boldsymbol{\varphi}_1 \approx [0 \ \phi_z \ 0]^T \quad \text{and} \quad \boldsymbol{\varphi}_2 \approx [0 \ 0 \ \phi_\theta]^T \tag{2.47}$$

with corresponding eigenfrequencies $\omega_1 = \omega_z$ and $\omega_2 = \omega_\theta$ and damping ratios $\zeta_1 = \zeta_z$ and $\zeta_2 = \zeta_\theta$, the impedance matrix becomes:

$$\hat{\mathbf{E}}_\eta(\omega_r, V_{cr}) = \left\{ \begin{bmatrix} 1 & 0 \\ 0 & 1 \end{bmatrix} - \begin{bmatrix} \kappa_{ae_{zz}} & \kappa_{ae_{z\theta}} \\ \kappa_{ae_{\theta z}} & \kappa_{ae_{\theta\theta}} \end{bmatrix} - \begin{bmatrix} (\omega_r/\omega_z)^2 & 0 \\ 0 & (\omega_r/\omega_\theta)^2 \end{bmatrix} + 2i \begin{bmatrix} \omega_r/\omega_z & 0 \\ 0 & \omega_r/\omega_\theta \end{bmatrix} \cdot \begin{bmatrix} \zeta_z - \zeta_{ae_{zz}} & -\zeta_{ae_{z\theta}} \\ -\zeta_{ae_{\theta z}} & \zeta_\theta - \zeta_{ae_{\theta\theta}} \end{bmatrix} \right\} \tag{2.48}$$

and

$$\kappa_{ae_{zz}} = \frac{\rho B^2}{2\tilde{m}_z} \left(\frac{\omega_z(V)}{\omega_z} \right)^2 H_4^* \frac{\int_L^{L_{exp}} \phi_z^2 \, dx}{\int_L \phi_z^2 \, dx} \quad \kappa_{ae_{z\theta}} = \frac{\rho B^3}{2\tilde{m}_z} \left(\frac{\omega_z(V)}{\omega_z} \right)^2 H_3^* \frac{\int_L^{L_{exp}} \phi_z \phi_\theta \, dx}{\int_L \phi_z^2 \, dx} \tag{2.49}$$

$$\kappa_{ae_{\theta z}} = \frac{\rho B^3}{2\tilde{m}_\theta} \left(\frac{\omega_\theta(V)}{\omega_\theta} \right)^2 A_4^* \frac{\int_L^{L_{exp}} \phi_\theta \phi_z \, dx}{\int_L \phi_\theta^2 \, dx} \quad \kappa_{ae_{\theta\theta}} = \frac{\rho B^4}{2\tilde{m}_\theta} \left(\frac{\omega_\theta(V)}{\omega_\theta} \right)^2 A_3^* \frac{\int_L^{L_{exp}} \phi_\theta^2 \, dx}{\int_L \phi_\theta^2 \, dx} \tag{2.50}$$

$$\zeta_{ae_{zz}} = \frac{\rho B^2}{4\tilde{m}_z} \frac{\omega_z(V)}{\omega_z} H_1^* \frac{\int_L^{L_{exp}} \phi_z^2 \, dx}{\int_L \phi_z^2 \, dx} \quad \zeta_{ae_{z\theta}} = \frac{\rho B^3}{4\tilde{m}_z} \frac{\omega_z(V)}{\omega_z} H_2^* \frac{\int_L^{L_{exp}} \phi_z \phi_\theta \, dx}{\int_L \phi_z^2 \, dx} \tag{2.51}$$

$$\zeta_{ae_{\theta z}} = \frac{\rho B^3}{4\tilde{m}_\theta} \frac{\omega_\theta(V)}{\omega_\theta} A_2^* \frac{\int_L^{L_{exp}} \phi_\theta \phi_z \, dx}{\int_L \phi_\theta^2 \, dx} \quad \zeta_{ae_{\theta\theta}} = \frac{\rho B^4}{4\tilde{m}_\theta} \frac{\omega_\theta(V)}{\omega_\theta} A_1^* \frac{\int_L^{L_{exp}} \phi_\theta^2 \, dx}{\int_L \phi_\theta^2 \, dx} \tag{2.52}$$

where $\tilde{m}_z$ and $\tilde{m}_\theta$ are the modally distributed masses, which in the case of constant m_z and m_θ along the length of the bridge, then $\tilde{m}_z = m_z$ and $\tilde{m}_\theta = m_\theta$. Also, ρ is the density of air, B is the width of the cross section and H_k, A_k are the aerodynamic derivatives as described in sec. 2.2.2.

2.3.2 Static divergence

Static divergence is a stability limit involving loss of torsional stiffness at an in-wind resonance frequency $\omega_r = 0$, i.e. the instability is static and not dynamic. Assuming a torsional mode of the type given in eq. 2.47, $\boldsymbol{\varphi}_2 \approx [0\ 0\ \phi_\theta]^T$, the impedance matrix reduces to:

$$\hat{E}_\eta(\omega_r = 0, V_{cr}) = 1 - \kappa_{ae_{\theta\theta}} \tag{2.53}$$

where $\kappa_{ae_{\theta\theta}}$ is given in eq. 2.50. Since this is a static type of instability the quasi-static version of the aerodynamic derivative involved may be used, here A_3^* may be replaced with $C'_M \hat{V}^2$ rendering the expression for the critical mean wind velocity for static divergence:

$$V_{cr} = B \cdot \omega_\theta \cdot \left(\frac{2\tilde{m}_\theta}{\rho B^4 C'_M} \cdot \frac{\int\limits_L \phi_\theta^2 \, dx}{\int\limits_{L_{exp}} \phi_\theta^2 \, dx} \right)^{1/2} \tag{2.54}$$

we see from eq. 2.54 above that the lowest V_{cr} will occur for the torsional mode with the lowest eigenfrequency ω_θ.

2.3.3 Galloping

Galloping is a dynamic stability limit involving vertical motion. Let $\boldsymbol{\varphi}_1 \approx [0\ \phi_z\ 0]^T$ be the lowest frequency vertical mode. The in-wind resonance frequency associated with this mode is $\omega_z(V)$, thus:

$$\omega_r = \omega_z(V_{cr}) \tag{2.55}$$

and the impedance matrix reduces to

$$\hat{E}_\eta(\omega_r, V_{cr}) = 1 - \kappa_{ae_{zz}} - (\omega_r/\omega_z)^2 + 2i(\zeta_z - \zeta_{ae_{zz}}) \cdot (\omega_r/\omega_z) \tag{2.56}$$

where κ_{aezz} and $\zeta_{ae_{zz}}$ are given in eq. 2.49 and eq. 2.51.

Setting the real and imaginary parts of eq. 2.56 equal to zero, a dynamic stability limit may be identify at an in-wind resonance frequency:

$$\omega_r = \omega_z \left(1 + \frac{\rho B^2}{2\tilde{m}_z} \cdot H_4^* \cdot \frac{\int\limits_{L_{exp}} \phi_z^2 \, dx}{\int\limits_L \phi_z^2 \, dx} \right)^{-1/2} \tag{2.57}$$

where at the same time the damping properties are:

$$\zeta_z = \zeta_{ae_{zz}} = \frac{\rho B^2}{4\tilde{m}_z}\frac{\omega_r}{\omega_z}H_1^*\frac{\int_{L_{exp}} \phi_z^2\,dx}{\int_L \phi_z^2\,dx} \tag{2.58}$$

It is evident by eq. 2.58 that H_1^* must attain positive values in order for the existence of a galloping stability limit.

2.3.4 Dynamic stability limit in torsion

The dynamic stability limit in torsion is the torsional equivalent to galloping. Let $\boldsymbol{\varphi}_2 \approx [0\ 0\ \phi_\theta]^T$ be the lowest frequency torsional mode, then the resonance frequency associated with this mode is given by $\omega_\theta(V)$ and thus:

$$\omega_r = \omega_\theta(V_{cr}) \tag{2.59}$$

The impedance matrix reduces to

$$\hat{E}_\eta(\omega_r, V_{cr}) = 1 - \kappa_{ae_{\theta\theta}} - (\omega_r/\omega_\theta)^2 + 2i(\zeta_\theta - \zeta_{ae_{\theta\theta}})\cdot(\omega_r/\omega_\theta) \tag{2.60}$$

where $\kappa_{ae_{\theta\theta}}$ and $\zeta_{ae_{\theta\theta}}$ are given in eq. 2.50 and 2.52. Setting the real and imaginary parts of eq. 2.60, a stability limit in torsion may be identified at an in-wind resonance frequency:

$$\omega_r = \omega_\theta \cdot \left(1 + \frac{\rho B^4}{2\tilde{m}_\theta}\cdot A_3^* \cdot \frac{\int_{L_{exp}} \phi_\theta^2\,dx}{\int_L \phi_\theta^2\,dx}\right)^{-1/2} \tag{2.61}$$

where at the same time the damping properties are:

$$\zeta_\theta = \zeta_{ae_{\theta\theta}} = \frac{\rho B^4}{4\tilde{m}_\theta}\frac{\omega_r}{\omega_\theta}A_2^*\frac{\int_{L_{exp}} \phi_\theta^2\,dx}{\int_L \phi_\theta^2\,dx} \tag{2.62}$$

It is seen from eq. 2.62 that any dynamic stability limit in torsion require A_2^* to attain positive values.

2.3.5 Flutter

The phenomenon known as flutter is an instability caused by coupling between vertical and torsional oscillations, r_z and r_θ. Mathematically this happens through the off-diagonal terms in the impedance matrix $\kappa_{ae_{z\theta}}$ and $\kappa_{ae_{\theta z}}$ and therefore requires shape-wise similar modes $\boldsymbol{\varphi}_1$ and $\boldsymbol{\varphi}_2$ as is evident by eq. 2.49-2.50.

For two-modes, one predominantly being vertical and one predominantly being torsional (as described in sec. 2.3.1), the flutter stability limit, because of coupling between r_z and r_θ, is identified by the case where $|\det(\hat{\mathbf{E}}_\eta(\omega_r, V_{cr})| = 0$ for a joint resonance frequency

$$\omega_r = \omega_z(V_{cr}) = \omega_\theta(V_{cr}) \tag{2.63}$$

A solution scheme to this two-mode flutter problem, as described in both [4] and [7], is given below.

Assuming that $L_{exp} = L$, and introducing the following notation:

$$\beta_z = \frac{\rho B^2}{\tilde{m}_z} \quad \beta_\theta = \frac{\rho B^4}{\tilde{m}_\theta} \tag{2.64}$$

$$\gamma = \frac{\omega_\theta}{\omega_z} \quad \hat{\omega}_r = \frac{\omega_r}{\omega_\theta} \tag{2.65}$$

$$\psi_z = \frac{\int\limits_L \phi_z \phi_\theta \, dx}{\int\limits_L \phi_z^2 \, dx} \quad \psi_\theta = \frac{\int\limits_L \phi_\theta \phi_z \, dx}{\int\limits_L \phi_\theta^2 \, dx} \tag{2.66}$$

Then the fully expanded real and imaginary parts of the determinant of $\hat{\mathbf{E}}_\eta$ may be written

$$\mathrm{Re}(\det(\hat{\mathbf{E}}_\eta)) = R_0 + R_2\hat{\omega}_r^2 + R_3\hat{\omega}_r^3 + R_4\hat{\omega}_r^4 = 0 \tag{2.67}$$

and

$$\mathrm{Im}(\det(\hat{\mathbf{E}}_\eta)) = I_0 + I_1\hat{\omega}_r + I_2\hat{\omega}_r^2 + I_3\hat{\omega}_r^3 \tag{2.68}$$

where

$$R_0 = 1$$

$$R_2 = -\left(1 + \gamma^2 + 4\zeta_z\zeta_\theta + \frac{\beta_z}{2}\gamma^2 H_4^* + \frac{\beta_\theta}{2}A_3^*\right)$$

$$R_3 = \gamma\left(\zeta_\theta\beta_z\gamma H_1^* + \zeta_z\beta_\theta A_2^*\right)$$

$$R_4 = \gamma^2\left[1 + \frac{\beta_z}{2}H_4^* + \frac{\beta_\theta}{2}A_3^* + \frac{\beta_z\beta_\theta}{4}(A_1^*H_2^*\psi_z\psi_\theta - A_2^*H_1^* + A_3^*H_4^* - A_4^*H_3^*\psi_z\psi_\theta)\right] \tag{2.69}$$

and where

$$I_0 = 2(\zeta_z\gamma + \zeta_\theta)$$

$$I_1 = -\frac{1}{2}(\beta_z\gamma^2 H_1^* + \beta_\theta A_2^*)$$

$$I_2 = -2\left[\zeta_z\left(\frac{\beta_\theta}{2}A_3^* + \gamma\right) + \zeta_\theta\gamma^2\left(\frac{\beta_z}{2}H_4^* + 1\right)\right]$$

$$I_3 = \gamma^2\left[\frac{\beta_z\beta_\theta}{4}(H_1^*A_3^* - H_2^*A_4^*\psi_z\psi_\theta - H_3^*A_1^*\psi_z\psi_\theta + H_4^*A_2^*) + \frac{1}{4}(\beta_z H_1^* + \beta_\theta A_2^*)\right] \tag{2.70}$$

The scheme here is to find roots of the real and imaginary parts for increasing values of $\hat{V} = V/(B\cdot\omega_r)$ until a common root $\hat{\omega}_r$ is found simultaneously, remembering to update the aerodynamic derivatives at each step as they are functions of $\hat{V}$. This may be done in a graphical manner, where the roots of the real and imaginary parts are plotted for increasing $\hat{V}$, and a solution is found at a point where their lines intersect. The resonance frequency is then given by $\omega_r = \hat{\omega}_r\cdot\omega_\theta$ and the critical wind velocity is given as $V_{cr} = \hat{V}\cdot B\cdot\omega_r$.

The flutter coupling is more prone to occur for shape-wise similar modes, this is because ψ_z and ψ_θ are the coupling terms and shape-wise similarity implies $\psi_z = \psi_\theta \approx 1$.

2.4 Buffeting response

2.4.1 Stochastic wind-load

The buffeting response of a structure is the response caused by forces of turbulence in the oncoming wind flow in addition to forces induced by the interaction between the flow and the oscillating body itself. The turbulence parts or fluctuating parts of the wind flow are usually seen as stochastic processes with statistical properties. The solutions which may be obtained for such processes are consequently also statistical. An illustration of the wind-flow, structural load and structural response in the time domain, and their frequency domain counterparts are shown in fig. 2.3.

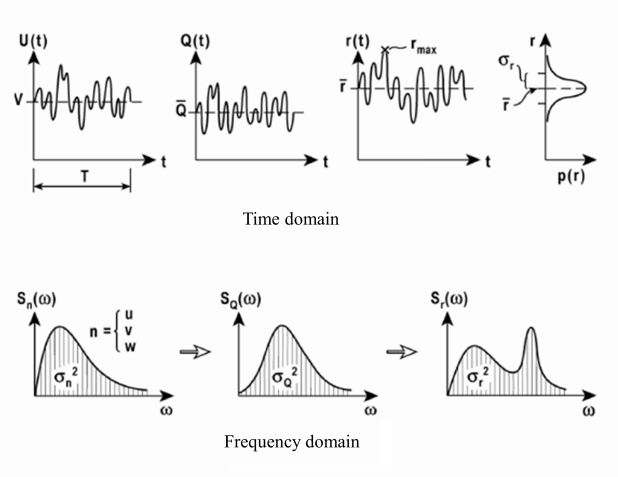

Figure 2.3: Time and frequency domain representation of load and response [4].

Where $S_n(\omega)$ is the fluctuating wind-flow spectrum for turbulence component $n = u(x,t),\ v(x,t)$ or $w(x,t)$, $S_Q(\omega)$ is the wind-load spectrum, and $S_r(\omega)$ is the response spectrum.

The transfer from a load spectrum to a response spectrum is via a frequency-response function $H(\omega)$ which was found for the modal case in sec. 2.3.1. The transfer from wind-*flow* spectrum to the wind-*load* spectrum is via the theory discussed in sec 2.2.1. These steps to arrive at the response spectrum is shown in the next section. When the response spectrum has been determined, the variance

of response r_i at position x_r is given as [4]

$$\sigma_{r_i}^2 = \int_0^\infty S_{r_i}(x_r, \omega)\, d\omega \tag{2.71}$$

A typical response variation with mean wind velocity was shown in fig. 1.1 in ch. 1.

When the variance is determined, the maximum response at a location may be computed by combining the static response and the standard deviation of the dynamic response multiplied by a peak factor k_p.

$$r_{max}(x_r) = \bar{r}_{max} + k_p \cdot \sigma_r(x_r) \tag{2.72}$$

For a narrow banded process the peak factor is approximately $k_p \approx \sqrt{2}$ [4].

A stochastic description of the wind flow turbulence components is required to calculate $S_q(\omega)$. An expression for the reduced auto spectral density of fluctuating wind flow components as proposed by Kaimal et. al. [8] is given by

$$\frac{f \cdot S_n(f)}{\sigma_n^2} = \frac{A_n \cdot \hat{f}}{(1 + 1.5 \cdot A_n \cdot \hat{f})^{5/3}} \quad n = u, v, w \tag{2.73}$$

where f is the frequency in Hz and $\hat{f} = f \cdot {}^{x_f}L_n/V$ where ${}^{x_f}L_n$ is the integral length scale of the relevant turbulence component, and V is the mean wind velocity.

Also employed in wind engineering is the so-called normalized co-spectrum given by

$$\hat{Co}_{nn}(\Delta s, f) = exp\left(-C_{ns} \cdot \frac{f \cdot \Delta s}{V}\right) \tag{2.74}$$

where $n = u, v, w,\ s = x_f, y_f, z_f$ and $\Delta s = \Delta x_f, \Delta y_f, \Delta z_f$.

As angular frequency – ω is preferred in this thesis, the transition is done using

$$S_n(f) = 2\pi \cdot S_n(\omega) \quad \text{and} \quad f = \frac{\omega}{2\pi} \tag{2.75}$$

Another parameter used in wind engineering is the turbulence intensity factor, defined as

$$I_n = \frac{\sigma_n}{V} \tag{2.76}$$

The subsequent steps to arrive at $S_r(\omega)$ is shown in the next section.

2.4.2 Response calculation

The following elaboration of the response spectrum assumes a general multi-modal approach, which allows modal coupling to occur and does not require modal eigenfrequencies to be well separated.

The general solution to the multi-modal approach is the three by three response variance matrix shown in the equation below.

$$\mathbf{Cov}_{rr}(x_r) = \begin{bmatrix} \sigma^2_{r_y r_y} & Cov_{r_y r_z} & Cov_{r_y r_\theta} \\ Cov_{r_z r_y} & \sigma^2_{r_z r_z} & Cov_{r_z r_\theta} \\ Cov_{r_\theta r_y} & Cov_{r_\theta r_z} & \sigma^2_{r_\theta r_\theta} \end{bmatrix} \tag{2.77}$$

This matrix is obtained by frequency domain integration as discussed in the previous section, the multi-mode equivalent to eq. 2.71 is given as [4]

$$\mathbf{Cov}_{rr}(x_r) = \int_0^\infty \mathbf{S}_{rr}(x_r, \omega)\, d\omega = \Phi_r(x_r) \left[\int_0^\infty \hat{\mathbf{H}}^*_\eta(\omega) \mathbf{S}_{\hat{Q}}(\omega) \hat{\mathbf{H}}^T_\eta(\omega)\, d\omega \right] \Phi^T(x_r) \tag{2.78}$$

where $\hat{\mathbf{H}}_\eta(\omega)$ and $\mathbf{S}_{\hat{Q}}$ are N_{mod} by N_{mod} matrices and $\Phi(x_r)$ is the three by N_{mod} mode matrix discussed in sec. 2.3.4 computed at the response location x_r. $\hat{\mathbf{H}}_\eta(\omega)$ is the frequency response matrix given by eq. 2.43 and includes the motion induced aerodynamic stiffness and damping, $\boldsymbol{\kappa}_{ae}$ and $\boldsymbol{\zeta}_{ae}$ given by eq. 2.44.

The matrix $\mathbf{S}_{\hat{Q}}(\omega)$ is what is called the normalized modal load matrix and is given by the definition of spectra as expressed by the Fourier amplitudes from the right hand side of eq. 2.41, i.e.

$$\mathbf{S}_{\hat{Q}}(\omega) = \lim_{T\to\infty} \frac{1}{\pi T} (\mathbf{a}^*_{\hat{Q}}(\omega) \cdot \mathbf{a}^T_{\hat{Q}}(\omega)) \tag{2.79}$$

Remembering that $\mathbf{a}_{\hat{Q}} = \tilde{\mathbf{K}}_0^{-1} \cdot \mathbf{a}_{\tilde{Q}}$ where $\mathbf{a}_{\tilde{Q}}$ is the Fourier amplitudes of the modal load vector $\tilde{\mathbf{Q}}(t)$, which by combining eq. 2.23 and 2.38 is given by

$$\tilde{Q}_i = \frac{\rho V^2 B}{2} \cdot \int_{L_{exp}} \boldsymbol{\varphi}_i^T \cdot \hat{\mathbf{B}}_q \cdot \mathbf{v}\, dx \tag{2.80}$$

The Fourier transform of this equation yields

$$a_{\tilde{Q}_i} = \frac{\rho V^2 B}{2} \cdot \int_{L_{exp}} \boldsymbol{\varphi}_i^T \cdot \hat{\mathbf{B}}_q \cdot \mathbf{a}_\upsilon \, dx \tag{2.81}$$

where $\mathbf{a}_\upsilon = [a_u \; a_w]^T$ contains the Fourier amplitudes of the u and w turbulence components. It may be shown then that the elements of the $\mathbf{S}_{\hat{Q}}(\omega)$ is given by

$$S_{\hat{Q}_i\hat{Q}_j}(\omega) = \frac{\rho B^3}{2\tilde{m}_i} \cdot \frac{\rho B^3}{2\tilde{m}_j} \cdot \left(\frac{V}{B\omega_i}\right)^2 \cdot \left(\frac{V}{B\omega_j}\right)^2 \cdot \hat{J}_{ij}^2 \tag{2.82}$$

where $\hat{J}_{ij}^2$ is the so-called joint acceptance function given by

$$\hat{J}_{ij}^2 = \frac{\int_{L_{exp}}\int \boldsymbol{\varphi}_i^T(x_1) \cdot \left\{\hat{\mathbf{B}}_q \cdot \left[\mathbf{I}_\upsilon^2 \cdot \hat{\mathbf{S}}_\upsilon(\Delta x, \omega)\right] \cdot \hat{\mathbf{B}}_q^T\right\} \cdot \boldsymbol{\varphi}_j(x_2) \, dx_1 dx_2}{\left(\int_{L_{exp}} \boldsymbol{\varphi}_i^T \cdot \boldsymbol{\varphi}_i \, dx\right) \cdot \left(\int_{L_{exp}} \boldsymbol{\varphi}_j^T \cdot \boldsymbol{\varphi}_j \, dx\right)} \tag{2.83}$$

where

$$\mathbf{I}_\upsilon = diag[I_u \;\; I_w] \tag{2.84}$$

and

$$\hat{\mathbf{S}}_\upsilon = diag[S_{uu}/\sigma_u^2 \;\; S_{ww}/\sigma_w^2] \tag{2.85}$$

It is in the above equation assumed that the cross spectra between flow components is negligible, that is to say $S_{uw} = S_{wu} \approx 0$. A response solution will require $N_{mod} \cdot N_{mod}$ joint acceptance functions.

For two modes, one predominantly vertical and one predominantly torsional, as was employed in sec. 2.3, i.e

$$\boldsymbol{\varphi}_1 \approx [0 \; \phi_z \; 0]^T \quad \text{and} \quad \boldsymbol{\varphi}_2 \approx [0 \; 0 \; \phi_\theta]^T \tag{2.86}$$

the joint acceptance functions become

$$\hat{J}_{zz}^2 = \iint_{L_{exp}} \phi_z(x_1)\phi_z(x_2) \left[(2\bar{C}_L)^2 I_u^2 \hat{S}_{uu} + \left(C_L' + \frac{D}{B}\bar{C}_D\right)^2 I_w^2 \hat{S}_{ww}\right] dx_1 dx_2 \tag{2.87}$$

$$\hat{J}^2_{z\theta} = \iint\limits_{L_{exp}} \phi_z(x_1)\phi_\theta(x_2) \left[4\bar{C}_L B \bar{C}_M I_u^2 \hat{S}_{uu} + \left(C'_L + \frac{D}{B}\bar{C}_D \right) B C'_M I_w^2 \hat{S}_{ww} \right] dx_1 dx_2 \tag{2.88}$$

$$\hat{J}^2_{\theta\theta} = \iint\limits_{L_{exp}} \phi_\theta(x_1)\phi_\theta(x_2) \left[(2B\bar{C}_M)^2 I_u^2 \hat{S}_{uu} + (BC'_M)^2 I_w^2 \hat{S}_{ww} \right] dx_1 dx_2 \tag{2.89}$$

where the reduced cross spectra $\hat{S}_{nn}$ may be replaced by

$$\hat{S}_{nn} = \frac{S_n(\omega)}{\sigma_n^2} \cdot \hat{Co}_{nn}(\Delta x, \omega) \quad n = u, w \tag{2.90}$$

and $\hat{J}^2_{\theta z} = \hat{J}^2_{z\theta}$.

The response spectrum and response variances may now readily be computed using the above theory.

Chapter 3

The suspension bridge

3.1 General composition

Suspension bridges are distinguished from other bridge-types by their ability to overcome long spans. Presently the longest bridge span in the world is the main span of the Akashi Kaikyō bridge in Japan, with a length of 1991 m [9].

Figure 3.1: The Akashi Kaikyō bridge [9].

The structural system of the suspension bridge can be divided into four main components [10], shown in fig. 3.2.

- the stiffening girder (or deck)
- the cable system supporting the stiffening girder
- the pylons (or towers)
- the anchor blocks supporting the cable system at the extreme ends

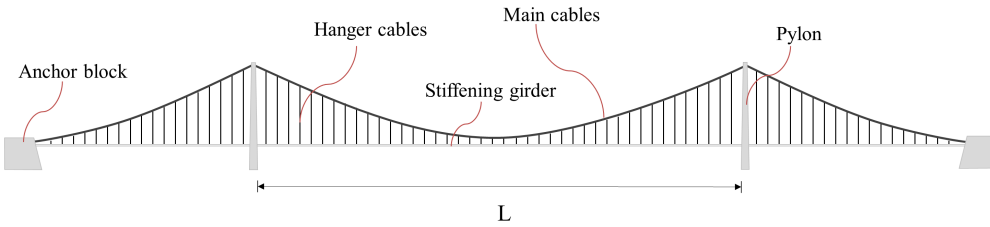

Figure 3.2: Three-span suspension bridge.

3.1.1 Cables and cable system

The cable system of a suspension bridge consists of main cables and hanger cables. The main cables are the main load-carrying components in the bridge and are designed to support the loads from the stiffening girder, the hanger cables and their own self-weight. The advantage of using suspended cables to carry load is that the large vertical forces from traffic and self-weight of the bridge are transferred through the main cables as pure tension. Pure tension is arguably the most efficient way of transferring loads, and thus the needed structural material is far less in the case of a cable as the main load-carrying element, as opposed to for instance a beam [10].

An important property of the cable as a load-carrying element is the sag ratio k, which is the ratio of the sag of the cable to the length of the cable span $k = e_c/L$, see fig. 3.7. The horizontal force H in the cable is inversely proportional to the sag ratio k. On the other hand deflections to non-uniform loads increases with increasing sag ratios and larger sag ratios also means higher pylons. Optimization may be done to find a suitable compromise between performance and cost when choosing sag ratio. Usually the main cables of suspension bridges have sag ratios between 1/9 and 1/11 [10].

3.1.2 Stiffening girder

The bridge deck, or stiffening girder, is the structural element that is subject to the majority of external loading. The main reason is that the traffic load is applied directly onto the deck of the stiffening girder, and also in most cases the dead load of the stiffening girder itself and its susceptibility to wind-load is larger than for the cable system.

The stiffening girder itself must be able to carry loads locally as well as transfer loads to the main cables via the hanger cables. The bridge is usually constructed in a way such that deck may be considered simply supported with the ability to move longitudinally at the pylons. The vertical forces at these supports are also considered to be small because the majority of the vertical force is carried by the cables.

In the traditional suspension bridge arrangement there are two vertical cable planes along the stiffening girder edges, see fig. 3.3 and 3.4, supporting the stiffening girder both vertically and torsionally.

Figure 3.3: Box cross section.

As the stiffening girder is more prone to wind-loads than the cable system it becomes a very important aspect of the bridge with respect to aerodynamics. The shape and type of stiffening girder cross section determines how it interacts with airflow from wind-loading. The stiffening girder's torsional stiffness is also an important property with respect to aerodynamic stability, as loss of torsional stiffness is involved in three out of four instability phenomenon.

The cross sections used in existing suspension bridges may generally be split into

three types: a cross section of trusses, a closed box-type cross section and a dual box cross section.

Cross section of trusses

Historically the cross sections of long span suspension bridges have been made with stiffening trusses, e.g. the Golden Gate bridge and also the Akashi bridge shown in fig. 3.1 have this kind of stiffening girder, see fig. 3.4.

In order to obtain sufficient torsional and bending stiffness, the truss cross sections are usually large, with depths up to $10\,m$ or more. The truss is still sometimes preferred today however, especially where traffic is designed to run in two stories.

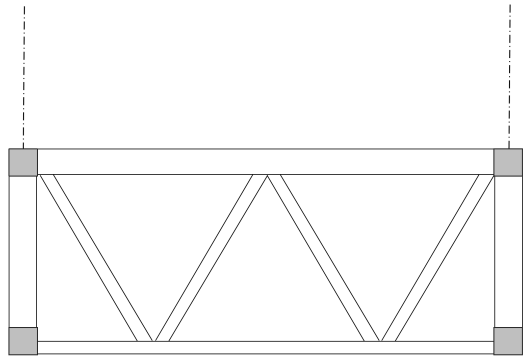

Figure 3.4: Cross section of trusses.

Box cross section

Modern suspension bridges are usually made with box girders. The closed box cross section may obtain sufficient torsional stiffness with smaller depths than the truss. With these box-shaped cross sections the aerodynamic behaviour is important as the bridge may become very slender for long spans. The aerodynamic properties of a box section may effectively be improved by altering the shape, for instance streamlining to reduce drag. The addition of guide vanes to reduce the effect of vortex shedding has also become increasingly popular. An illustration of a basic box cross section is shown in fig. 3.3.

Dual box cross section

The newest addition to cross section types is the so-called vented box girder, or dual box girder. This cross section consists of two box girders connected by transverse girders incorporated between each pair of hanger cables along the length of the bridge. This type of stiffening girder has shown very good aerodynamic properties in wind tunnel tests. The Xihoumen bridge in China, with currently the second longest main span in the world with a length of 1650 m [11], has a dual box cross section, see fig. 3.5.

Figure 3.5: Xihoumen bridge [12].

3.1.3 Pylons

The function of the pylons is to elevate the main cables, and thus the height of the pylons will depend on the span length and chosen sag ratio. As opposed to regular tower structures the main design force for the pylons is not drag from wind load, but the large axial force caused by the main cables [10]. Pylons are made with either reinforced concrete or steel sections. Whereas steel was more in use earlier, modern suspension bridges often have reinforced concrete pylons, as concrete is a superb material for withstanding large compressive forces.

3.1.4 Anchor blocks

The anchor blocks are the structural element of the suspension bridge that transfers the large axial forces of the cables to the earth.

3.2 Single-span suspension bridge

3.2.1 Structural system

In the single-span suspension bridge only the main span is supported by the cable system and the main cables are continued as freely suspended backstays to the anchor blocks, see fig 3.6. Single-span suspension bridges are often used at bridge sites where the placement of intermediate pylons is not possible. Such sites may be for instance a deep body of water or a valley.

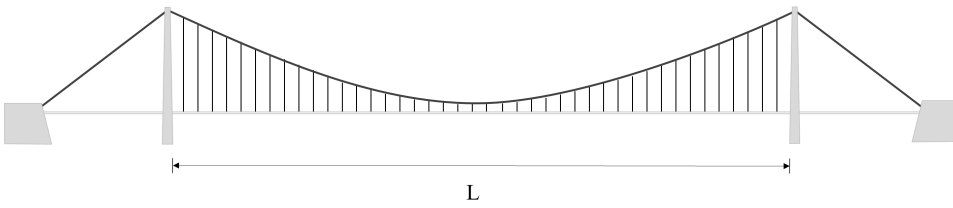

Figure 3.6: Single-span suspension bridge.

3.2.2 Dynamics of a single-span suspension bridge

An approach to identify the eigenfrequencies and corresponding vibrational modes of the single-span suspension bridge is presented thoroughly in [5]. As this approach is quite mathematical, only the general ideas are reproduced here.

The approach is based on the shallow cable theory, also presented in [5]. The assumptions are that the bridge behaves as two cables (in two identical cable planes) and a beam, where the hanger forces are evenly distributed along the length of the bridge. The flexibility of hangers, pylons and back-stays are for simplicity ignored, considered to only cause small discrepancies in the calculation of eigenvalues [5]. Under such circumstances the main girder and the two cable planes move in perfect harmony and the motion may consequently be split into three independent components, one out of plane horizontal motion, one in plane vertical motion and a torsional motion.

The out of plane horizontal motion includes both a component for the motion of the main cables and a component for the motion of the bridge deck. For the vertical and torsional components the bridge deck and the cables are assumed to move congruently. Thus, the four fundamental vibrational modes found from this theory are of the type:

$$\begin{aligned} \boldsymbol{\varphi}_i &= [\phi_{y_i}\ 0\ 0]^T \quad \boldsymbol{\varphi}_i = [\phi_{c_i}\ 0\ 0]^T \\ \boldsymbol{\varphi}_i &= [0\ \phi_{z_i}\ 0] \quad \boldsymbol{\varphi}_i = [0\ 0\ \phi_{\theta_i}]^T \end{aligned} \tag{3.1}$$

where the subscript c indicate cable mode and the rest are as discussed in ch. 2.

The computer program ALVSAT[1] [1] is based on this theory and is used in this thesis to determine frequencies and vibrational modes.

3.2.3 Cable forces

The overall stiffness properties of a single-span suspension bridge depends greatly on the axial force in the main cables, the static forces in the cables must therefore be quantified before a dynamic analysis may be performed. It is assumed that the construction procedure is such that all the weight of the beam is transferred to the main cables via the hangers, and further into the earth through the backstays and pylons. The horizontal force in a single cable is then given by [5]:

$$\bar{H} = \frac{m_z g L^2}{16 e_c} \left\{ 1 + \frac{2m_c}{m_z} \left[1 + \frac{4}{3} \left(\frac{e_c}{L} \right)^2 \right] \right\} \tag{3.2}$$

where g, L and e_c is the gravitational acceleration, main span length and cable sag respectively, m_z is the total distributed mass of the stiffening girder in the vertical direction, m_c is the distributed mass of a single main cable, see fig. 3.7. Note that the distributed mass of the hanger cables are included in m_z and m_c.

[1] ALVSAT is a computer program developed at SINTEF for calculation of single-span suspension bridge vibrational modes and wind-load induced static and dynamic response.

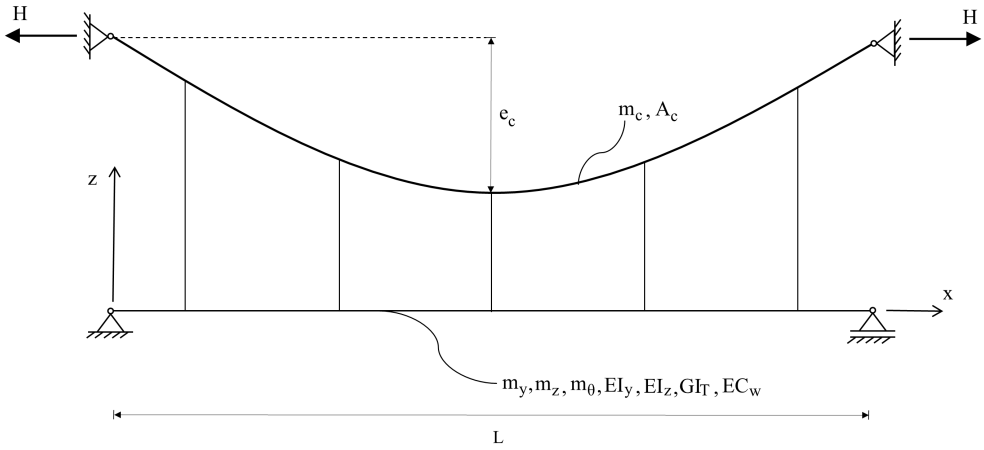

Figure 3.7: Single-span suspension bridge idealized structural system.

The maximum axial force in the cable will be at the pylons and knowing the horizontal force component it may be calculated using:

$$\bar{N}_{max} = \bar{H} \cosh\left(\frac{qL}{2\bar{H}}\right) \tag{3.3}$$

where q is the total static load on a single cable given by:

$$q = g \cdot \left(\frac{m_z}{2} + m_c\right) \tag{3.4}$$

Chapter 4

The Sognefjord bridge

4.1 Overview

As a part of the new coastal highway route E39 project of the NPRA, the possibility of a bridge crossing the Sognefjord is being looked at. Because the fjord quickly becomes to deep to place intermediate pylons, a single-span suspension bridge with a main span of $3700\,m$ is being considered. This span length accompanied by its proposed slenderness means that the design with respect to aerodynamics is highly important. An illustration of the bridge is shown below.

Figure 4.1: Illustration of the Sognefjord bridge [13].

The proposed bridge, referred to as the Sognefjord bridge, is a single-span suspension bridge with $455\,m$ high reinforced concrete pylons placed on either side of the slopes down towards the fjord. The cable sag is $e_c = 370\,m$ which leads to a

sag ratio $k = 0.1$. The free back-stays are lead to anchor blocks embedded within the rock of the adjacent mountain sides, see fig. 4.2. Design specifics and figures in this chapter have been provided by the NPRA [14].

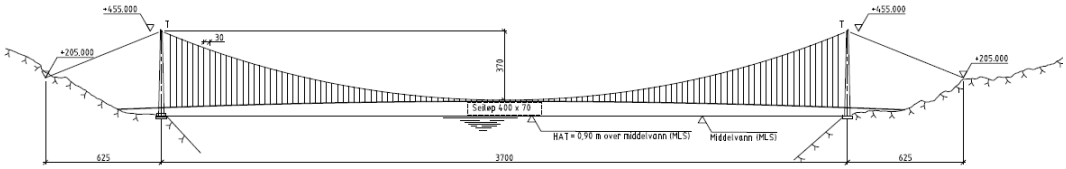

Figure 4.2: Sognefjord bridge.

A super long span suspension bridge such as this requires a cross section with great aerodynamic properties, therefore a dual box section as discussed in sec. 3.1.2 has been proposed. In this thesis such a cross section has been used to investigate the aerodynamic stability limits. The cross section is based on two box girders which are identical to the one used in the Dalsfjord bridge.

Three different configurations with the two box girders at different center-to-center distances have been investigated, specifically $15\,m$, $20\,m$ and $30\,m$. The cross section with 20 m center-to-center distance (c/c) is shown in fig. 4.3. Hollow steel sections are used as transverse girders to join the two box girders, the transverse girders are incorporated between each pair of hanger cables at every $30\,m$.

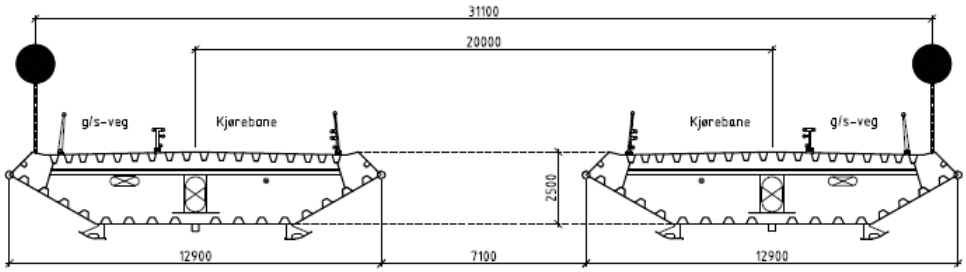

Figure 4.3: Dual box cross-section with c/c $20\,m$.

4.2 Dalsfjord bridge cross-sectional properties

The properties of the stiffening girder of the Sognefjord bridge is calculated from the properties of the box cross section of Dalsfjord bridge which has been provided by the NPRA [14] and are given in tables 4.1-4.3 (structural axes are as shown in fig. 2.1). The cross section width (B) is 12.9 m and height (D) is 2.5 m, as seen in fig. 4.4.

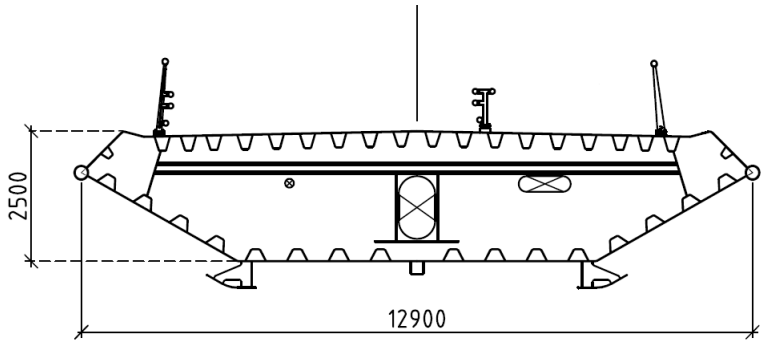

Figure 4.4: Dalsfjord bridge cross section.

The centroid, shear center and center of gravity are given in table 4.1 below.

Table 4.1: Cross-sectional centra of single box.

Center	$y\,[mm]$	$z\,[mm]$
Centroid (cc)	6450	1589
Shear center (sc)	6450	1436
Center of gravity (cg)	6450	1819

where z is measured from the bottom of the cross section, and $y = 6450\ mm$ is in the center in the y-direction of the cross section. The stiffness properties of the cross section are given in table 4.2.

Table 4.2: Cross-sectional properties of a single box section.

Property	Unit	Value
A_{sb}	m^2	0.4472
$I_{y,sb}$	m^4	0.4398
$I_{z,sb}$	m^4	6.2420
$I_{T,sb}$	m^4	1.0780
$C_{w,sb}$	m^6	0.8698
E	N/mm^2	$210 \cdot 10^3$
G	N/mm^2	$80 \cdot 10^3$

where A is the area, I_i is the second moment of area about axis i, I_T is the torsional constant, C_w is the warping constant and E and G are the modulus of elasticity and shear modulus respectively.

The individual contributions to the total distributed mass of the cross section is shown in the table below.

Table 4.3: Distributed mass of a single box section.

Description	Distributed mass $[kg/m]$
Longitudinal steel ($\rho_{steel} = 7850\,kg/m^3$)	3511
Guide vanes	112
Bulkheads	603
Lower hanger cable fastening	30
Railing with fastening plates	136
Pavement (membrane and wearing course)	1885
Electrical installations etc.	240
Surface treatment	26
Sum single box ($m_{z,sb}$)	6543

The distributed rotational mass of the single-box girder is given as:

$$m_{\theta,sb} = 82\,505\ kgm^2/m \tag{4.1}$$

4.3 Dual box cross-sectional properties

The cross-sectional properties of the different configurations is calculated using the properties of the single box section and transverse girder.

4.3.1 Transverse girders

The two box girders are connected with a transverse girder between each pair of hanger cables every $30\,m$ along the main span of the bridge. The cross section of the transverse girder is shown in fig. 4.5.

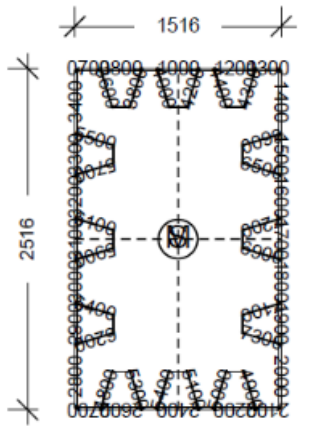

Figure 4.5: Cross section of transverse girder.

For simplicity the stiffness contribution of the transverse girders are assumed negligible. Only their mass contribution is accounted for in the following calculations.

With an area of $0.1790\,m^2$, the distributed mass of the steel transverse girder is $m_{tg} = 1405\,kg/m$ along its own length. The contribution to the total distributed mass is calculated simply by

$$m_{z,tg} = m_{tg} \cdot L_{tg}/(30\,m) \tag{4.2}$$

The contribution to the rotational mass moment of inertia from the transverse girder is

$$m_{\theta,tg} = \frac{m_{tg} \cdot L_{tg}^3}{12}/(30\,m) \tag{4.3}$$

Table 4.4: Mass contribution of transverse girder.

		c/c		
Property	Unit	15 m	20 m	30 m
L_{tg}	m	25	30	40
$m_{z,tg}$	kg/m	1171	1405	1873
$m_{\theta,tg}$	kgm^2/m	60981	105375	249778

The assumed lengths and computed values for the mass contributions of the transverse girder to the different cross section configurations is presented in table 4.4.

4.3.2 Stiffness

The stiffness of the dual box section is calculated from the stiffness of the single box, given in sec. 4.2. The stiffness contribution from the transverse girder is assumed to be negligible, and so is the distance from the centroid to the shear center.

With the assumptions above the second moment of area about the y-axis and the torsional constant may be estimated using

$$I_y = 2 \cdot I_{y,sb} \tag{4.4}$$

and

$$I_T = 2 \cdot I_{T,sb} \tag{4.5}$$

The second moment of area about the z-axis is estimated using the well known parallel axis theorem

$$I_z = I_{cc} + A \cdot r^2 \tag{4.6}$$

where r is the distance from the centroid (cc) to a parallel axis about which I_z is calculated and A is the area of the section. The bending stiffness about the z-axis for the dual box section, with r being half the center-to-center distance, is then found by:

$$I_z = 2 \cdot (I_{z,sb} + A_{sb} \cdot r^2) \tag{4.7}$$

The warping constant may be estimated using the formula [15]:

$$C_w = I_f \cdot \frac{h^2}{2} \tag{4.8}$$

where the cross section is seen as an I-section with the two boxes corresponding to the flanges and the cross beam being the web. Thus $I_f = I_{y,sb}$ and h is the distance center-to-center between the boxes.

The obtained stiffness values for the configurations is shown in table 4.5.

Table 4.5: Stiffness properties of the dual box cross sections.

		c/c		
Property	Unit	15 m	20 m	30 m
I_y	m^4	0.8796	0.8796	0.8796
I_z	m^4	62.794	101.924	213.724
I_T	m^4	2.156	2.156	2.156
C_w	m^6	49.4775	87.96	197.91

4.3.3 Mass

The calculation of the distributed mass in the vertical direction is a simple summation of the contribution from the box sections and the transverse girders. In addition, half of the mass of the hanger cables is added to the mass of the girder, while the other half is added to the mass of the main cables, thus

$$m_z = 2 \cdot m_{z,sb} + m_{z,tg} + m_{hc} \tag{4.9}$$

It is here taken for granted that the mass of the hanger cables added to the bridge girder is $m_{hc} = 280\,kg/m$, the specific calculation is shown in the next section.

The rotational mass may be found using the parallel axis theorem as before, which for rotational mass moment of inertia is given as

$$M_\theta = M_{\theta,cg} + M \cdot r^2 \tag{4.10}$$

where $M_{\theta,cg}$ is the rotational mass moment of inertia about the center of gravity (cg) and M_θ is the inertia about a parallel axis at a distance r from the center of gravity. M is the total mass of the body.

The rotational mass of the box girder is then

$$m_{\theta,girder} = 2 \cdot (m_{z,sb} \cdot (r^2 + e^2) + m_{\theta,sb}) \tag{4.11}$$

where r is half the center-to-center distance of the two box sections and e is the eccentricity between the center of gravity and shear center. For the hanger cables and main cables, assuming that half of the hanger cable is mass included in the main cable mass, whereas m_{hc} is the half added to the girder, the cable system contribution becomes

$$m_{\theta,c} = 2 \cdot (m_{hc} + m_c) \cdot r_c^2 \tag{4.12}$$

where r_c is half the center-to-center distance of the main cables. The total rotational mass of inertia is then given by

$$m_\theta = m_{\theta,girder} + m_{\theta,tg} + m_{\theta,c} \tag{4.13}$$

The distributed masses obtained is shown in table 4.3 below. It has been taken for granted that the mass of the main cables including the added weight from the hanger cables is $m_c = 9677\,kg/m$. The cable calculations are shown in the next section.

Table 4.6: Mass properties of dual box girder.

		c/c		
Property	Unit	15 m	20 m	30 m
m_z	kg/m	$14.538 \cdot 10^3$	$14.773 \cdot 10^3$	$15.241 \cdot 10^3$
m_θ	kgm^2/m	$4.3304 \cdot 10^6$	$6.3514 \cdot 10^6$	$11.676 \cdot 10^6$

4.4 Cable dimensions

The cable system of the Sognefjord bridge is the traditional suspension system with two main cables connected to the deck by 121 pairs of hanger cables along the bridge length. The main cables are assumed to have a minimum tensile strength

of $f_{cbu} = 1770\,N/mm^2$ and elasticity module of $E_c = 200 \cdot 10^3\,N/mm^2$.

Hanger cables of the type Bridon LC100 have been suggested by the NPRA, and are assumed to meet the necessary requirements. The weight of the hanger cables are distributed to the main cables and the girder as discussed in sec. 5.2. The mass contribution of the hanger cables are given in the table below.

Table 4.7: Hanger cable composition and load distribution.

Description	Unit	Value
Total length of hangers	m	32594
Mass per length	kg/m	56.2
Total mass hanger cables	kg	$1832 \cdot 10^3$
Cable socket (per socket)	kg	439
Total weight of sockets	kg	$212 \cdot 10^3$
Mass added to stiffening girder	kg/m	280
Mass per cable clamp	kg	3000
Total mass upper hanger cable	kg	$1748 \cdot 10^3$
Mass added to each main cable	kg/m	232

The main cable dimensions are chosen to meet the requirements of NPRA given in [16](5.10.3.2), i.e. maximum cable force should not exceed:

$$F_{Rd} = \frac{F_{uk}}{1.5 \cdot \gamma_m} \tag{4.14}$$

where $\gamma_m = 1.2$ and

$$F_{uk} = f_{cbu} \cdot A_c \tag{4.15}$$

where f_{cbu} is the minimum tensile strength of the cable and A_c is the effective steel area of the cable. For wire strands with $f_{cbu} = 1770\,N/mm^2$ and a suggested effective steel area of $A_c = 1.15\,m^2$, the allowable force in the a single cable is:

$$F_{Rd} = 1130.83 \cdot 10^6\,N \tag{4.16}$$

The maximum cable force is calculated with a specified traffic-load of $9\,kN/m$ per roadway lane and $2\,kN/m$ per walking/bicycle path. These loads are specified in [16] for bridges with main spans less than $500\,m$ but will be assumed to be

the design traffic load for the Sognefjord bridge as well as larger spans are not specified in [16]. With two roadway lanes and two walking/bicycle paths the total design traffic load for the Sognefjord bridge is $q_T = 22\,kN/m$.

Safety factors specified in [16] are $\gamma_G = 1.2$ for self-weight and $\gamma_T = 1.3$ for traffic-load. The horizontal force in the main cables may now be calculated using eq. 3.2, with $m_{z,Ed} = \gamma_G \cdot m_z + \gamma_T \cdot (q_T/g)$ and $m_{c,Ed} = \gamma_G \cdot m_c$. This yields the horizontal forces as shown in the table below.

Table 4.8: Horizontal force in main cables.

		c/c		
Description	Unit	15 m	20 m	30 m
$\bar{H}$	MN	995.83	1002.21	1014.96

The maximum axial force may now be calculated with eq. 3.4 where

$$q = \frac{q_T}{2} + \frac{m_z \cdot g}{2} + m_c \cdot g \tag{4.17}$$

which yields:

Table 4.9: Maximum axial force in main cables.

		c/c		
Description	Unit	15 m	20 m	30 m
$\bar{N}_{max}$	MN	1075.42	1082.31	1096.09
Utilization	%	95	96	97

As seen by table 4.9 an effective steel area of $1.15\,m^2$ per main cable is sufficient for all three cross section cases.

4.5 Aerodynamic derivatives

At the time of writing this thesis experimentally found aerodynamic derivatives for the exact cross sections are not available. The aerodynamic derivatives used are from wind tunnel tests of different configurations of the proposed bridge called

Brusymfonien [3], which has a similar dual box bridge girder. The Brusymfonien bridge however, has a girder width of only $B = 7.5\,m$ opposed to $B = 12.9\,m$ for the Sognefjord bridge. This difference is assumed to be negligible in the calculations and $B = 12.9\,m$ is used. An illustration of the configurations for Brusymfonien is shown below.

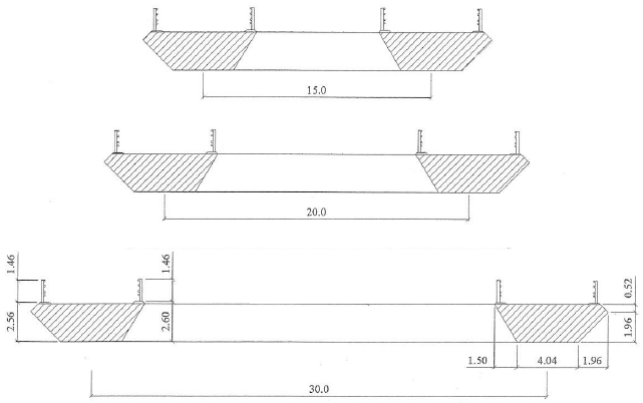

Figure 4.6: Dual box configurations of Brusymfonien wind tunnel tests [3].

The static aerodynamic load coefficients from these wind tunnel tests are shown in the table below.

Table 4.10: Static aerodynamic load coefficients – Brusymfonien wind tunnel tests [3].

c/c	C_D	C_L	C'_L	C_M	C'_M
$15\,m$	1.523	-0.145	5.46	0.134	0.04
$20\,m$	1.754	0.118	6.37	0.185	-0.80
$30\,m$	1.819	-0.200	6.96	0.194	-3.24

The experimentally found aerodynamic derivatives are found by curve fitting of test results, and given by

$$AD_i = p_3\hat{V}_i^3 + p_2\hat{V}_i^2 + p_1\hat{V}_i + p_0 \tag{4.18}$$

where p_i are constants and $\hat{V}_i = V/(B{\cdot}\omega_i(V))$. In the case of vertical and torsional

movement only:

$$AD_i = \begin{bmatrix} H_i^* \\ A_i^* \end{bmatrix}, \; i = 1 \ldots 4 \tag{4.19}$$

The figure below shows the aerodynamic derivatives plotted for the different center-to-center distances.

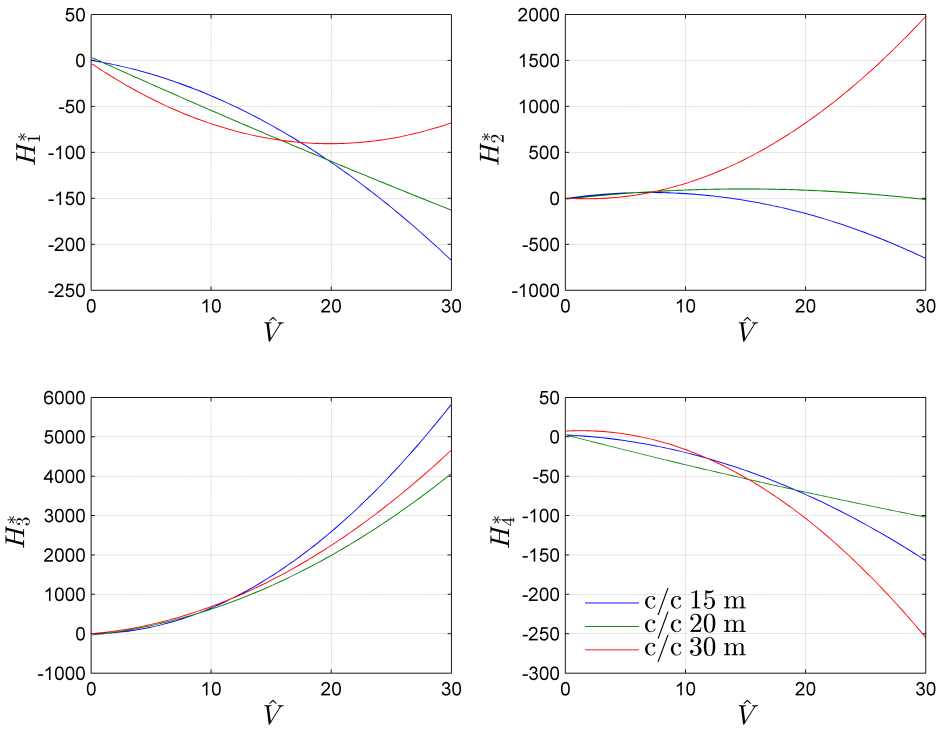

Figure 4.7: Aerodynamic derivatives, $H_k^*, k = 1 \ldots 4$.

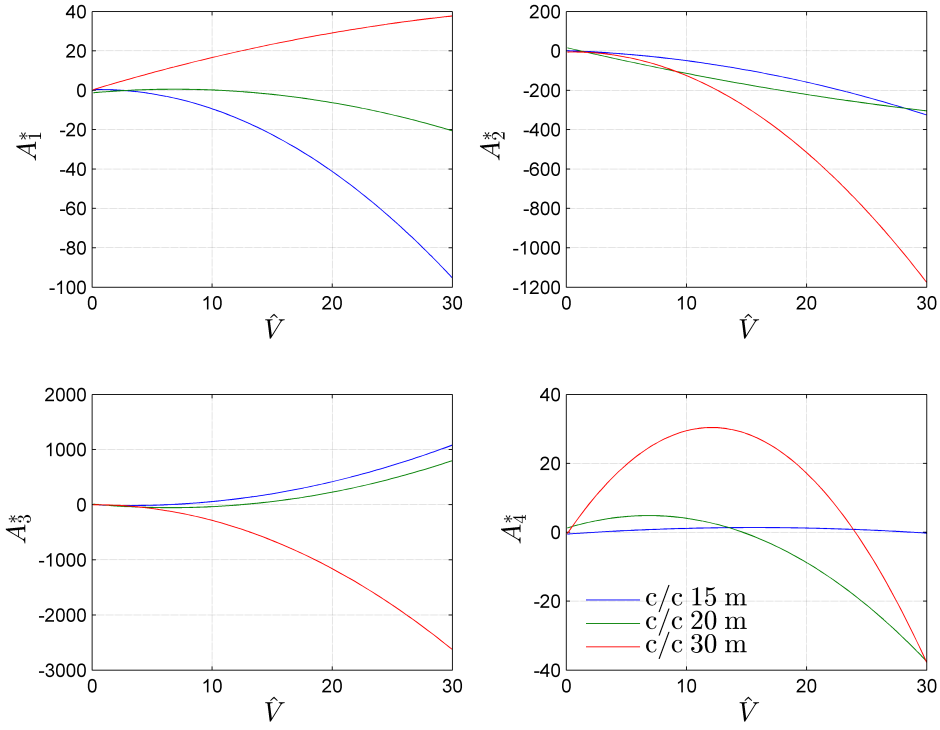

Figure 4.8: Aerodynamic derivatives, $A_k^*, k = 1 \ldots 4$.

It should be noted that the wind tunnel tests were only carried out for wind velocities up to a maximum reduced velocity of $\hat{V} = 16.2$, values above these are thus extrapolated from test data. Full tables containing all coefficients for aerodynamic derivatives are presented in app. C.

4.6 Wind properties at bridge site

For long span suspension bridges such as the proposed Sognefjord bridge, defined as class III bridges, the design mean wind velocity should be determined from measurements as stated in the Norwegian building standard NS-EN 1991-1-4 [17]. The project has not reached a stage where this has been done however, therefore as a first estimate the design wind velocity is taken from the equations given by [16, 17]

$$V_m(z) = c_r(z) \cdot c_0(z) \cdot V_b \tag{4.20}$$

where $V_m(z)$ is the mean wind velocity at height z, $c_0(z)$ is the orography factor here taken as 1.0, and $c_r(z)$ is the terrain roughness factor given by

$$c_r(z) = k_r \cdot ln\left(\frac{z}{z_0}\right) \tag{4.21}$$

where z_0 is the roughness length and k_r is a roughness factor given by

$$k_r = 0.19 \cdot \left(\frac{z_0}{0.05}\right)^{0.07} \tag{4.22}$$

The basic wind velocity, V_b, is given as

$$V_b = c_{dir} \cdot c_{season} \cdot V_{b,0} \tag{4.23}$$

where the directional and seasonal factors c_{dir} and c_{season} may be set to 1.0 as recommended by the standard. $V_{b,0}$ is the fundamental value of the basic wind velocity, which is site specific and found to be

$$V_{b,0} = 29\,m/s \tag{4.24}$$

for the proposed bridge site in Gulen municipality [14].

With a roughness length of $z_0 = 0.01\,m$, $k_r \approx 0.17$ and the terrain roughness factor at $z = 70\,m$ is

$$c_r(70) = 0.17 \cdot ln\left(\frac{70}{0.01}\right) = 1.505 \tag{4.25}$$

this yields a design mean wind velocity of

$$V_m(70) = 1.505 \cdot 29\,m/s = 43.6\,m/s \tag{4.26}$$

According to point 2.5.2.5 in [16], the critical mean wind velocity of a class III bridge should meet the requirement

$$\frac{V_{cr}}{\gamma_{cr}} \geq V_m(z) \tag{4.27}$$

where $\gamma_{cr} = 1.6$. The requirement for the critical mean wind velocity is thus

$$V_{cr} \geq 1.6 \cdot 43.6\, m/s = 69.8\, m/s \tag{4.28}$$

The turbulence intensity is given by [16, 17] to be

$$I_u(z) = \frac{k_1}{c_0(z) \cdot ln(z/z_0)} \tag{4.29}$$

where the turbulence intensity factor is given as $k_1 = 1.2$ [14], this yields and intensity

$$I_u(70) = \frac{1.2}{1.0 \cdot ln(70/0.01)} \approx 0.14 \tag{4.30}$$

also from section 2.5 in [16] the following values are found for the wind turbulence properties

$$I_w = \frac{1}{2} \cdot I_u = 0.07 \tag{4.31}$$

and

$$\begin{array}{ll} A_u = 6.8 & A_w = 9.4 \\ C_{ux} = 10 & C_{wx} = 3 \end{array} \tag{4.32}$$

and the integral length scales given by [14]

$${}^{x_f}L_u = 360\, m \quad {}^{x_f}L_w = 30\, m \tag{4.33}$$

are all the values needed for generating a wind spectrum according to eq. 2.73. The wind spectra are shown in fig. 4.9.

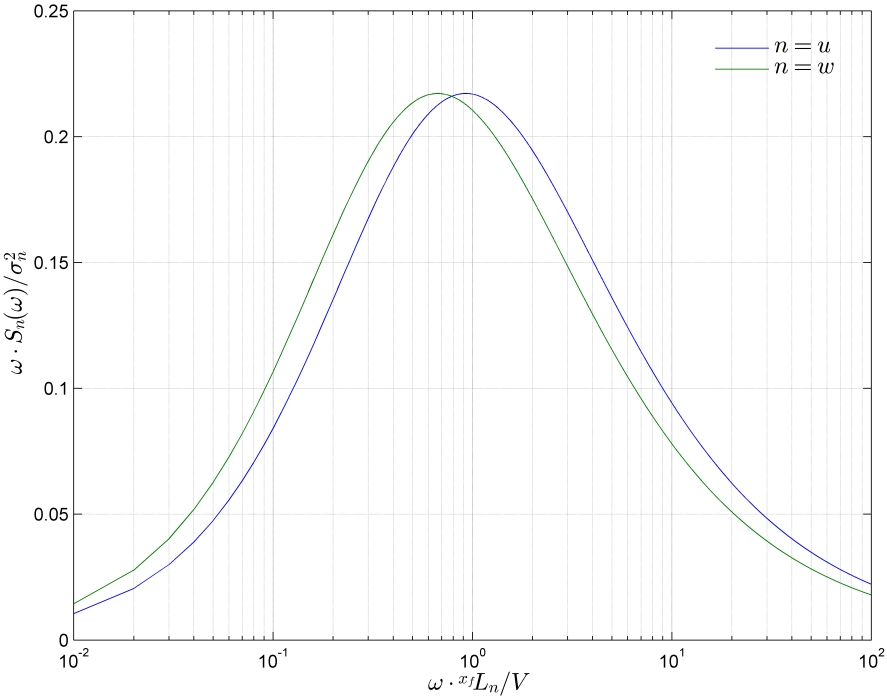

Figure 4.9: Kaimal spectra of turbulence components.

Chapter 5

Numerical results

5.1 Introduction

This chapter presents the numerical results found for the three cross sectional configurations discussed in sec. 4.3. The eigenmodes and corresponding mode shapes have been found using the computer program ALVSAT, which was mentioned in sec. 3.2.2. See app. A for all the ALVSAT input values as well as an example output.

The computation of mode shapes (from Fourier coefficients), stability limits and dynamic response has been done using self written MATLAB [2] scripts, all of which are given in app. D. The scripts have been verified against examples given in [4]. The calculations follow the theory given in ch. 2 and focuses only on the vertical r_z and torsional r_θ degrees of freedom, since these are the ones associated with the aerodynamic stability limits.

For the computation of the stability limits and dynamic response, the modally distributed masses $\tilde{m}_z$ and $\tilde{m}_\theta$ are needed. The distributed masses of the bridge are assumed constant over the entire span, rendering the modally distributed masses:

$$\tilde{m}_z = m_z + 2 \cdot m_c \tag{5.1}$$

and

$$\tilde{m}_\theta = m_\theta \tag{5.2}$$

where m_z, m_θ and m_c are given in ch. 4.

5.2 Eigenfrequencies and modes of vibration

The eigenfrequencies and the vibrational modes of the bridge has been determined using the computer program ALVSAT. The program computes the mode shapes using a Fourier series solution to the eigenvalue problem (eq. 2.8) and consequently the output is the Fourier coefficients $a_{i_{j,k}}$ where $i = 1 \ldots N_{mod}$ is the mode number $j = y, z, \theta$ or c and $k = 1 \ldots N_C$ is the Fourier coefficients. The vibrational modes are then generated using a MATLAB script which computes them with the following expression

$$\phi_{i_j} = \sum_{k=1}^{N_C} a_{i_j,k} \cdot \sin(k\pi\hat{x}) \tag{5.3}$$

where $\hat{x} = x/L$.

As stated in ch. 2 and the previous section only vertical and torsional movement is associated with aerodynamic stability limits, therefore only vertical and torsional vibrational modes have been determined using ALVSAT. A total of 8 vertical modes and 8 torsional modes have been computed using 8 Fourier coefficients for each mode, in accordance with [1] which states that the number of Fourier coefficients should be atleast equal to the number of modes in each direction of motion. The number of coefficients has also be deemed sufficient by observing that the last few of the 8 coefficients are close to or exactly zero.

The eigenfrequencies found from ALVSAT are shown in table 5.1 for all three cross section configurations.

Table 5.1: Eigenfrequencies for the Sognefjord bridge.

c/c	15 m	20 m	30 m
Mode		$\omega\,[rad/s]$	
VA1	0.3863	0.3865	0.3869
VS1	0.4947	0.4967	0.4936
TA1	0.5629	0.5238	0.4804
TS1	0.6734	0.6466	0.5998
VS2	0.6808	0.6876	0.6766
VA2	0.7412	0.7410	0.7410
TS2	0.9001	0.8584	0.7989
VS3	0.9402	0.9410	0.9396
TA2	1.0963	1.0168	0.9281
VA3	1.1125	1.1125	1.1124
TS3	1.3776	1.2802	1.1706
VS4	1.3022	1.3023	1.3019
VA4	1.4851	1.4850	1.4849
TA3	1.6405	1.5224	1.3907
TS4	1.9160	1.7788	1.6256
TA4	2.1859	2.0290	1.8542

V=Vertical, T=Torsional, S=Symmetric, A=Asymmetric.

It is seen that the eigenfrequencies of the vertical modes are very similar for all configurations, as we might expect considering the stiffness and mass in the vertical direction are practically equal. The torsional modes take on slightly different values due to the changes in rotational mass and bending stiffness about the z-axis. As $\omega \propto \sqrt{K/M}$ it is seen by the decrease in ω that the rotational mass becomes more dominant for larger center-to-center distances.

A plot of the mode shapes corresponding to the 4 lowest eigenfrequencies is shown in fig. 5.1, note that the normalized mode shapes are nearly identical for the three configurations. For plots of all 16 mode shapes see app. B.

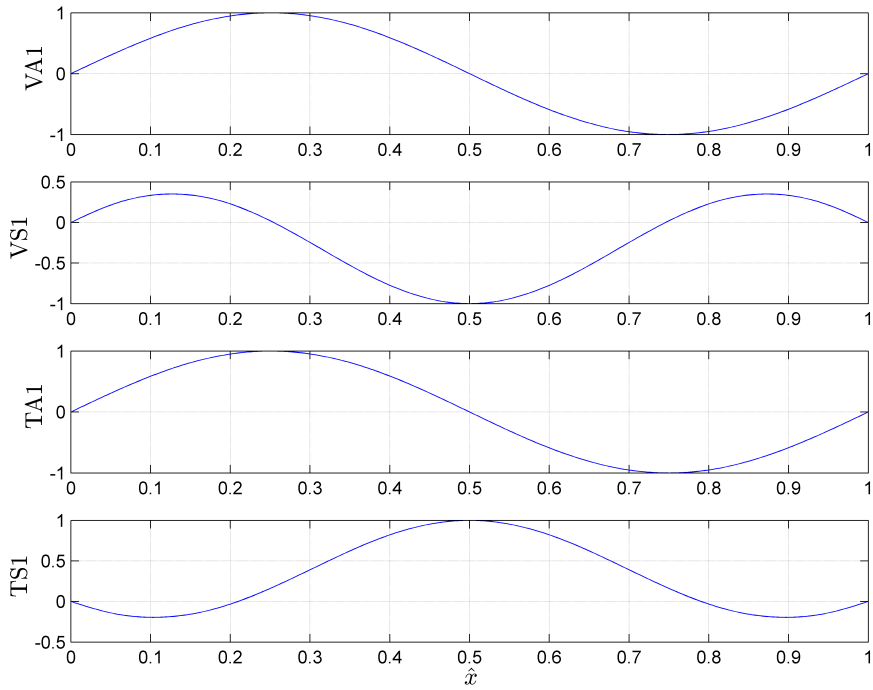

Figure 5.1: Four lowest frequency mode shapes.

As stated in sec. 2.3.5, shape-wise similar and low frequency modes in vertical and torsional movement are prone to coupling in a flutter instability. By inspecting the four lowest modes it is seen that VA1 and TA1 look identical, and in addition their frequency ratio is close to 1, these modes are consequently the most likely modes to couple in a flutter instability. The flutter and response calculations presented in the next section will therefore focus on these modes. For all three cross-sectional configurations the shape-wise similarity for these modes are such that $\psi_z = \psi_\theta \approx 1$.

5.3 Stability limits

5.3.1 Dual box 15 m c/c

The configuration with 15 m center-to-center distance have the following properties:

Table 5.2: Structural properties for stability limit calculation 15 m c/c.

$\rho\,[kg/m^3]$	$B\,[m]$	$\zeta_z = \zeta_\theta$	$\tilde{m}_z\,[kg/m]$	$\tilde{m}_\theta\,[kgm^2/m]$	C'_M
1.25	12.9	0.005	33893	$4.3304 \cdot 10^6$	0.04

Static divergence

The torsional mode with the lowest frequency is TA1 as shown in table 5.1, with an eigenfrequency of $\omega_\theta = 0.5629$. Using eq. 2.54 critical mean wind velocity for static divergence is found to be:

$$V_{cr} = 12.9m \cdot 0.5629\,rad/s \cdot \left(\frac{2 \cdot 4.3304 \cdot 10^6\,kgm^2/m}{1.25\,kg/m^3 \cdot (12.9\,m)^4 \cdot 0.04} \cdot 1 \right)^{1/2} \approx 574\,m/s \tag{5.4}$$

which is obviously very high. However solving the general expression given eq. 2.53 with a MATLAB script reveals a stability limit in static divergence far lower at

$$V_{cr} = 93.6\,m/s \tag{5.5}$$

which is then the critical mean wind velocity for static divergence.

Galloping and dynamic stability limit in torsion

By inspecting the aerodynamic derivatives in fig. 4.7 and fig. 4.8 we see that both H_1^* and A_2^* are negative for all relevant values of $\hat{V}$ (it is only positive at $\hat{V} \approx 0$), thereby rendering any galloping limit and dynamic stability limits in torsion non existent.

Flutter

For flutter calculation the two low eigenfrequency modes, one vertical and one torsional, which are the most shape-wise similar are critical. From table 5.1 and

fig. 5.1 it is seen that this is the first asymmetric vertical mode (VA1) and the first asymmetric torsional mode (TA1) as stated in the previous section. These modes have the following frequencies:

Table 5.3: Frequencies VA1/TA1, 15 m c/c.

$\omega_z\,[rad/s]$	$\omega_\theta\,[rad/s]$	$\gamma = \omega_\theta/\omega_z$
0.3863	0.5629	1.457

The solution of the flutter equations is shown in fig. 5.2 below.

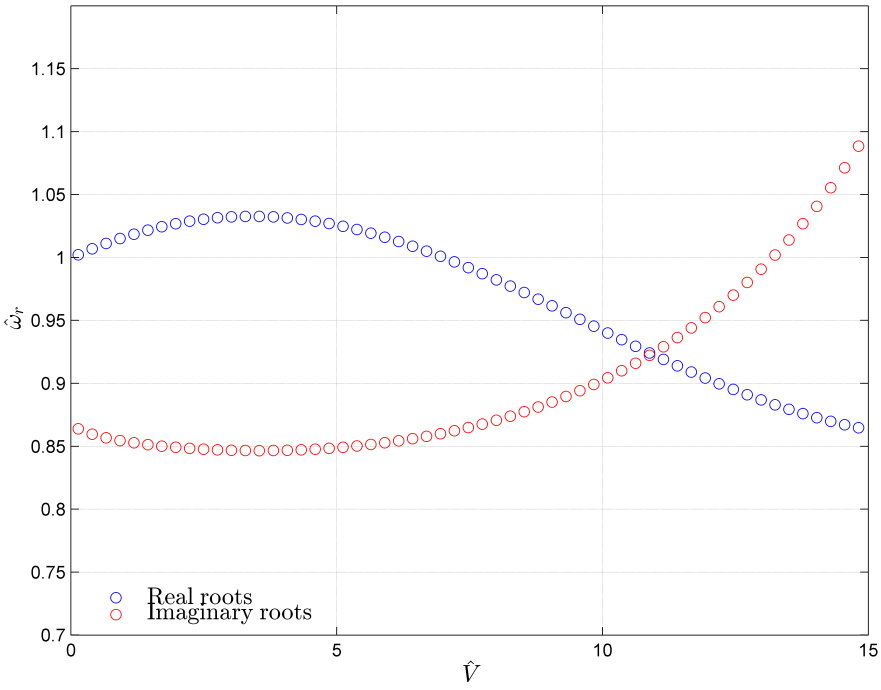

Figure 5.2: Development of the flutter equations for increasing $\hat{V}$.

The real part and imaginary parts intersect at approximately $(\hat{V}, \hat{\omega}_r) = (11.1, 0.924)$ leading to a resonance frequency:

$$\omega_r = \omega_\theta \cdot \hat{\omega}_r = 0.5629 \cdot 0.924 = 0.520\, rad/s \tag{5.6}$$

at a critical mean wind velocity of:

$$V_{cr} = \hat{V} \cdot B \cdot \omega_r = 11.1 \cdot 12.9 \cdot 0.520 = 74.5\, m/s \tag{5.7}$$

which is close to, but above the critical wind speed requirement of $69.8\, m/s$.

5.3.2 Dual box 20 m c/c

The configuration with 20 m center to center distance have the following properties:

Table 5.4: Structural properties for stability limit calculation 20 m c/c.

$\rho\,[kg/m^3]$	$B\,[m]$	$\zeta_z = \zeta_\theta$	$\tilde{m}_z\,[kg/m]$	$\tilde{m}_\theta\,[kgm^2/m]$	C'_M
1.25	12.9	0.005	34128	$6.3514 \cdot 10^6$	-0.8

Static divergence

As shown in the table above, the quasi-static aerodynamic property C'_M is negative. Consequently eq. 2.54 will not yield a real V_{cr} so it may not identify a stability limit. A static divergence limit was not found with eq. 2.53 either.

Galloping and dynamic stability limit in torsion

The aerodynamic derivatives H_1^* is negative for all relevant values of $\hat{V}$ and thus a galloping stability limit may not be identified.

For the case of dynamic stability in torsion however, it is seen that if the aerodynamic derivative A_2^* is developed for high $\hat{V}$ it goes from negative to positive at around $\hat{V} = 120$, see fig. 5.3.

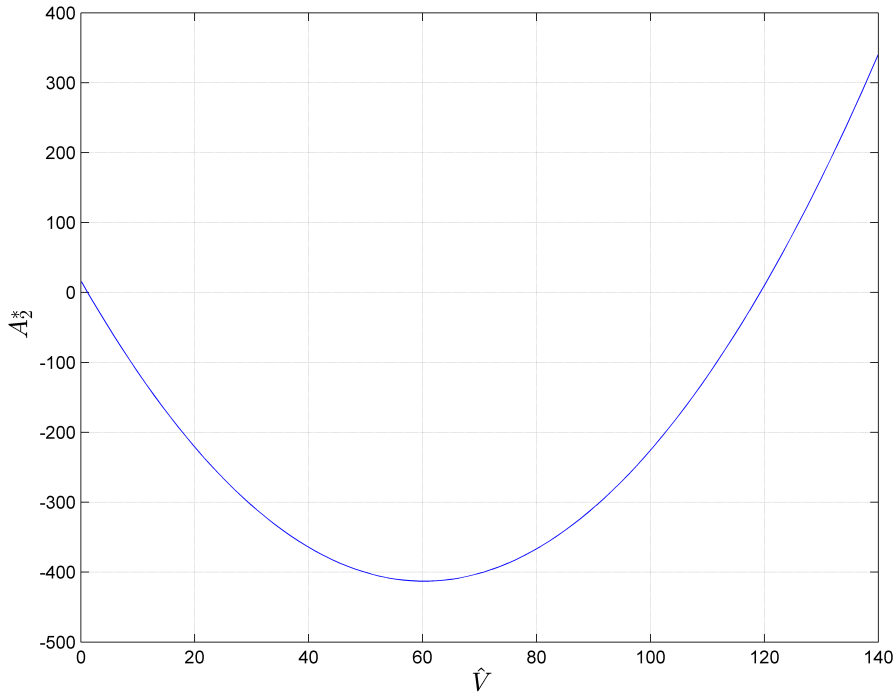

Figure 5.3: A_2^* - 20 m c/c.

This yields a dynamic stability limit in torsion at $\hat{V} = 121.2$ and thus a critical mean wind velocity and resonance frequency of

$$V_{cr} = 109\,m/s \quad \omega_r = 0.07\,rad/s \tag{5.8}$$

This stability limit is however questionable as the values of $\hat{V}$ is extrapolated way beyond the wind tunnel test results.

Flutter

A flutter calculation for the 20 m c/c configuration has been done for the modes VA1 and TA1. The frequencies of the modes are presented in table 5.5 below.

Table 5.5: Frequencies VA1/TA1, 20 m c/c

$\omega_z\,[rad/s]$	$\omega_\theta\,[rad/s]$	$\gamma = \omega_\theta/\omega_z$
0.3865	0.5238	1.355

The solution to the flutter equations is shown in fig. 5.4.

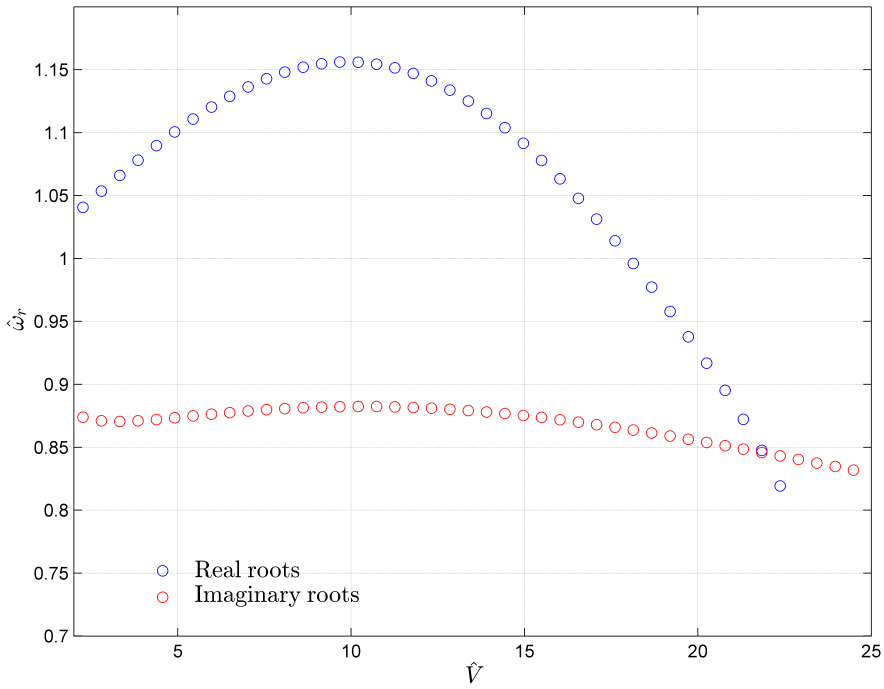

Figure 5.4: Development of the flutter equations for increasing $\hat{V}$.

The intersection between the real and the imaginary parts occur at $(\hat{V}, \hat{\omega}_r) = (21.9, 0.845)$. This gives an in-wind resonance frequency:

$$\omega_r = \omega_\theta \cdot \hat{\omega}_r = 0.5238 \cdot 0.845 = 0.443\, rad/s \tag{5.9}$$

at a critical mean wind velocity of:

$$V_{cr} = \hat{V} \cdot B \cdot \omega_r = 21.9 \cdot 12.9 \cdot 0.443 = 125\, m/s \tag{5.10}$$

5.3.3 Dual box 30 m c/c

The girder configuration with 30 m center to center distance have the following properties:

Table 5.6: Structural properties for stability limit calculation 30 m c/c.

$\rho\,[kg/m^3]$	$B\,[m]$	$\zeta_z = \zeta_\theta$	$\tilde{m}_z\,[kg/m]$	$\tilde{m}_\theta\,[kgm^2/m]$	C'_M
1.25	12.9	0.005	34596	$11.676 \cdot 10^6$	-3.24

Static divergence

The configuration with 30 m c/c also has a negative C'_M, thus a static divergence stability limit may not be identified.

Galloping and dynamic stability limit in torsion

A dynamic stability limit in torsion may not be identified, as for all practical values of $\hat{V}$, A_2^* is negative. For galloping it is seen that H_1^* is not strictly negative, however because H_4^* grows negative quickly, the resonance frequencies become complex values, and thus a stability limit in galloping is not found.

Flutter

A flutter calculation for the 30 m c/c configuration has been done for modes VA1 and TA1, the two modes have the following frequencies:

Table 5.7: Frequencies VA1/TA1, 30 m c/c.

$\omega_z\,[rad/s]$	$\omega_\theta\,[rad/s]$	$\gamma = \omega_\theta/\omega_z$
0.3869	0.4804	1.242

A solution of the flutter equations is not found for the 30 m c/c case. The development of the real and imaginary parts is shown in fig. 5.5.

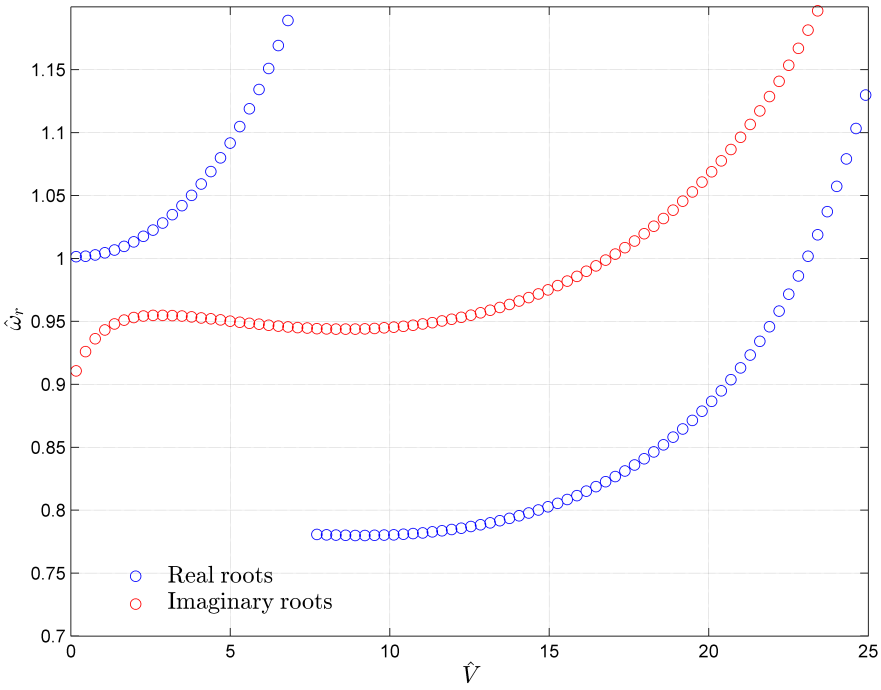

Figure 5.5: Development of the flutter equations for increasing $\hat{V}$.

For higher $\hat{V}$ the real and imaginary roots will just continue to increase in the same exponential manner as shown in fig. 5.5.

5.4 Dynamic response

5.4.1 Joint acceptance function

The determination of the joint acceptance functions is the most computationally demanding part of finding the dynamic response. The numerical integration required to obtain the joint acceptance functions may be done by a double summation of the form

$$I(\beta) = \frac{1}{N^2} \sum_{n=1}^{N} \sum_{m=1}^{N} \phi_i(\hat{x}_n)\phi_j(\hat{x}_m) \cdot exp\{-\beta \cdot \Delta\hat{x}_{nm}\} \tag{5.11}$$

where $\Delta\hat{x}_{nm} = |\hat{x}_n - \hat{x}_m|$ and $\beta = C_{nx} \cdot \omega \cdot L/V$, $n = u, w$. Because these integrals are dependent on the discretization of $\hat{x}$, i.e. the number N. It was found helpful to study the convergence rate of the integrals with respect to N as to determine the needed number of points for a sound solution to the response. A plot of these integrals for the mode shapes VA1 and TA1 for three cases of N is shown in fig. 5.6.

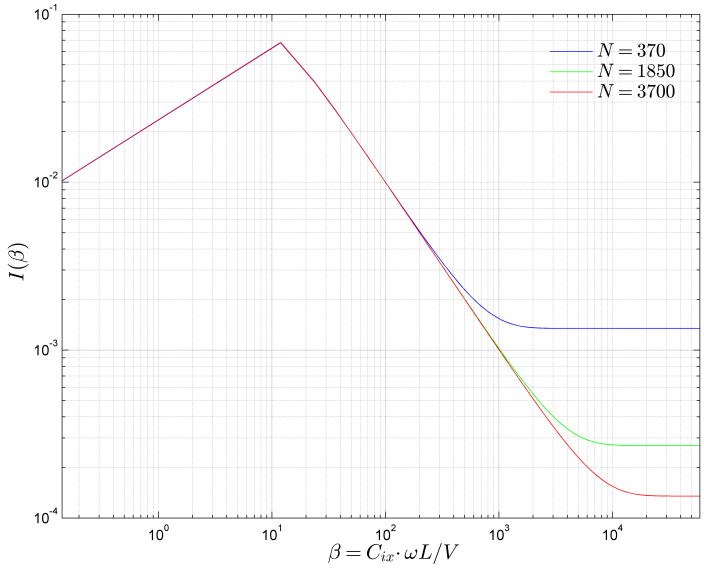

Figure 5.6: Joint acceptance integral convergence.

It is seen by the figure that only at large β values do the integrals not converge, and that at these large values of β the integrals are small. With the resonant

eigenfrequencies of modes VA1 and TA1 being less than 0.6 the relevant beta values will only reach the divergence point for wind velocities less than around $5\,m/s$. Based on this a discretization of $N = 370$ is chosen for computational efficiency.

5.4.2 Dual box 15 m c/c

The dynamic response for the $15\,m$ center-to-center configuration was computed using a two mode approach with VA1 and TA1 at response location $x_r/L = 0.25$. The resulting dynamic response variances are shown in fig. 5.7.

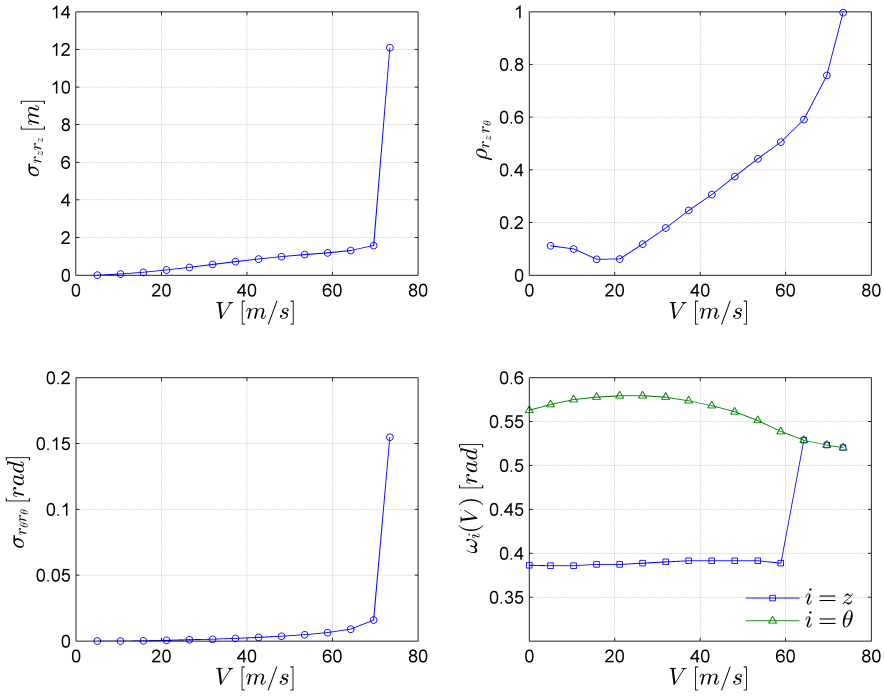

Figure 5.7: Top left: dynamic response in the vertical direction. Top right: covariance coefficient. Lower left: dynamic response in torsion. Lower right: development of in-wind resonance frequencies.

The response calculation for this cross-sectional configuration confirms the existence the flutter limit in vicinity of the one found in sec. 5.3, the largest standard deviation was found for $73.4\,m/s$ as opposed to the computed flutter limit of

$74.5\,m/s$. The in-wind resonance frequency plot shows that the two modes oscillates at the same frequency at a mean wind velocity of approximately $65\,m/s$. A comparison of the response spectra at mean wind veloctites of $V = 40\,m/s$ and $V = 73.4\,m/s$ is shown in fig 5.8.

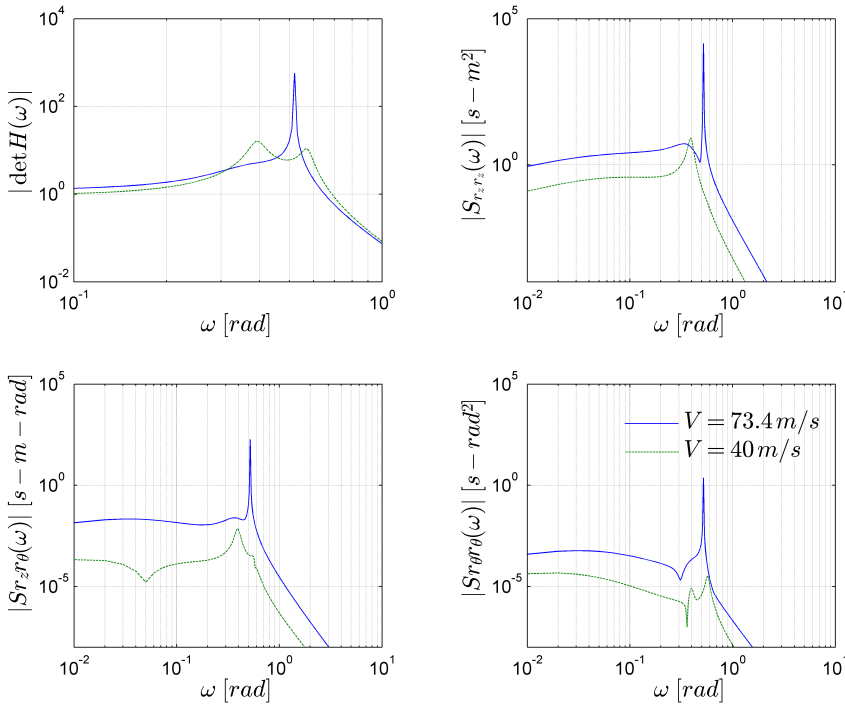

Figure 5.8: Top left: frequency-response spectrum. Top right: response spectrum in vertical movement. Lower left: cross spectrum between vertical and torsional movement. Lower right: response spectrum in torsional movement.

The figure shows the coupling effect of the modes in the frequency-response plot where at $V = 40\,m/s$ there are two peaks, but for $V = 73.4$ there is only a single high peak at the flutter frequency. The response spectrum consequently also shows a very large peak at the flutter frequency. A time series simulation of $V = 40\,m/s$ and $V = 73.4\,m/s$ is shown in fig. 5.9.

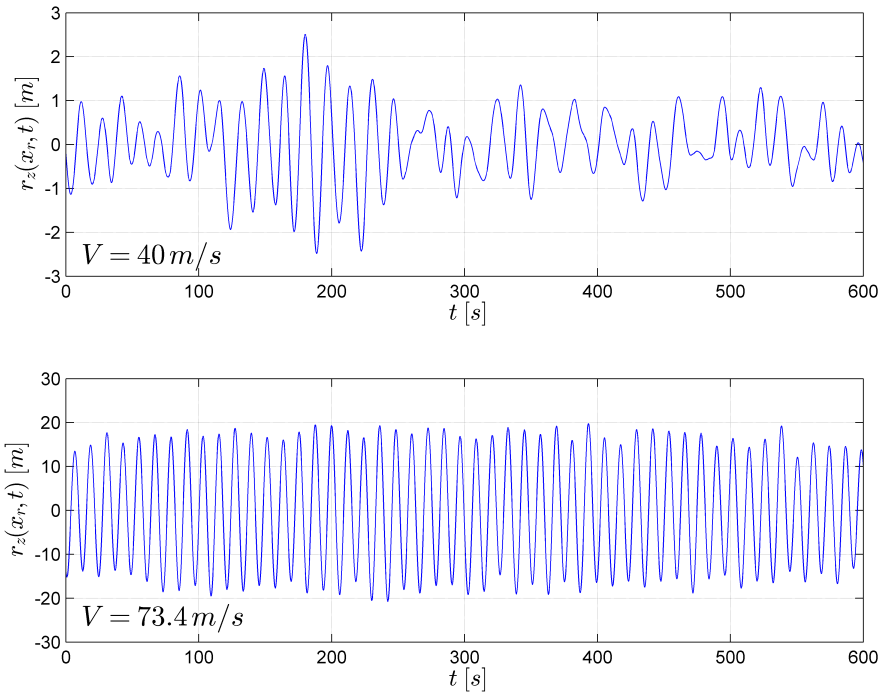

Figure 5.9: Time series simulation of dynamic response.

The time series simulation shows how the motion induced effect dominates at flutter velocity, making the response more narrow banded as opposed to the more broad banded response at 40 m/s.

5.4.3 Dual box 20 m c/c

The dynamic response for the $20\,m$ center to center configuration was also computed using a two mode approach with VA1 and TA1 at response location $x_r/L = 0.25$. The results are shown in fig. 5.10.

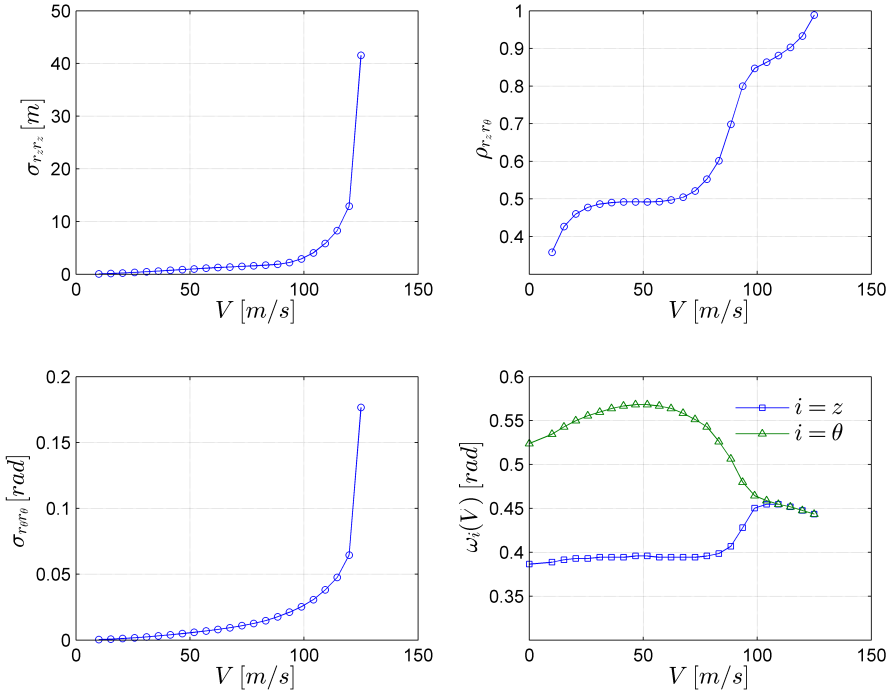

Figure 5.10: Top left: dynamic response in the vertical direction. Top right: covariance coefficient. Lower left: dynamic response in torsion. Lower right: development of in-wind resonance frequencies.

The response calculation confirms the stability limit in flutter at $125\,m/s$, in this case equal to the calculated critical velocity in sec. 5.3. The in-wind resonance frequency development shows a coupled frequency at about $100\,m/s$. The response spectra for $V = 40\,m/s$ and $V = 125\,m/s$ is shown in fig. 5.11.

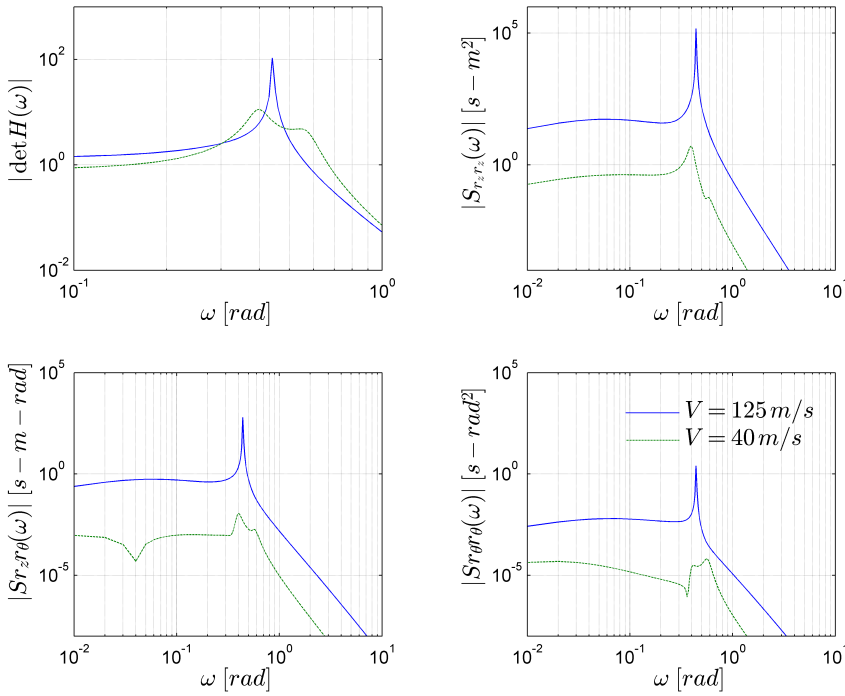

Figure 5.11: Top left: frequency-response spectrum. Top right: response spectrum in vertical movement. Lower left: cross spectrum between vertical and torsional movement. Lower right: response spectrum in torsional movement.

The different response spectra for this cross-sectional configuration also show a clear difference from having two peaks and a fairly broad banded response spectrum at the lower mean wind velocity, to having a peak at the flutter frequency for the flutter mean wind velocity. A time series simulation of $V = 40\,m/s$ and $V = 125\,m/s$ is presented in fig. 5.12. The time series simulation plots show the same effect that the motion induced effects have on the response, making it more narrow banded whilst at the lower wind velocity the response is more broad banded.

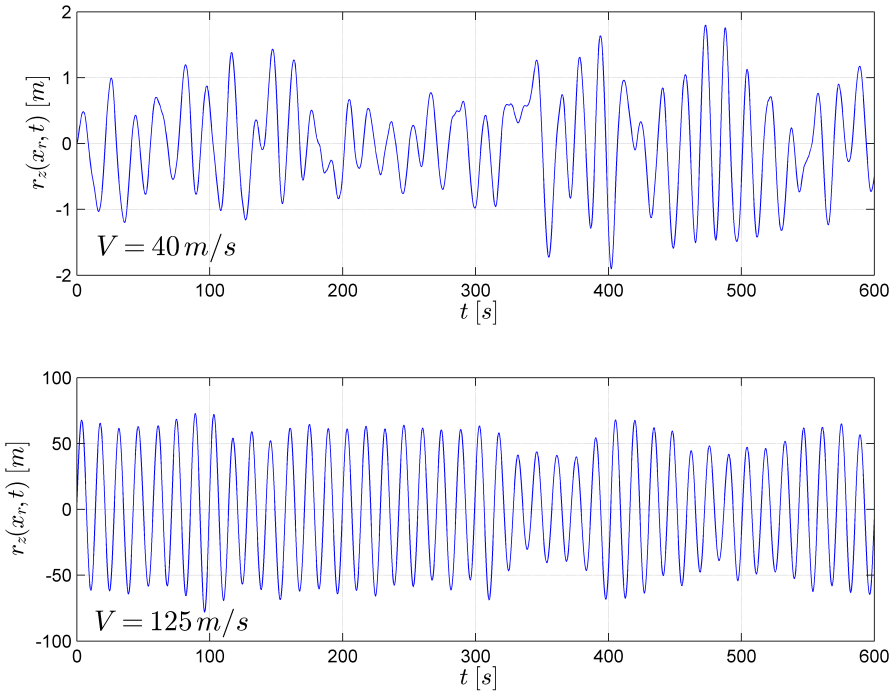

Figure 5.12: Time series simulation of dynamic response.

5.4.4 Dual box 30 m c/c

For the case of 30 m center-to-center configuration no stability limits were found in sec. 5.3, which is also the case for the response calculation. A response calculation was done up to $V = 140\,m/s$ and is shown in fig. 5.13.

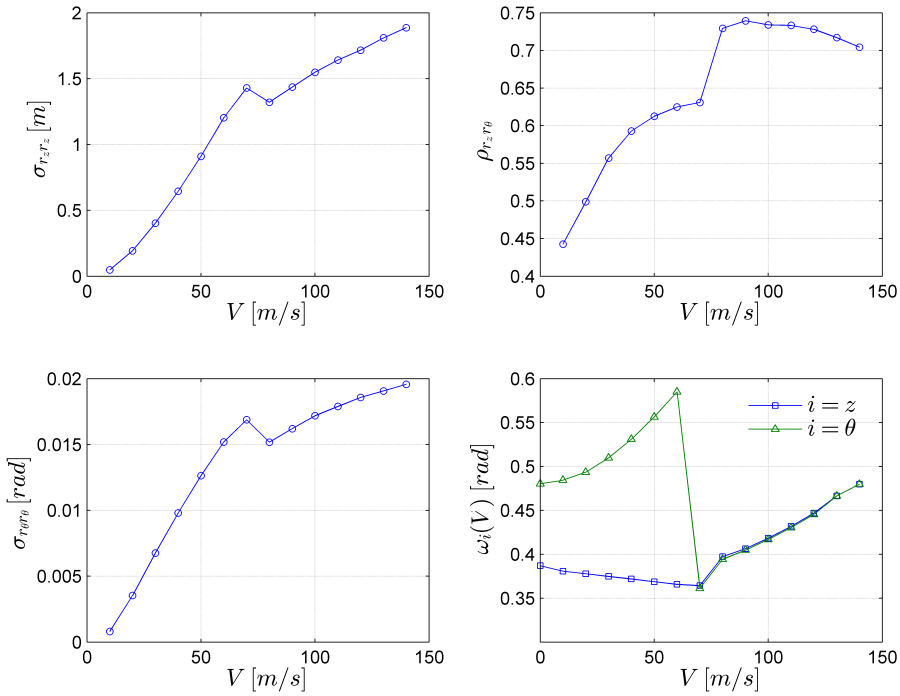

Figure 5.13: Top left: dynamic response in the vertical direction. Top right: covariance coefficient. Lower left: dynamic response in torsion. Lower right: development of in-wind resonance frequencies.

The response variances for the 30 m c/c configuration show a numerical instability around $V = 70\,m/s$ although no flutter limit was identified in sec. 5.3. The in-wind resonance frequencies show a coupling effect at the same point, however the convergence of the eigenfrequencies was found to be very unstable around $V = 70\,m/s$. The response spectra for mean wind velocities of $V = 40$, 70 and 140 m/s is shown in fig. 5.14.

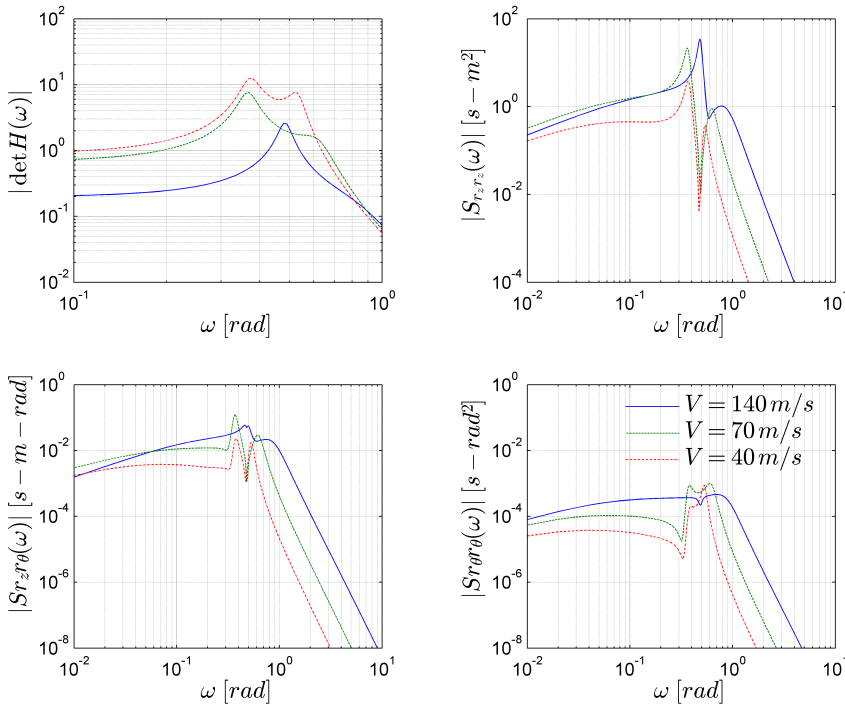

Figure 5.14: Top left: frequency-response spectrum. Top right: response spectrum in vertical movement. Lower left: cross spectrum between vertical and torsional movement. Lower right: response spectrum in torsional movement.

The frequency response spectrum shows a coupling effect for the highest mean wind velocity, but at the same time the absolute values of the frequency-response decreases with increasing V. The values of the response spectra are almost unchanged for the different velocities. A time series simulation was not done as no stability limits were found.

5.5 Summary and discussion

A summary of the stability limits found in sec. 5.3 are presented in table 5.8.

Table 5.8: Summary of stability limits.

c/c	15 m		20 m		30 m	
Stability limit	V_{cr} m/s	ω_r rad	V_{cr} m/s	ω_r rad	V_{cr} m/s	ω_r rad
Static divergence	93.6	0	-	-	-	-
Galloping	-	-	-	-	-	-
Dynamic limit in torsion	-	-	109[a]	0.07	-	-
Flutter	74.5	0.520	125	0.443	-	-

"-": stability limit was not identified.

a: limit found for highly extrapolated $\hat{V}$.

It is seen that all the stability limits calculated lie above the requirement of $V = 69.8\,m/s$ presented in sec. 4.6. The cross section with 15 m center-to-center gap is the one with the lowest critical velocities, and the flutter limit is close to the requirement but still above. When increasing the center-to-center distance to 20 m the critical velocities increase, and for the 30 m configuration none were identified at all.

The response results confirm the stability limits in flutter for the 15 m and 20 m configurations and shows what appears to be a stabilizing effect at lower wind velocities for these configurations. The stabilizing effect is shown in fig. 5.15, which plots the rate of change of the standard deviation in z-direction. It is seen for the 15 m and 20 m cases that the stabilization ends at the point where the modal coupling begins at around 60 m/s and 90 m/s. Also the drop at around 70 m/s for the 30 m c/c configuration is shown in the plot.

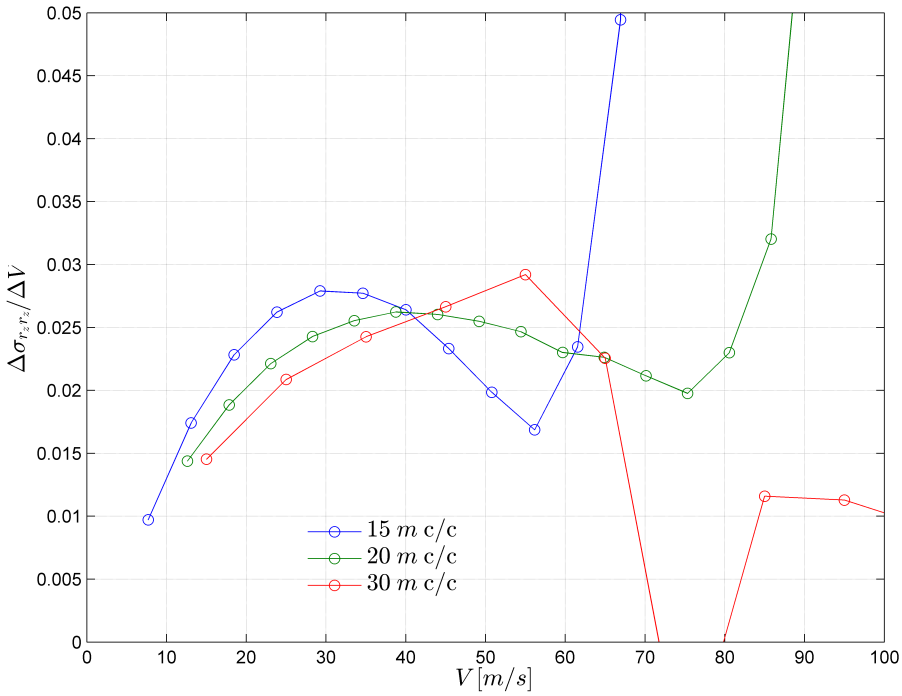

Figure 5.15: Rate of change of vertical dynamic response.

For the two smallest center-to-center configurations the rate of change of the response turns at the point of modal coupling. But for the 30 m c/c case the stabilization effect just continues, this is shown by fig. 5.14 where it is seen that $|\det H(\omega)|$ is decreasing with increasing wind loads, as the motion induced effects stabilizes the structure.

These results are highly governed by the aerodynamic derivatives, and thus they represent a significant uncertainty in the calculations. This uncertainty is further strengthened by the fact that the employed aerodynamic derivatives are not for the exact cross sections used and it is also observed that all stability limits obtained are in an extrapolated domain of the polynomial fits of the wind tunnel tests. This includes a stability limit found for the 20 m case at $\hat{V} = 121.2$ which is extrapolated far beyond the reduced velocities in the wind tunnel tests. The 30 m c/c case has a pair of aerodynamic derivatives that are very different from the other two cases, which may cause the numerical instability at around $V = 70\,m/s$.

Chapter 6

Conclusions

The numerical results indicate that the dual box girder has the required aerodynamic properties for slender suspension bridges with spans up to 3700 m. All identified stability limits were for larger critical mean wind velocity than what is required by standards.

It has been seen that increasing the center-to-center distance of the box sections leads to an increase of the critical mean wind velocity of the aerodynamic stability limits. For the widest dual box no stability limits were found at all.

From an aerodynamic stability point of view, the results suggest that a single-span suspension bridge with a dual box girder is a viable option for a bridge crossing the Sognefjord.

To ensure the validity of the stability limits, further work should include calculations using aerodynamic derivatives found by wind tunnel tests for the exact cross section in consideration.

Appendix A

ALVSAT

This appendix includes the input data for used to calculate the eigenfrequencies and eigenmodes in ALVSAT, as well as an example output.

A.1 ALVSAT input for the different configurations

Table A.1: ALVSAT input

	c/c		
Input	15 m	20 m	30 m
DG $[m]$	2.5	2.5	2.5
DC $[m]$	1.21	1.21	1.21
BG $[m]$	12.9	12.9	12.9
L $[m]$	3700	3700	3700
HM $[m]$	5.0	5.0	5.0
F $[m]$	370	370	370
NY $[m]$	34.24	34.24	34.24
{L1}	0	0	0
{L2}	0	0	0
MG $[kg/m]$	$14.54 \cdot 10^3$	$14.77 \cdot 10^3$	$15.24 \cdot 10^3$
MC $[kg/m]$	9677	9677	9677
H $[N]$	$774.8 \cdot 10^6$	$780.1 \cdot 10^6$	$790.7 \cdot 10^6$
EIZ $[Nm^2]$	$13.19 \cdot 10^{12}$	$21.4 \cdot 10^{12}$	$44.88 \cdot 10^{12}$
G $[m/s^2]$	9.807	9.807	9.807
S0 $[N]$	0	0	0
{S0}	0	0	0
{STR}	0	0	0
PI1 [-]	0.1819	0.1819	0.1819
PI2 [-]	0.1819	0.1819	0.1819
FI1 $[rad]$	0.3805	0.3805	0.3805
FI2 $[rad]$	0.3805	0.3805	0.3805
HR $[m]$	0.68	0.68	0.68
BC $[m]$	13.05	15.55	20.55
M $[kgm^2/m]$	$4.33 \cdot 10^6$	$6.351 \cdot 10^6$	$11.68 \cdot 10^6$
AC $[m^2]$	1.15	1.15	1.15
EIX $[Nm^2]$	$0.1847 \cdot 10^{12}$	$0.1847 \cdot 10^{12}$	$0.1847 \cdot 10^{12}$
EIW $[Nm^4]$	$10.39 \cdot 10^{12}$	$18.47 \cdot 10^{12}$	$41.56 \cdot 10^{12}$
GIT $[Nm^2]$	$0.1725 \cdot 10^{12}$	$0.1725 \cdot 10^{12}$	$0.1725 \cdot 10^{12}$
EC $[N/m^2]$	$200 \cdot 10^9$	$200 \cdot 10^9$	$200 \cdot 10^9$

A.2 Example output

```
 0000000000000000000000000000000000000000000000000000000000000000000000000000000000000000000000000000
 0.0                                                                                                  0.0
 0.0 SOGNEFJORDBRUA c/c 15m. rev. 23.05.2013                                                          0.0
 0.0 Dempning: 0,5 % strukturell dempning           0.0
 0.0 Lastfaktor på vind er 1.0 (r.p. 50 år)                                                           0.0
 0.0                                                                                                  0.0
 0000000000000000000000000000000000000000000000000000000000000000000000000000000000000000000000000000
 0.0..................................................................................................0.0
 0.0..................................................................................................0.0
 0.0.............................. Analysed by ......................................................0.0
 0.0..................................................................................................0.0
 0.0..................................................................................................0.0
 0.0..................................................................................................0.0
 0.0.....000.....0000........000.....000...0000000.......000.....00000000000.0.0
 0.0....0   0....0  0........0 0.....0 0..0       0.....0   0....0         0.0.0
 0.0...0     0...0  0........0 0.....0 0.0         0...0     0...0         0.0.0
 0.0..0       0..0  0........0 0.....0 0.0         0..0       0..0         0.0.0
 0.0.0    0    0.0  0........0 0.....0 0.0   000   0.0    0    0.00000 00000.0.0
 0.0.0   0.0   0.0  0........0 0.....0 0.0  0...0000.0   0.0   0.....0 0.....0.0
 0.0.0  0...0  0.0  0........0 0.....0 0.0  0........0  0...0  0.....0 0.....0.0
 0.0.0  0...0  0.0  0........0 0.....0 0.0   0.......0  0...0  0.....0 0.....0.0
 0.0.0  0...0  0.0  0........0  0...0  0.0    0......0  0...0  0.....0 0.....0.0
 0.0.0  0...0  0.0  0........0  0...0  0..0    0.....0  0...0  0.....0 0.....0.0
 0.0.0  0...0  0.0  0........0  0...0  0...0    0....0  0...0  0.....0 0.....0.0
 0.0.0  0...0  0.0  0.........0  0.0  0.....0    0..0  0...0  0.....0 0.....0.0
 0.0.0  0...0  0.0  0.........0  0.0  0......0    0.0  0...0  0.....0 0.....0.0
 0.0.0  00000  0.0  0.........0  0.0  0.......0    0.0  00000  0.....0 0.....0.0
 0.0.0         0.0  0..........0  0  0.........0   0.0         0.....0 0.....0.0
 0.0.0         0.0  0..........0  0  0..........0  0.0         0.....0 0.....0.0
 0.0.0         0.0  0..........0     0..........0  0.0         0.....0 0.....0.0
 0.0.0  00000  0.0  0...........0   0...........0  0.0  00000  0.....0 0.....0.0
 0.0.0  0...0  0.0  0...........0   0....0000...0  0.0  0...0  0.....0 0.....0.0
 0.0.0  0...0  0.0  00000000....0   0....0   000   0.0  0...0  0.....0 0.....0.0
 0.0.0  0...0  0.0         0.....0 0.....0         0.0  0...0  0.....0 0.....0.0
 0.0.0  0...0  0.0         0.....0 0.....0         0.0  0...0  0.....0 0.....0.0
 0.0.0  0...0  0.0         0.....000......0       0..0  0...0  0.....0 0.....0.0
 0.0.0000...0000.00000000000......0........0000000...0000...0000.....000.....0.0
 0.0..................................................................................................0.0
 0.0..................................................................................................0.0
 0.0.....................                                          ......................0.0
 0.0..................... Version 3.7 / 940628 /                    ......................0.0
 0.0.....................                                          ......................0.0
 0.0..................................................................................................0.0
 0.0..................................................................................................0.0
 0.0...000000000000000000000000000000000000000000000000000000000000000000000000000000000000000...0.0
 0.0...0                                                                                        0...0.0
 0.0...0  Developed by:   SINTEF div. of Structural Engineering                                 0...0.0
 0.0...0                  N-7034 TRONDHEIM  NTH                                                 0...0.0
 0.0...0                                                                                        0...0.0
 0.0...0                  Excecuted 13-05-24 at 10:57:14                                        0...0.0
 0.0...0                                                                                        0...0.0
 0.0...0000000000000000000000000000000000000000000000000000000000000000000000000000000000000000...0.0
 0.0..................................................................................................0.0
 0.000000000000000000000000000000000000000000000000000000000000000000000000000000000000000000000.0
 0....................................................................................................0.0
 0000000000000000000000000000000000000000000000000000000000000000000000000000000000000000000000000000
1RUN MODES

                           HOR   VER   TOR
        FRECUENCY ANALYSES:  0     1     1
        STATIC    ANALYSES:  0     0     0
        DYNAMIC   ANALYSES:  0     0     0
     STRUCTURAL PARAMETERS :

        LENGTH OF BRIDGE SPAN             L    =  3700.
        MINIMUM HANGER LENGTH             HM   =  5.000
        SAG OF MAIN CABLES                F    =  370.0
        HOGGING OF THE GIRDER             NY   =  34.24
        LENGTH OF SIDE SPAN SECOND. CABLE L1   =  .0000
        SAG OF SECONDARY CABLES           FS   =  .0000
        MASS   OF GIRDER                  MG   =  .1454E+05
        MASS   OF MAIN CABLES (ONE CABLE) MC   =  9677.
```

```
          TENSION IN MAIN CABLE (ONE CABLE) H    =  .7748E+09
          RIGIDITY OF GIRDER                EI   =  .1319E+14
          ACCELERATION OF GRAVITY           G    =  9.807
          TYPICAL DIMENSION OF GIRDER       DG   =  2.500
          TYPICAL DIMENSION OF ONE CABEL    DC   =  1.210
          TYPICAL WIDTH OF THE GIRDER       BG   =  12.90
          TENSION IN GIRDER                 SO   =  .0000
          TENSION IN SECOND. CABLES         FO   =  .0000
          INITIAL STRAIN IN SECOND. CABLES  STR  =  .0000
          LENGTH OF BACKSTAYS IN % OF       PI1  =  .1819
          THE LENGTH OF THE BRIDGE SPAN     PI2  =  .1819
          CABLE SLOPE OF BACKSTAY 1:        FI1  =  .3805
          CABLE SLOPE OF BACKSTAY 2:        FI2  =  .3805
          DISTANCE BETWEEN POINT OF ATTACHMENT
          FOR HANGERS AND THE CENTER OF
          GYRATION                          HR   =  .6800
          HALF THE DISTANCE BETWEEN
          THE CABLES                        BC   =    13.0500
          MASS MOMENT OF INERTIA            M    =  .4330E+07
          HORIZONTAL COMPONENT OF
          CROSS SECTION OF EACH CABLE       AC   =  1.150
          BENDING STIFFNESS OF GIRDER       EIX  =  .1847E+12
          WARPING RESISTANCE                EIW  =  .1039E+14
          TORSIONAL STIFFNESS               GIT  =  .1725E+12
          MODULUS OF ELASTICITY OF CABLE    EC   =  .2000E+12

1DATA FOR FREQUENCY ANALYSES

                                              HOR VER TOR
          NUMBER OF COEFFICIENTS (NFC):       8    8    8
          NUMBER OF NORMAL MODES (NNM):       8    8    8


          FREQUENCY RANGE FOR ITERATION SEARCH :

          LOWER LIMIT FOR VERTICAL MODE    VOMI =  .0000
          UPPER LIMIT FOR VERTICAL MODE    VOMA =  .0000
          LOWER LIMIT FOR TORSIONAL MODE   TOMI =  .0000
          UPPER LIMIT FOR TORSIONAL MODE   TOMA =  .0000
          MAXIMUM NUMBER OF ITERATIONS     NMAX =   30
          NO. OF INTERVALS IN
          FREQUENCY RANGE IN ASYM          ITFR =   50
          BRIDGE HELD/FREE AT THE ENDS     LC   =    1
          LC=0 : FREE  LC=1 : HELD AT ONE END

 ENVIRONMENTAL DATA

          ESDU  SPECTRUM (ISTYP=2)
          ------------------------
          WIND SPEED AT THE LEVEL OF THE BRIDGE (UREF) =   38.60
          INTEGRAL LENGTH SCALE OF U IN X-DIR (XLU)    =   448.2
          TURBULENCE INTENSITY U COMPONENT             =   .1370
          CHARACTERISTIC HEIGHT ABOVE THE
          GROUND OF THE BRIDGE DECK                    =   62.00
          WIND VELOCITY 10 M ABOVE THE GROUND          =   29.16
          TURBULENCE INTENSITY OF VERTICAL VELOCITY    =   .7551E-01
          INTEGRAL LENGTH SCALE OF U IN Y-DIR          =   127.4
          INTEGRAL LENGTH SCALE OF U IN Z-DIR          =   81.11
          INTEGRAL LENGTH SCALE OF W IN X-DIR          =   37.56
          INTEGRAL LENGTH SCALE OF W IN Y-DIR          =   21.35
          INTEGRAL LENGTH SCALE OF W IN Z-DIR          =   27.18
          ALFA VALUE IN MODIFIED VON KARMAN SPECTRUM   =   .5884
          BETA1 IN MODIFIED VON KARMAN SPECTRUM        =   .6259
          BETA2 IN MODIFIED VON KARMAN SPECTRUM        =   .3741
          TERRAIN ROUGHNESS (Z0)                       =   .2320E-01


          ESDU   COHERENCE FUNCTION (ICTYP=2)
          -----------------------------------
          DECAY FACTOR HORIZONTAL SEPARATION (U,W)=    1.000        1.000
          DECAY FACTOR VERTICAL SEPARATION  (U,W) =    1.000        1.000
          AVERAGE CORRELATION BETWEEN LOADS
          ON GIRDER AND CABLES                    =    .9000
          DENSITY OF AIR:                         =    1.250

 COEFFICIENTS (FORM FACTORS)
```

```
          CDG(1:5) :   .8260       .0000       .0000       .0000       .8260
          CDDG(1:5):   .0000       .0000       .0000       .0000       .0000
          CDC(1:5) :   1.000       .0000       .0000       .0000       1.000
          CLG(1:5) :  -.2510       9.700       2.000       1.000      -.2510
          CLDG(1:5):   2.401       9.700       2.000       1.000       2.401
          CMG(1:5) :   .2000E-02   9.700       2.000       1.000       .2000E-02
          CMDG(1:5):   .7700       9.700       2.000       1.000       .7700



1DATA FOR STATIC ANALYSIS

          NUMBER OF INTERVAL FOR RESPONS CALCULATION
                  HOR VER  TOR
                 10   10   10



 DATA FOR DYNAMIC ANALYSES

                                          HOR    VER   TOR
          CROSS TERMS BETWEEN MODES:      1      1      1
          IRS                       :     0      0      0



          DURATION OF STORM         :    600.




          CRITICAL DAMPING RATIOS :

          CRDR( 1,1:3) :   .5000E-02 -.7400E-02  .1410E-01
          CRDR( 2,1:3) :   .5000E-02 -.7700E-02  .9600E-02
          CRDR( 3,1:3) :   .5000E-02 -.6200E-02  .7400E-02
          CRDR( 4,1:3) :   .5000E-02 -.5900E-02  .6500E-02
          CRDR( 5,1:3) :   .5000E-02 -.4300E-02  .6100E-02
          CRDR( 6,1:3) :   .5000E-02  .3100E-02  .5900E-02
          CRDR( 7,1:3) :   200.0      200.0      200.0
          CRDR( 8,1:3) :   200.0      200.0      200.0
1         ******************************************
         ********** VERTICAL   RESPONSE *************
         ******************************************

         ***** OUTPUT FROM THE FREQUENCY ANALYSIS *****



          **********  SYMMETRIC  MODES  **********


           MODE       PERIOD      FREQUENCY
           NO:          SEC        RAD/SEC

              1      12.69690        .49486

              2       9.22855        .68084

              3       6.68290        .94019

              4       4.82508       1.30219

          FOURIER CONSTANTS :

  MODE      1           2           3           4

        -.9095E+00    .1000E+01    .1484E+00    .3896E-01
```

```
        .1000E+01    .9243E+00    .7306E-01    .1556E-01

        .6241E-01   -.2172E+00    .1000E+01    .1547E-01

        .1898E-01   -.5015E-01   -.2244E-01    .1000E+01

        .8360E-02   -.2046E-01   -.7343E-02   -.6556E-02

        .4418E-02   -.1049E-01   -.3470E-02   -.2362E-02

        .2618E-02   -.6108E-02   -.1944E-02   -.1192E-02

        .1678E-02   -.3873E-02   -.1206E-02   -.7005E-03


  MODES OF VIBRATION :         1         2         3         4

     OBSERVATION
     POINT :
           .00            .0000E+00  .0000E+00  .0000E+00  .0000E+00
        185.00            .3889E+00  .3390E+00  .7302E+00  .9047E+00
        370.00            .6031E+00  .8047E+00  .1088E+01  .8495E+00
        555.00            .6053E+00  .1247E+01  .8592E+00 -.1048E+00
        740.00            .3986E+00  .1515E+01  .1785E+00 -.9120E+00
        925.00            .1241E-01  .1535E+01 -.5401E+00 -.6845E+00
       1110.00           -.4793E+00  .1286E+01 -.8681E+00  .3262E+00
       1295.00           -.9966E+00  .8613E+00 -.6047E+00  .1012E+01
       1480.00           -.1447E+01  .3914E+00  .8981E-01  .6204E+00
       1665.00           -.1752E+01  .2849E-01  .7971E+00 -.4198E+00
       1850.00           -.1861E+01 -.1036E+00  .1093E+01 -.9658E+00
1         **********  ASYMMETRIC MODES  **********/

          MODE       PERIOD      FREQUENCY
          NO:          SEC        RAD/SEC

             1      16.26597        .38628

             2       8.47854        .74107

             3       5.64770       1.11252

             4       4.23090       1.48507


         FOURIER CONSTANTS :

  MODE      1           2           3           4

        .1000E+01    .3691E-02    .7302E-03    .2582E-03

       -.3691E-02    .1000E+01    .3641E-03    .1030E-03

       -.7288E-03   -.3668E-03    .1000E+01   -.2260E-06

       -.2578E-03   -.1039E-03    .0000E+00    .1000E+01

       -.1190E-03   -.4445E-04    .0000E+00    .0000E+00

       -.6405E-04    .0000E+00    .0000E+00    .0000E+00

       -.3812E-04    .0000E+00    .0000E+00    .0000E+00

       -.2435E-04    .0000E+00    .0000E+00    .0000E+00


  MODES OF VIBRATION :         1         2         3         4

     OBSERVATION
     POINT :
           .00            .0000E+00  .0000E+00  .0000E+00  .0000E+00
        185.00            .3051E+00  .5878E+00  .8090E+00  .9511E+00
        370.00            .5845E+00  .9511E+00  .9511E+00  .5878E+00
        555.00            .8085E+00  .9511E+00  .3090E+00 -.5878E+00
        740.00            .9531E+00  .5878E+00 -.5878E+00 -.9511E+00
        925.00            .1003E+01 -.4551E-07 -.1000E+01  .9103E-07
       1110.00            .9531E+00 -.5878E+00 -.5878E+00  .9511E+00
```

```
        1295.00            .8085E+00 -.9511E+00  .3090E+00  .5878E+00
        1480.00            .5845E+00 -.9511E+00  .9511E+00 -.5878E+00
        1665.00            .3051E+00 -.5878E+00  .8090E+00 -.9511E+00
        1850.00           -.4464E-07  .9103E-07 -.1365E-06  .1821E-06


         ONE START FREQUENCY TRIED IN ASYM
         NUMBER OF ITERATIONS NECESSARY:      4
1        ******************************************
        ********** TORSIONAL  RESPONSE *************
        ******************************************


        ***** OUTPUT FROM THE FREQUENCY ANALYSIS *****



         **********  SYMMETRIC  MODES  **********


          MODE       PERIOD      FREQUENCY
          NO:          SEC        RAD/SEC

             1       9.32999        .67344

             2       6.98058        .90009

             3       4.56113       1.37755

             4       3.27937       1.91598


         FOURIER CONSTANTS :

  MODE      1           2           3           4

        .1000E+01    .5351E+00    .7116E-01    .2148E-01

       -.5393E+00    .1000E+01    .3522E-01    .8570E-02

       -.5238E-01   -.7354E-01    .1000E+01    .8560E-02

       -.1645E-01   -.1947E-01   -.1041E-01    .1000E+01

       -.7321E-02   -.8234E-02   -.3434E-02   -.3598E-02

       -.3902E-02   -.4288E-02   -.1633E-02   -.1303E-02

       -.2327E-02   -.2525E-02   -.9192E-03   -.6604E-03

       -.1499E-02   -.1615E-02   -.5725E-03   -.3895E-03


  MODES OF VIBRATION :         1         2         3         4

     OBSERVATION
     POINT :
           .00            .0000E+00  .0000E+00  .0000E+00  .0000E+00
        185.00           -.1543E+00  .4526E+00  .7187E+00  .8986E+00
        370.00           -.1907E+00  .8875E+00  .1043E+01  .8314E+00
        555.00           -.1039E+00  .1192E+01  .7801E+00 -.1280E+00
        740.00            .9029E-01  .1284E+01  .8541E-01 -.9296E+00
        925.00            .3692E+00  .1145E+01 -.6271E+00 -.6946E+00
       1110.00            .6861E+00  .8054E+00 -.9365E+00  .3184E+00
       1295.00            .1000E+01  .3574E+00 -.6577E+00  .1001E+01
       1480.00            .1263E+01 -.8511E-01  .4312E-01  .6058E+00
       1665.00            .1437E+01 -.4076E+00  .7500E+00 -.4351E+00
       1850.00            .1499E+01 -.5239E+00  .1044E+01 -.9811E+00
1        **********  ASYMMETRIC MODES  **********/

          MODE       PERIOD      FREQUENCY
          NO:          SEC        RAD/SEC

             1      11.16264        .56288
```

```
           2       5.73101       1.09635

           3       3.82996       1.64054

           4       2.87441       2.18590

        FOURIER CONSTANTS :

MODE      1           2           3           4

       .1000E+01    .1123E-02    .2240E-03    .7981E-04

      -.1123E-02    .1000E+01    .1119E-03    .3190E-04

      -.2238E-03   -.1122E-03    .1000E+01   -.2145E-07

      -.7977E-04   -.3199E-04    .0000E+00    .1000E+01

      -.3714E-04   -.1379E-04    .0000E+00    .0000E+00

      -.2020E-04    .0000E+00    .0000E+00    .0000E+00

      -.1217E-04    .0000E+00    .0000E+00    .0000E+00

      -.7881E-05    .0000E+00    .0000E+00    .0000E+00


MODES OF VIBRATION :         1         2         3         4

   OBSERVATION
   POINT :
         .00            .0000E+00  .0000E+00  .0000E+00  .0000E+00
       185.00           .3078E+00  .5878E+00  .8090E+00  .9511E+00
       370.00           .5868E+00  .9511E+00  .9511E+00  .5878E+00
       555.00           .8089E+00  .9511E+00  .3090E+00 -.5878E+00
       740.00           .9517E+00  .5878E+00 -.5878E+00 -.9511E+00
       925.00           .1001E+01 -.4551E-07 -.1000E+01  .9103E-07
      1110.00           .9517E+00 -.5878E+00 -.5878E+00  .9511E+00
      1295.00           .8089E+00 -.9511E+00  .3090E+00  .5878E+00
      1480.00           .5868E+00 -.9511E+00  .9511E+00 -.5878E+00
      1665.00           .3078E+00 -.5878E+00  .8090E+00 -.9511E+00
      1850.00          -.4525E-07  .9103E-07 -.1365E-06  .1821E-06


       ONE START FREQUENCY TRIED IN ASYM
       NUMBER OF ITERATIONS NECESSARY:      5

       ***** CPU-TIME USED =    12.1200 *****
```

Appendix B

Eigenmodes

This appendix contains plots of all 16 mode shapes found with ALVSAT.

B.1 Mode shape plots

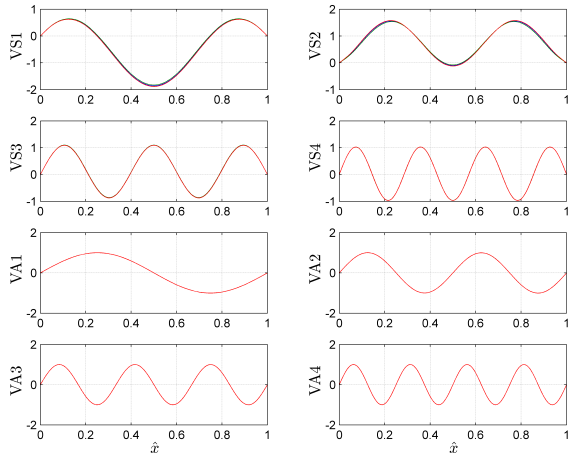

Figure B.1: Vertical eigenmodes. Line colors: *blue = 15 m c/c, green = 20 m c/c and red = 30 m c/c.*

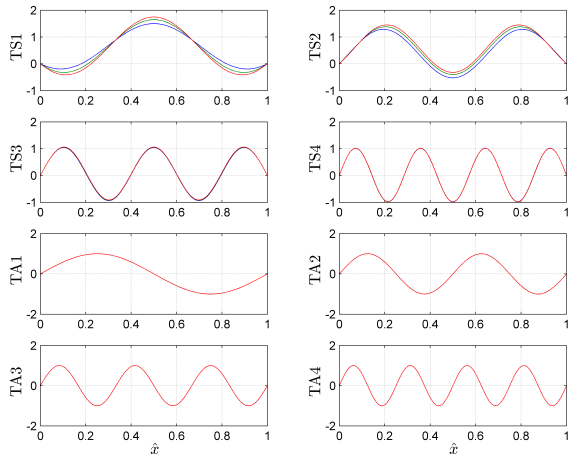

Figure B.2: Torsional eigenmodes. Line colors: *blue = 15 m c/c, green = 20 m c/c and red = 30 m c/c.*

Appendix C

Aerodynamic derivative coefficients

This appendix contains tables with coefficients used in the polynomial fit of the aerodynamic derivatives.

Table C.1: Bridge with 15 m c/c between box sections [3]

$U\,[m/s]$	$U/(n_r b)\,[-]$	$U/(n_\phi b)\,[-]$	$\sigma_{r/h}\,[\%]$	$\sigma_\phi\,[\text{deg}]$	H_1^*	H_2^*	H_3^*	H_4^*	A_1^*	A_2^*	A_3^*	A_4^*
1.51*	18.07	13.54	3.78	0.47	-20.17	5.7	46.04	1.04	-2.11	-4.36	-6.3	0.71
2.57	31	22.85	7.52	0.61	-16.06	17.47	108.05	10.79	-0.58	-3.88	-12.34	-3.99
3.47	40.52	30.62	10.78	0.46	-14.73	96.46	159.19	-18.25	-2.21	-18.21	-13.73	5.37
4.43	51.07	39.72	10.14	0.45	-35.2	51.44	231.56	-24.16	-9.7	-31.38	2.7	1.17
5.37	63.16	49.04	14.53	0.64	-36.38	60.8	414.43	-12.92	-7.97	-29.03	17.94	0.08
				$\mathbf{c}_2$	-0.0043	-0.0344	0.1638	-0.0039	-0.0028	-0.0074	0.0385	-0.0002
				$\mathbf{c}_1$	-0.3443	3.0294	0.0040	-0.1118	0.0208	-0.3430	-1.5172	0.0392
				$\mathbf{c}_0$	0.1591	-3.4781	4.2271	2.3987	0.3247	1.3018	0.1633	-0.5460

* wind speeds with derivatives not included in the polynomial fit

$P\{U_r\} = c_2 U_r^2 + c_1 U_r + c_0 \quad U_r = U/(nb)$

In-wind frequencies at model scale, n_r and n_ϕ in Hz.

Table C.2: Bridge with 20 m c/c between box sections [3]

$U\,[m/s]$	$U/(n_r b)\,[-]$	$U/(n_\phi b)\,[-]$	$\sigma_{r/h}\,[\%]$	σ_ϕ [deg]	H_1^*	H_2^*	H_3^*	H_4^*	A_1^*	A_2^*	A_3^*	A_4^*
1.39*	16.56	12.41	3.63	0.37	-16.34	22.24	43.98	-4.71	-5.3	-22.35	-26.52	2.86
2.47	29.44	21.81	7.18	0.48	-18.88	33.25	92.73	-3.1	-1.39	-26.07	-34.87	3.97
3.48	40.3	30.84	7.86	0.51	-28.05	21.44	171.6	-28.15	-4.21	-25.84	-26.73	9.88
4.4	50.11	38.6	10.45	0.42	-41.14	56.52	210.68	-31.37	1.49	-47.89	-45.89	1.28
5.33	61.02	46.59	11.35	0.39	-65.46	35.05	403.16	-43.58	5.57	-46.33	-32.52	10.59
6.36	72.01	53.96	16.34	0.4	-52.47	201.51	447.87	-34.25	2.69	-138.31	-80.83	0.78
7.15	79.6	62.61	20.63	0.46	-78.1	76.32	798.82	-40.75	-2.9	-156.3	-49.76	-0.52
8.21	87.58	73.97	26.25	0.57	-80.99	40.13	816.83	-51.29	-5.45	-158.52	-33.74	-3.75
9.06	101.98	84.17	31.74	0.6	-83.54	120.71	940.17	-58.25	-2.34	-112.58	48.01	3.16
				$\mathbf{c}_2$	0.0003	-0.0128	0.0896	0.0004	-0.0010	0.0030	0.0392	-0.0020
				$\mathbf{c}_1$	-0.9396	2.3909	4.8589	-0.6300	0.0861	-2.2708	-3.2142	0.1788
				$\mathbf{c}_0$	3.5081	-9.8447	-35.0403	2.5589	-1.3091	16.8237	12.1639	1.1391

* wind speeds with derivatives not included in the polynomial fit

$P\{U_r\} = c_2 U_r^2 + c_1 U_r + c_0 \quad U_r = U/(nb)$

In-wind frequencies at model scale, n_r and n_ϕ in Hz.

Table C.3: Bridge with 30 m c/c between box sections [3]

$U\,[m/s]$	$U/(n_r b)\,[-]$	$U/(n_\phi b)\,[-]$	$\sigma_{r/h}\,[\%]$	$\sigma_\phi\,[\text{deg}]$	H_1^*	H_2^*	H_3^*	H_4^*	A_1^*	A_2^*	A_3^*	A_4^*
1.42*	17.61	13.91	3.68	0.49	-29.99	11.79	72.02	-8.04	-15.28	-33.57	-5.34	6.41
2.55	33.02	24.66	7.53	0.66	-44.62	11.69	150.03	22.56	7.28	-44.43	-24.62	15.14
3.53	45.05	32.49	9.51	0.76	-61.19	49.14	263.46	5.2	18.04	-17.2	-119.27	25.6
4.39	55.63	40.42	12.97	0.69	-74.55	10.58	353.02	-23.34	12.15	-51.44	-79.37	46.54
5.41	65.23	47.57	17.04	0.77	-63.4	84.68	460.77	-30.95	16.27	-91.31	-207.26	9.54
6.47	80.49	56.42	24.7	0.84	-61.44	119.22	537.97	-36.38	17.88	-69.93	-184.31	34.7
7.32	90.01	61.89	30.53	0.88	-82.97	148.06	647.03	-47.58	25.17	-83.66	-236.88	34.5
8.28	99.74	65.13	35.49	0.83	-98.14	188.41	768.39	-52.37	23.72	-182.19	-359.06	23.93
8.96*	105.3	74.57	41.74	0.85	-117.17	58.7	1023.7	-61.89	21.28	-255.54	-269.66	8.96
				$\mathbf{c}_2$	0.0056	0.0635	0.1096	-0.0081	-0.0005	-0.0343	-0.0749	-0.0054
				$\mathbf{c}_1$	-1.3998	-1.4858	4.0865	0.1358	0.2937	0.2520	0.1815	0.8218
				$\mathbf{c}_0$	-3.0938	3.9778	-0.6063	7.2128	0.1443	-5.8488	-1.3881	-0.8680

* wind speeds with derivatives not included in the polynomial fit

$P\{U_r\} = c_2 U_r^2 + c_1 U_r + c_0 \quad U_r = U/(nb)$

In-wind frequencies at model scale, n_r and n_ϕ in Hz.

Appendix D

MATLAB scripts

D.1 Mode shapes

The mode shapes were generated from Fourier coefficient using the script *MODEGEN.m*, where the Fourier coefficients and eigenfrequencies were loaded from separate files.

MODEGEN.m

```
%Mode shape generator
%This script generates plots of the mode shapes, and also a mode ...
    shape
%matrices PHI. rev. 2 | 11.04.2013 SLW
close all
clear all
%***USER INPUT***
%Inputfiles and current directory
cd('C:\Users\Simen\Master 2013\MyFolder');
InputFC='FC 15m cc.txt';
InputOMEGA='Omega 15m cc.txt';


%MODEGEN Output
writeOP=0;
Outputname='PHI 15m cc.txt';

%PLOT OPTIONS
plotmode=0;
normalize=0;
loadPHI=0;
twomodeOP=1;

%Structural properties
L=3700;
Np=370; %Number of points

%Specify number of modes (Number of Lateral, Vertical or ...
    Torsional modes)
NL=0; NV=8; NT=8;

NFC=8; %Number of fourier coefficients. For computational ...
    purposes NFC=NL/V/T.

%***END USER INPUT***
%There are always an even number of modes, where half of them ...
    are symmetric
%and the other half are antisymmetric.
NLS=NL/2; NLA=NLS; NVS=NV/2; NVA=NVS; NTS=NT/2; NTA=NTS;
```

```
36
37 %Total number of modes
38 NMOD=NLS+NLA+NVS+NVA+NTS+NTA;
39
40 %Importing the coefficients from .txt file. The coefficients ...
       should be
41 %arranged as in ALVSAT result: VS,VA,TS,TA (provided no ...
       horizontal modes).
42 if loadPHI==0;
43
44 FCS=importdata(InputFC);
45
46 FVS=FCS(1:NFC,1:NVS);
47
48 FVA=FCS(NFC+1:2*NFC,1:NVA);
49
50 FTS=FCS(2*NFC+1:3*NFC,1:NTS);
51
52 FTA=FCS(3*NFC+1:4*NFC,1:NTA);
53
54 clear FCS
55 FCS=[FVS,FVA,FTS,FTA];
56
57
58 %Generating mode shapes
59 x=linspace(0,L,Np);
60 xred=x./L;
61
62 %Modeshapes
63 PVS=zeros(Np,NVS);
64 PVA=zeros(Np,NVA);
65 PTS=zeros(Np,NTS);
66 PTA=zeros(Np,NTA);
67
68 for k=1:NFC
69     PVS=PVS + sin((2*k-1)*pi*xred')*FVS(k,:);
70     PVA=PVA + sin((2*k)*pi*xred')*FVA(k,:);
71     PTS=PTS + sin((2*k-1)*pi*xred')*FTS(k,:);
72     PTA=PTA + sin((2*k)*pi*xred')*FTA(k,:);
73 end
74
75 PHI=[PVS,PVA,PTS,PTA];
76
77 if writeOP==1;
78 dlmwrite(Outputname,PHI,'\t');
79 end
80 end
81
82 OMEGA=importdata(InputOMEGA);
```

```
83  OMEGA=OMEGA(:,3);
84
85  %Normalize plots
86  if normalize==1;
87     for n=1:NMOD
88         c=max(abs(PHI(:,n)));
89         PHI(:,n)=(1/c).*PHI(:,n);
90     end
91  end
92
93
94  %Generate plots for all modes
95  if plotmode==1
96  NW=floor(NMOD/4);
97  NPLOT=NMOD;
98  NWEND=0;
99  if rem(NMOD,4)≠0;
100      NWEND=1;
101      NPLOTEND=rem(NMOD,4);
102 end
103
104 %Modenumbers
105 modnum=[1:1:NV,1:1:NT];
106
107
108 for n=1:NW
109     figure
110     for m=1:4;
111         k=(4*(n-1)+m);
112         subplot(4,1,m)
113         plot(xred,PHI(:,k));
114         xlabel('x/L');
115         str0=num2str(modnum(k));
116         if k>NV;
117             str1=strcat('\phi_{\theta',str0,'}');
118         else
119             str1=strcat('\phi_{z',str0,'}');
120         end
121         ylabel(str1);
122         grid on
123     end
124 end
125
126 if NWEND==1;
127     figure
128     for n=1:NPLOTEND
129         k=4*NW+n;
130         subplot(4,1,m)
131         plot(xred,PHI(:,k));
```

```
132          xlabel('x/L');
133          if k>NV;
134              str1=strcat('\phi_{\theta',str0,'}');
135          else
136              str1=strcat('\phi_{z',str0,'}');
137          end
138          ylabel(str1);
139          grid on
140      end
141  end
142  end
143
144
145  %Generate two mode output?
146  if  twomodeOP==1;
147      modes=input('Which modes?[\phi_z \phi_{theta}]');
148      opname=input('Output filename?(no extension) ');
149      str1=strcat(opname,'.txt');
150      opPHI=[PHI(:,modes(1)),PHI(:,modes(2))];
151      dlmwrite(str1,opPHI,'\t');
152      str2=strcat(opname,'_omega.txt');
153      opOMEGA=[OMEGA(modes(1)),OMEGA(modes(2))];
154      dlmwrite(str2,opOMEGA,'\t');
155  end
```

D.2 Flutter

The flutter solutions were calculated using a script *Flutter.m* shown below, if the Theodorsen aerodynamic derivatives are used they are generated with the script *aeroplate.m*.

Flutter.m

```
%This script computes the critical wind velocity of flutter ...
    instability
%using two modes.
%—Simen L Walbaekken 16.04.2013
cd('C:\Users\Simen\Master 2013\MyFolder')

clear all
close all

%Basic structural properties, options for aerodynamic ...
    derivatives and the
%two modes including eigenfrequencies are imported from text files.
%User input: filenames and wind velocity search
Nv=100;
Vmin=1;
Vmax=130;
plotAD=0;
ADalt=1;

Inp=dlmread('Data 15m cc.txt','\t',[2,0,2,9]);
OMEGA=importdata('15m cc VA1—TA1(5—13)_omega.txt');
PHI=dlmread('15m cc VA1—TA1(5—13).txt');
ADfile='AD 15m cc.txt';



mZ=Inp(1); mT=Inp(2); zetaZ=Inp(3); zetaT=Inp(4); rho=Inp(7);
B=Inp(8); L=Inp(9);

omegaZ=OMEGA(1);
omegaT=OMEGA(2);

betaZ=(rho*B^2)/mZ;
betaT=(rho*B^4)/mT;
alfa=omegaT/omegaZ;

%Modeshapes
phiZ=PHI(:,1);
phiT=PHI(:,2);
```

```
38
39 %Modeshapeintegrals note: Lexp=L
40 gammaZ=(phiT'*phiZ)/(phiZ'*phiZ);
41 gammaT=(phiT'*phiZ)/(phiT'*phiT);
42 gamma=gammaZ*gammaT;
43
44 omegamin=omegaZ;
45 omegamax=omegaT;
46
47 Vredmin=Vmin/(B*omegamax);
48 Vredmax=Vmax/(B*omegamin);
49
50 Vred=linspace(Vredmin,Vredmax,Nv);
51 if ADalt==1;
52    pAD=dlmread(ADfile,'\t',[1,1,8,4]);
53    H1=zeros(1,Nv);
54    H2=zeros(1,Nv);
55    H3=zeros(1,Nv);
56    H4=zeros(1,Nv);
57    A1=zeros(1,Nv);
58    A2=zeros(1,Nv);
59    A3=zeros(1,Nv);
60    A4=zeros(1,Nv);
61    for n=1:4;
62        H1=H1+pAD(1,n)*((2*pi).*Vred).^(4-n);
63        H2=H2+pAD(2,n)*((2*pi).*Vred).^(4-n);
64        H3=H3+pAD(3,n)*((2*pi).*Vred).^(4-n);
65        H4=H4+pAD(4,n)*((2*pi).*Vred).^(4-n);
66        A1=A1+pAD(5,n)*((2*pi).*Vred).^(4-n);
67        A2=A2+pAD(6,n)*((2*pi).*Vred).^(4-n);
68        A3=A3+pAD(7,n)*((2*pi).*Vred).^(4-n);
69        A4=A4+pAD(8,n)*((2*pi).*Vred).^(4-n);
70    end
71 else
72 %Aerodynamic derivatives, from the function aeroplate.m (Theodorsen)
73 [H1,H2,H3,H4,A1,A2,A3,A4]=aeroplate(Vred);
74 end
75
76 if plotAD==1;
77     subplot(2,2,1)
78     plot(Vred,H1)
79     xlabel('V/(B*\omega)')
80     ylabel('H^*_1')
81     xlim([Vredmin,Vredmax])
82     grid on
83
84     subplot(2,2,2)
85     plot(Vred,H2)
86     xlabel('V/(B*\omega)')
```

```
87      ylabel('H^*_2')
88      xlim([Vredmin,Vredmax])
89      grid on
90
91      subplot(2,2,3)
92      plot(Vred,H3)
93      xlabel('V/(B*\omega)')
94      ylabel('H^*_3')
95      xlim([Vredmin,Vredmax])
96      grid on
97
98      subplot(2,2,4)
99      plot(Vred,H4)
100     xlabel('V/(B*\omega)')
101     ylabel('H^*_4')
102     xlim([Vredmin,Vredmax])
103     grid on
104
105     figure
106     subplot(2,2,1)
107     plot(Vred,A1)
108     xlabel('V/(B*\omega)')
109     ylabel('A^*_1')
110     xlim([Vredmin,Vredmax])
111     grid on
112
113     subplot(2,2,2)
114     plot(Vred,A2)
115     xlabel('V/(B*\omega)')
116     ylabel('A^*_2')
117     xlim([Vredmin,Vredmax])
118     grid on
119
120     subplot(2,2,3)
121     plot(Vred,A3)
122     xlabel('V/(B*\omega)')
123     ylabel('A^*_3')
124     xlim([Vredmin,Vredmax])
125     grid on
126
127     subplot(2,2,4)
128     plot(Vred,A4)
129     xlabel('V/(B*\omega)')
130     ylabel('A^*_4')
131     xlim([Vredmin,Vredmax])
132     grid on
133 end
134
135
```

```
%Solving for roots
ReRoots=zeros(1,Nv);
ImRoots=zeros(1,Nv);


for n=1:Nv
    %Real part
    R0=1;
    R1=0;

    R2=-(1+alfa^2+4*alfa*zetaZ*zetaT...
        +(betaZ/2)*alfa^2*H4(n)+(betaT/2)*A3(n));

    R3=alfa*(zetaT*betaZ*alfa*H1(n)+zetaZ*betaT*A2(n));

    R4=alfa^2*(1+(betaZ/2)*H4(n)+(betaT/2)*A3(n)...
        +(betaT*betaZ/4)*((A1(n)*H2(n)*gamma)-A2(n)*H1(n)+A3(n)*H4(n)...
        -(A4(n)*H3(n)*gamma)));

    ReC=[R4,R3,R2,R1,R0];
    ReS=roots(ReC);
    ReR=0;
    j=1;

    for i=1:4;
        if isreal(ReS(i))==1 && ReS(i)<alfa && ReS(i)>0;
            ReR(j)=ReS(i);
            j=j+1;
        end
    end
    ReRoots(n)=max(ReR);


    %Imaginary part roots
    I0=2*(zetaZ*alfa+zetaT);

    I1=-0.5*(betaZ*alfa^2*H1(n)+betaT*A2(n));

    I2=-2*(zetaZ*((betaT/2)*A3(n)+alfa)...
        +zetaT*(alfa^2)*((betaZ/2)*H4(n)+1));

    I3=2*alfa^2*((betaZ*betaT/8)*(H1(n)*A3(n)-(H2(n)*A4(n)*gamma)...
        -(H3(n)*A1(n)*gamma)+H4(n)*A2(n))+1/4*(betaZ*H1(n)+betaT*A2(n)));

    ImC=[I3,I2,I1,I0];
    ImS=roots(ImC);
    ImR=0;
    j=1;
    for i=1:3;
```

```
185         if isreal(ImS(i))==1 && ImS(i) < alfa && ImS(i)>0;
186             ImR(j)=ImS(i);
187             j=j+1;
188         end
189     end
190     ImRoots(n)=max(ImR);
191 end
192
193 set(0,'DefaultTextFontname','Times New Roman')
194 fig1=figure(1);
195 plot(Vred,ReRoots,'bo',Vred,ImRoots,'ro','LineWidth',1.25);
196 title('Solution of flutter equations VA1—TA1, 15m c/c',...
197     'Interpreter','latex')
198 xlabel('$\hat{V}$','Interpreter','latex','Fontsize',11)
199 ylabel('$$\hat{\omega}_r$','Interpreter','latex','Fontsize',11)
200 grid on
201 h=legend('RealRoots','ImagRoots');
202
203 set(h,'Interpreter','latex','Location','SouthWest')
204
205 legend('boxoff')
```

aeroplate.m

```
function [H1,H2,H3,H4,A1,A2,A3,A4] = aeroplate(Vred)
%Function calculates aerodynamic derivatives of a flat plate,
%input is reduced velocity Vh.
X=0.5.*(1./Vred);
J0=besselj(0,X);
J1=besselj(1,X);
Y0=bessely(0,X);
Y1=bessely(1,X);

%Vh is reduced velocity = V/(B*w(V)) and J_n, Y_n is the bessel ...
    functions
%F and G are the real and imaginary parts of the so called ...
    Theodorsen's
%circulatory function

F=(J1.*(J1+Y0)+Y1.*(Y1-J0))./((J1+Y0).^2+(Y1-J0).^2);

G=-((J1.*J0)+(Y1.*Y0))./((J1+Y0).^2+(Y1-J0).^2);

H1=-2*pi.*F.*Vred;
H2=(pi/2).*(1+F+4.*G.*Vred).*Vred;
H3=(2*pi).*(F.*Vred-G./4).*Vred;
H4=(pi/2).*(1+4.*G.*Vred);

A1=(-pi/2).*(F.*Vred);
A2=(-pi/8).*(1-F-4.*G.*Vred).*Vred;
A3=(pi/2).*(F.*Vred-G./4).*Vred;
A4=(pi/2).*G.*Vred;
end
```

The static divergence and dynamic stability limit in torsion were found with the following script.

StatDiv.m

```
%Static divergence calculation using A^*_3

cd('C:\Users\Simen\Master NTNU 2013\Beregninger final\20 m ...
    cc\Static div')

clear all
close all

%Basic structural properties, options for aerodynamic ...
    derivatives and the
%two modes including eigenfrequencies are imported from text files.
%User input: filenames and wind velocity range
Nv=10000;
Vmin=10;
Vmax=120;
ADalt=1;
wMin=1e-2; wMax=1e2; Nw=500;

Inp=dlmread('Data 15m cc.txt','\t',[2,0,2,9]);
OMEGA=importdata('15m cc VA1-TA1 (5-13)_omega.txt');
PHI=dlmread('15m cc VA1-TA1 (5-13).txt');
ADfile='AD 15m cc.txt';

tol=0.001;

mZ=Inp(1); mT=Inp(2); zetaZ=Inp(3); zetaT=Inp(4); rho=Inp(7);
B=Inp(8); L=Inp(9);

omegaT=OMEGA(2);

phiT=PHI(:,2);

V=linspace(Vmin,Vmax,Nv);
OmegaT=zeros(1,Nv+1); OmegaT(1)=omegaT;
w=linspace(wMin,wMax,Nw);
K=zeros(1,Nv);

for n=1:Nv
    Vn=V(n);
    omegaTn=OmegaT(n);
    flag=0;
    while flag==0;
        Vred=Vn/(B*omegaTn);
```

```
42
43          if ADalt==1;
44              pAD=dlmread(ADfile,'\t',[1,1,8,4]);
45              A2=0;
46              A3=0;
47              for i=1:4;
48                  A2=A2+pAD(6,i)*((2*pi).*Vred).^(4-i);
49                  A3=A3+pAD(7,i)*((2*pi).*Vred).^(4-i);
50              end
51          else
52              %Aerodynamic derivatives, from the function ...
                    aeroplate.m (Theodorsen)
53              [H1,H2,H3,H4,A1,A2,A3,A4]=aeroplate(Vred);
54          end
55
56          KaeTT=(rho*B^4)/(2*mT)*(omegaTn/omegaT)^2*A3;
57
58          CaeTT=(rho*B^4)/(4*mT)*(omegaTn/omegaT)*A2;
59
60          E=1-KaeTT-(w./omegaT).^2 + 2*1i*(zetaT-CaeTT).*(w./omegaT);
61
62          H=1./abs(E);
63
64          [~,Pos1]=max(H);
65
66          omegaTi=w(Pos1);
67
68          if abs(omegaTi-omegaTn)<tol
69              flag=1;
70          else
71              omegaTn=omegaTi;
72          end
73      end
74
75      OmegaT(n+1)=omegaTi;
76      K(n)=KaeTT;
77
78      if abs((1-KaeTT))<tol;
79          Vcr=Vn;
80          fprintf('Static divergence reached at Vcr= %5.2f m/s\n',Vcr)
81          break
82      end
83  end
84
85  plot(V,K,'bo',[0,Vmax],[1,1],'k--','LineWidth',1.25)
86
87  %%
88  %Dynamic stability limit in torsion
89  for n=1:Nv
```

```
90      Vn=V(n);
91      omegaTn=OmegaT(n);
92      flag=0;
93      while flag==0;
94          Vred=Vn/(B*omegaTn);
95
96          if ADalt==1;
97              pAD=dlmread(ADfile,'\t',[1,1,8,4]);
98              A2=0;
99              A3=0;
100             for i=1:4;
101                 A2=A2+pAD(6,i)*((2*pi).*Vred).^(4-i);
102                 A3=A3+pAD(7,i)*((2*pi).*Vred).^(4-i);
103             end
104         else
105             %Aerodynamic derivatives, from the function ...
                    aeroplate.m (Theodorsen)
106             [H1,H2,H3,H4,A1,A2,A3,A4]=aeroplate(Vred);
107         end
108
109         KaeTT=(rho*B^4)/(2*mT)*(omegaTn/omegaT)^2*A3;
110
111         CaeTT=(rho*B^4)/(4*mT)*(omegaTn/omegaT)*A2;
112
113         E=1-KaeTT-(w./omegaT).^2 + 2*1i*(zetaT-CaeTT).*(w./omegaT);
114
115         H=1./E;
116
117         [~,Pos1]=max(abs(H));
118
119         omegaTi=w(Pos1);
120
121         if abs(omegaTi-omegaTn)<tol
122             flag=1;
123         else
124             omegaTn=omegaTi;
125         end
126     end
127
128     OmegaT(n+1)=omegaTi;
129     K(n)=KaeTT;
130
131     [MinE,PosE]=min(abs(E));
132
133     if abs(MinE)<tol;
134         disp('Dynamic stability limit in torsion found')
135         Ncr=n;
136         omegaR=w(PosE);
137         Vcr=Vn;
```

```
138             break
139         end
140     end
```

D.3 Response calculation

The MATLAB scripts *response_main.m* calculates the dynamic response in a two-modal approach employing the subscripts *ModLoad.m*, *FreqResp.m* and *JAF.m*.

response_main.m

```
%Buffeting response calculation with two modes
%Main script
%By Simen L. W. | 27.05.2013
%
clear all
%*********USER INPUT*****************
cd('C:\Users\Simen\Master 2013\MyFolder')

Datafile='Data 15m cc.txt';
Modesfile='15m cc VA1-TA1(5-13)'; %no extension
ADfile='AD 15m cc.txt';
Windfile='Wind data 15m cc.txt';


Freqfile=strcat(Modesfile,'_omega.txt');
Modesfile=strcat(Modesfile,'.txt');

%Modes 1=Z, 2=T
Mode1=1;
Mode2=2;

%Computational options
Vmin=73.4; Vmax=73.4; Nv=1;  %Mean-wind velocity
OmegaMin=1e-2; OmegaMax=1e1; Nw=1000; %Frequency range

runplot=1;
%Frequency iterations, specify max number of iterations
%and tolerance
iMax=20; tol=0.001;
%Response location
Xr=3700/4;

%**********END USER INPUT**************

%**********DATA IMPORT*****************
DAT=dlmread(Datafile,'\t',[2,0,2,10]);
OMEGA=importdata(Freqfile);
PHI=dlmread(Modesfile);
WIND=dlmread(Windfile,'\t',[2,1,9,1]);
LC=dlmread(Windfile,'\t',[11,1,16,1]);
pAD=dlmread(ADfile,'\t',[1,1,8,4]);
```

```
42
43 m1=DAT(1); m2=DAT(2); zeta1=DAT(3); zeta2=DAT(4); rho=DAT(7); ...
       B=DAT(8);
44 D=DAT(9); L=DAT(10);
45
46 omega1=OMEGA(1); omega2=OMEGA(2); phi1=PHI(:,1); phi2=PHI(:,2);
47
48 Nx=length(phi1); x=linspace(0,L,Nx); xh=x./L;
49
50 Iu=WIND(1); Iw=WIND(2); Lu=WIND(3); Lw=WIND(4); Au=WIND(5); ...
       Aw=WIND(6);
51 Cux=WIND(7); Cwx=WIND(8);
52
53 CbD=LC(1); CD=LC(2); CbL=LC(3); CL=LC(4); CbM=LC(5); CM=LC(6);
54
55 clear DAT OMEGA PHI WIND LC
56 %********END DATA IMPORT***************
57
58 %********MODE INTEGRALS****************
59 P11=trapz(x,phi1.^2); P22=trapz(x,phi2.^2); P12=trapz(x,phi1.*phi2);
60
61 gamma1=P12/P11; gamma2=P12/P22;
62 %************************************
63
64 %********WIND SPECTRA******************
65 w=linspace(OmegaMin,OmegaMax,Nw);
66
67 Au=Au/(2*pi); Aw=Aw/(2*pi);  %Change to rad/s instead of Hz
68
69 Cux=Cux/(2*pi); Cwx=Cwx/(2*pi); %Change to rad/s instead of Hz
70
71 %************************************
72
73 %**********Response location*********
74
75 [¬,Xi]=min(abs(x-Xr));
76
77 if Mode1==1 && Mode2==2
78 phiXR=[phi1(Xi),0;0,phi2(Xi)];
79 elseif Mode1==1 && Mode2==1
80 phiXR=[phi1(Xi),phi2(Xi);0,0];
81 elseif Mode1==2 && Mode2==2
82 phiXR=[0,0;phi1(Xi),phi2(Xi)];
83 end
84
85 %********Computation******************
86 V=linspace(Vmin,Vmax,Nv);
87 OM1=zeros(1,Nv+1); OM1(1)=omega1;
88 OM2=zeros(1,Nv+1); OM2(1)=omega2;
```

```
89
90  SQQ11=zeros(Nv,Nw);
91  SQQ12=zeros(Nv,Nw);
92  SQQ22=zeros(Nv,Nw);
93
94  SRR11=zeros(Nv,Nw);
95  SRR12=zeros(Nv,Nw);
96  SRR21=zeros(Nv,Nw);
97  SRR22=zeros(Nv,Nw);
98
99  H11=zeros(Nv,Nw);
100 H12=zeros(Nv,Nw);
101 H21=zeros(Nv,Nw);
102 H22=zeros(Nv,Nw);
103
104 DE=zeros(Nv,Nw);
105 DH=zeros(Nv,Nw);
106
107 sig1=zeros(1,Nv);
108 sig2=zeros(1,Nv);
109 cov12=zeros(1,Nv);
110 cov21=zeros(1,Nv);
111
112 %%
113 tic;
114 for n=1:Nv
115 Vn=V(n);
116 %Normalized modal load matrix
117 run('ModLoad.m');
118
119 %Frequency-response matrix
120 omega1n=OM1(n);
121 omega2n=OM2(n);
122 run('FreqResp.m');
123
124 OM1(n+1)=omega1i;
125 OM2(n+1)=omega2i;
126
127 for k=1:Nw
128     Hk=[H11(n,k),...
129         H12(n,k);....
130         H21(n,k),...
131         H22(n,k)];
132
133     SQQk=[SQQ11(n,k),...
134         SQQ12(n,k);...
135         SQQ12(n,k),...
136         SQQ22(n,k)];
137
```

```
138      SRRk=conj(Hk)*SQQk*Hk';
139
140      SRR11(n,k)=SRRk(1,1);
141      SRR12(n,k)=SRRk(1,2);
142      SRR21(n,k)=SRRk(2,1);
143      SRR22(n,k)=SRRk(2,2);
144  end
145
146  CovRR=[trapz(w,abs(SRR11(n,:))),...
147      trapz(w,abs(SRR12(n,:)));...
148      trapz(w,abs(SRR21(n,:))),...
149      trapz(w,abs(SRR22(n,:)))];
150
151  Cov=phiXR*CovRR*phiXR';
152
153  sig1(n)=sqrt(Cov(1,1));
154  sig2(n)=sqrt(Cov(2,2));
155  cov12(n)=Cov(1,2);
156  cov21(n)=Cov(2,1);
157  end
158
159  runtime=toc;
160  fprintf('Script finished in %5.3f seconds\n',toc)
161  clear tic toc
162
163  if runplot==1
164  run('RespPlot.m')
165  end
166
167  if Nv>1
168  figure
169  plot(V,sig1,'o-')
170  grid on
171  xlabel('$V \, [m/s]$','Interpreter','latex')
172  ylabel('$\sigma_{r_z \, r_z} \,[m]$','Interpreter','latex')
173  else
174  fprintf('Sigma1= %5.4f [m]\n',sig1)
175  fprintf('Sigma2= %5.4f [rad]\n',sig2)
176  end
```

ModLoad.m

```
%Modal load part of frequency response
%Result is normalized modal load matrix

%*****WIND LOAD*******
%Reduced auto spectral density and beta for coherence function
%Coh=exp(-beta*dx).

Su=((Au.*Lu./Vn)./((1+1.5.*Au.*w.*Lu./Vn).^(5/3)));
Sw=((Aw.*Lw./Vn)./((1+1.5.*Aw.*w.*Lw./Vn).^(5/3)));

Beta_un=Cux.*L.*w./Vn;
Beta_wn=Cwx.*L.*w./Vn;

%Function JAF is used to calculate the Joint Acceptance function
%integrals
Iu11=JAF(phi1,phi1,xh,Beta_un);
Iw11=JAF(phi1,phi1,xh,Beta_wn);

Iu12=JAF(phi1,phi2,xh,Beta_un);
Iw12=JAF(phi1,phi2,xh,Beta_wn);

Iu22=JAF(phi2,phi2,xh,Beta_un);
Iw22=JAF(phi2,phi2,xh,Beta_wn);

%Joint Acceptance function Squared (JS)
if Mode1==1 && Mode2==2
JS11=(L^2).*((2*CbL)^2*Iu^2*Iu11.*Su +...
    (CL+(D/B).*CbD)^2.*Iw.^2.*Iw11.*Sw);

JS12=(L^2).*((4*CbL*B*CbM*Iu.^2).*Iu12.*Su +...
(CL+(D/B)*CbD)*B*CM*Iw^2.*Iw12.*Sw);

JS22=(L^2).*((2*B*CbM)^2*Iu^2*Iu22.*Su +...
    (B*CM)^2*Iw^2.*Iw22.*Sw);

elseif Mode1==1 && Mode2==1
JS11=(L^2).*((2*CbL)^2*Iu^2*Iu11.*Su +...
    (CL+(D/B).*CbD)^2.*Iw.^2.*Iw11.*Sw);

JS12=(L^2).*((2*CbL)^2*Iu^2*Iu12.*Su +...
    (CL+(D/B).*CbD)^2.*Iw.^2.*Iw12.*Sw);

JS22=(L^2).*((2*CbL)^2*Iu^2*Iu22.*Su +...
    (CL+(D/B).*CbD)^2.*Iw.^2.*Iw22.*Sw);

elseif Mode1==2 && Mode2==2
```

```
47 JS11=(L^2).*((2*B*CbM)^2*Iu^2*Iu11.*Su +...
48      (B*CM)^2*Iw^2.*Iw11.*Sw);
49
50 JS12=(L^2).*((2*B*CbM)^2*Iu^2*Iu12.*Su +...
51      (B*CM)^2*Iw^2.*Iw12.*Sw);
52
53 JS22=(L^2).*((2*B*CbM)^2*Iu^2*Iu22.*Su +...
54      (B*CM)^2*Iw^2.*Iw22.*Sw);
55 end
56
57 %Reduced Joint Acceptance functions (JSred)
58 JS11red=(JS11)./(P11^2);
59 JS12red=(JS12)./(P11*P22);
60 JS22red=(JS22)./(P22^2);
61
62 for i=1:Nw
63 SQQ11(n,i)=((rho*B^3)/(2*m1))*((rho*B^3)/(2*m1))*(Vn/(B*omega1))^2*...
64      (Vn/(B*omega1))^2*JS11red(i);
65 SQQ12(n,i)=((rho*B^3)/(2*m1))*((rho*B^3)/(2*m2))*(Vn/(B*omega1))^2*...
66      (Vn/(B*omega2))^2*JS12red(i);
67 SQQ22(n,i)=((rho*B^3)/(2*m2))*((rho*B^3)/(2*m2))*(Vn/(B*omega2))^2*...
68      (Vn/(B*omega2))^2*JS22red(i);
69 end
```

JAF.m

```
%Joint Acceptance Function
%Calculation. x is the reduced length vector. Large Nx/Nf should ...
    be used.
function [IJ] = JAF(f1,f2,x,beta)

Nf1=length(f1);
%Nf2=length(f2);
Nx=length(x);
Nb=length(beta);

if Nf1≠Nx
    disp('Lengths of f(x) and x does not coincide')
    return
end

S=zeros(1,Nb);
for k=1:Nb
    for n=1:Nx
        for m=1:Nx

            dx=abs(x(n)-x(m));
            S(k)=S(k)+f1(n)*f2(m)*exp(-beta(k)*dx);

        end
    end
end
IJ=(1/Nx^2).*S;
end
```

FreqResp.m

```
%Frequency response matrix computation which updates resonance ...
    frequencies by
%iteration. Two modes - vertical and/or torsional.
%This is the part of the script response_main.m

Ni=-1; %Iteration counter

flag=0;
while flag==0;
if Ni == iMax
    break
end
Ni=Ni+1;

Vred1=Vn/(B*omega1n);
Vred2=Vn/(B*omega2n);

%Calculates relevant aerodynamic stiffness and damping dependent on
%input modes.

%***Z-T modes***
if Mode1==1 && Mode2==2
    H1Z1=0;
    H2Z1=0;
    H3Z1=0;
    H4Z1=0;
    A1T2=0;
    A2T2=0;
    A3T2=0;
    A4T2=0;
    %Aerodynamic derivatives
    for q=1:4;
        H1Z1=H1Z1+pAD(1,q)*((2*pi).*Vred1).^(4-q);
        H2Z1=H2Z1+pAD(2,q)*((2*pi).*Vred1).^(4-q);
        H3Z1=H3Z1+pAD(3,q)*((2*pi).*Vred1).^(4-q);
        H4Z1=H4Z1+pAD(4,q)*((2*pi).*Vred1).^(4-q);
        A1T2=A1T2+pAD(5,q)*((2*pi).*Vred2).^(4-q);
        A2T2=A2T2+pAD(6,q)*((2*pi).*Vred2).^(4-q);
        A3T2=A3T2+pAD(7,q)*((2*pi).*Vred2).^(4-q);
        A4T2=A4T2+pAD(8,q)*((2*pi).*Vred2).^(4-q);
    end

        Cae11=((rho*B^2)/(4*m1*omega1))*H1Z1*omega1n;
        Cae12=(((rho*B^3)/(4*m1*omega1))*H2Z1*gamma1)*omega1n;
        Cae21=(((rho*B^3)/(4*m2*omega2))*A1T2*gamma2)*omega2n;
        Cae22=((rho*B^4)/(4*m2*omega2))*A2T2*omega2n;
```

```
46
47          Kae11=((rho*B^2)/(2*m1*omega1^2))*H4Z1.*(omega1n^2);
48          Kae12=((rho*B^3)/(2*m1*omega1^2))*H3Z1*gamma1.*(omega1n^2);
49          Kae21=((rho*B^3)/(2*m2*omega2^2))*A4T2*gamma2.*(omega2n^2);
50          Kae22=((rho*B^4)/(2*m2*omega2^2))*A3T2.*(omega2n^2);
51
52  %***Z-Z modes***
53  elseif Mode1==1 && Mode2==1
54      H1Z1=0;
55      H4Z1=0;
56      H1Z2=0;
57      H4Z2=0;
58
59      for q=1:4;
60          H1Z1=H1Z1+pAD(1,q)*((2*pi).*Vred1).^(4-q);
61          H4Z1=H4Z1+pAD(4,q)*((2*pi).*Vred1).^(4-q);
62          H1Z2=H1Z2+pAD(1,q)*((2*pi).*Vred2).^(4-q);
63          H4Z2=H4Z2+pAD(4,q)*((2*pi).*Vred2).^(4-q);
64      end
65
66          Cae11=((rho*B^2)/(4*m1*omega1))*H1Z1*omega1n;
67          Cae12=((rho*B^2)/(4*m1*omega1))*H1Z1*gamma1*omega1n;
68          Cae21=((rho*B^2)/(4*m2*omega2))*H1Z2*gamma2*omega2n;
69          Cae22=((rho*B^2)/(4*m2*omega2))*H1Z2*omega2n;
70
71          Kae11=((rho*B^2)/(2*m1*omega1^2))*H4Z1.*(omega1n^2);
72          Kae12=((rho*B^2)/(2*m1*omega1^2))*H4Z1.*gamma1*(omega1n^2);
73          Kae21=((rho*B^2)/(2*m2*omega2^2))*H4Z2.*gamma2*(omega2n^2);
74          Kae22=((rho*B^2)/(2*m2*omega2^2))*H4Z2.*(omega2n^2);
75
76  %***T-T modes***
77  elseif Mode1==2 && Mode2==2
78      A2T1=0;
79      A2T2=0;
80      A3T1=0;
81      A3T2=0;
82
83      for q=1:4;
84
85          A2T1=A2T1+pAD(6,q)*((2*pi).*Vred1).^(4-q);
86          A3T1=A3T1+pAD(7,q)*((2*pi).*Vred1).^(4-q);
87          A2T2=A2T2+pAD(6,q)*((2*pi).*Vred2).^(4-q);
88          A3T2=A3T2+pAD(7,q)*((2*pi).*Vred2).^(4-q);
89
90      end
91
92          Cae11=((rho*B^4)/(4*m1*omega1))*A2T1*omega1n;
93          Cae12=((rho*B^4)/(4*m1*omega1))*A2T1*gamma1*omega1n;
94          Cae21=((rho*B^4)/(4*m2*omega2))*A2T2*gamma2*omega2n;
```

```
95          Cae22=((rho*B^4)/(4*m2*omega2))*A2T2*omega2n;
96
97          Kae11=((rho*B^4)/(2*m1*omega1^2))*A3T1.*(omega1n^2);
98          Kae12=((rho*B^4)/(2*m1*omega1^2))*A3T1.*gamma1*(omega1n^2);
99          Kae21=((rho*B^4)/(2*m2*omega2^2))*A3T2.*gamma2*(omega2n^2);
100         Kae22=((rho*B^4)/(2*m2*omega2^2))*A3T2.*(omega2n^2);
101
102 end
103
104     I=eye(2,2);
105
106
107     for k=1:Nw %Frequency Response for omega_k and determinant ...
            calculation
108
109         En=I - [Kae11,Kae12;Kae21,Kae22] - ...
110             [(w(k)/omega1)^2,0;0,(w(k)/omega2)^2]...
111             + ...
                    2*1i*[w(k)/omega1,0;0,w(k)/omega2]*([zeta1,0;0,zeta2]...
112             -[Cae11,Cae12;Cae21,Cae22]);
113
114         Hn=inv(En);
115
116         H11(n,k)=Hn(1,1); H12(n,k)=Hn(1,2);
117         H21(n,k)=Hn(2,1); H22(n,k)=Hn(2,2);
118
119         DE(n,k)=det(En);
120         DH(n,k)=det(Hn);
121
122     end
123
124     %Find new resonance frequencies
125     [¬,Posw1]=max(abs(H11(n,:))); [¬,Posw2]=max(abs(H22(n,:)));
126
127     omega1i=w(Posw1);  omega2i=w(Posw2);
128
129     %Control of new resonance frequencies
130     if abs(omega1i-omega1n)≤tol && abs(omega2i-omega2n)≤tol;
131         flag=1;
132     else
133         omega1n=omega1i;
134         omega2n=omega2i;
135     end
136 end
137
138 NI(n)=Ni; %Iterations used
```

Bibliography

[1] D. Fergestad, J. Høyte, and H.-P. Brathaug, *BRUKERMANUAL til ALVSAT versjon 3.7: Analyse av lineære svingninger av hengebru i vinduro*. SINTEF Bygg og miljøteknikk, Konstruksjonsteknikk, 1996.

[2] MATLAB, *version 8.0.0 (R2012b)*. Natick, Massachusetts: The MathWorks Inc., 2012.

[3] S. O. Hansen et. al., *Brusymfonien: Static and dynamic wind tunnel tests with a section model*. Svend Ole Hansen ApS, 2005.

[4] E. N. Strømmen, *Theory of Bridge Aerodynamics*. Springer Verlag, 2 ed., 2010.

[5] E. N. Strømmen, *Structural Dynamics*. Springer Verlag, to be published 2013.

[6] A. K. Chopra, *Dynamics of structures: Theory and applications to earthquake engineering*. Prentice Hall, Upper Saddle River, NY, 3 ed., 2007.

[7] C. Dyrbye and S. O. Hansen, *Wind loads on structures*. John Wiley & Sons, 1996.

[8] J. Kaimal, J. Wyngaard, Y. Izumi, and O. Coté, "Spectral characteristics of surface-layer turbulence," *Quarterly Journal of the Royal Meteorological Society*, vol. 98, no. 417, pp. 563–589, 1972.

[9] Wikipedia, "Akashi kaikyō bridge." `http://en.wikipedia.org/wiki/Akashi_Kaikyo_Bridge`.

[10] N. J. Gimsing and C. T. Georgakis, *Cable supported bridges: concept and design*. Wiley, 2011.

[11] Wikipedia, "Xihoumen bridge." `http://en.wikipedia.org/wiki/Xihoumen_Bridge`.

[12] Highestbridges.com. http://highestbridges.com/wiki/images/5/50/Xihoumen.jpg.

[13] http://www.vegvesen.no.

[14] K. Berntsen. Private communication.

[15] P. K. Larsen, A. H. Clausen, and A. Aalberg, *Stålkonstruksjoner: Profiler og Formler*. Tapir Akademisk Forlag, 3 ed., 2007. Table 5.3, p. 44.

[16] Statens vegvesen, *Bruprosjektering, Eurokodeutgave*, håndbok 185 ed., 2011. www.vegvesen.no.

[17] Standard Norge, Lysaker, *Eurokode 1: Laster på konstruksjoner, Del 1-4, Allmenne laster. Vindlaster*, 2009.